

# **Smooth Muscle Titin in Embryo Implantation and Angiogenesis**

vorgelegt von  
Diplom-Ingenieurin  
Nora Bergmann  
aus Berlin

Von der Fakultät III – Prozesswissenschaften  
der Technischen Universität Berlin  
zur Erlangung des akademischen Grades  
Doktorin der Naturwissenschaften  
Dr. rer. nat.

genehmigte Dissertation

Promotionsausschuss:

Vorsitzender: Prof. Dr. Roland Lauster

Berichter: Prof. Dipl.-Ing. Dr. Ulf Stahl

Berichter: Prof. Dr. med. Michael Gotthardt

Tag der wissenschaftlichen Aussprache: 21.5.2010

Berlin 2010

D83



---

Die Dissertation wurde angefertigt am  
Max-Delbrück-Centrum für Molekulare Medizin Berlin-Buch  
Arbeitsgruppe von Professor Dr. med. Michael Gotthardt  
Neuromuskuläre und kardiovaskuläre Zellbiologie  
Robert-Rössle-Str. 10  
13125 Berlin





---

Das Staunen ist eine Sehnsucht nach Wissen.

Thomas von Aquin



---

## Acknowledgements

It is my pleasure to acknowledge the people, who supported me to this day.

I thank Professor Dr. med. Michael Gotthardt for the opportunity to work on a fascinating project. He not only offered excellent working conditions, but also the freedom of research. I am most grateful for all the inspiring discussions and his trust during the last years.

Prof. Dipl.-Ing. Dr. Ulf Stahl offered me plenty of time and gave me motivation as well as support. I am deeply thankful for following up and assisting my research.

For the pleasant working atmosphere and the close cooperation I am much obliged to all the current and former members of the Gotthardt-lab. My research was also supported by their expert assistance. I like to thank especially Katharina Rost for her helpfulness and Beate Goldbrich-Hannig for assisting me with the mouse genotyping. I am also grateful to the Hübner-lab for the DNA sequencing and the Hecker-lab for the mass spectrometry. Furthermore, I have enjoyed the opportunity to interact with and learn from members of the Willnow-lab.

My immense gratitude belongs to my parents Elfie and Reinhard Bergmann for their love, patience, guidance, and encouragement. Without them, I would never have enjoyed so many opportunities. I am deeply indebted to my brother Ulf Bergmann for all his advice and the scientific ambition that we share. To my friends I am deeply grateful for their effort and understanding. I am fortunate for all the support I have experienced during my life.



# Table of Contents

<b>List of Figures .....</b>	<b>XIII</b>
<b>List of Tables .....</b>	<b>XV</b>
<b>Abbreviations .....</b>	<b>XVI</b>
<b>Abbreviations of genes and proteins .....</b>	<b>XIX</b>
<b>1 Abstract.....</b>	<b>1</b>
<b>2 Zusammenfassung.....</b>	<b>2</b>
<b>3 Introduction.....</b>	<b>4</b>
3.1 Structure and Function of Muscle .....	4
3.1.1 Smooth Muscle.....	4
3.1.2 Striated Muscle .....	5
3.1.3 Muscle contraction .....	6
3.2 Titin .....	8
3.2.1 Titin's structure and localization within the sarcomere .....	8
3.2.2 Titin isoforms .....	9
3.2.3 Titin binding partners .....	11
3.2.3.1 Z-disc region proteins .....	11
3.2.3.2 I-band region proteins .....	11
3.2.3.3 A-band region proteins .....	12
3.2.3.4 M-band region proteins.....	12
3.2.4 Titin's kinase.....	13
3.3 Smooth muscle titin.....	14
3.4 Embryo spacing and implantation .....	15
3.4.1 The female reproductive system.....	15
3.4.2 Embryo implantation .....	16

3.5	Angiogenesis .....	18
3.5.1	Sprouting angiogenesis.....	18
3.5.2	Uterine angiogenesis during embryo implantation.....	19
3.6	Knockout and knockin technology .....	20
3.7	Aim of the study .....	21
<b>4</b>	<b>Materials and Methods.....</b>	<b>23</b>
4.1	Materials .....	23
4.1.1	Chemicals .....	23
4.1.2	Enzymes .....	23
4.1.3	Bacterial strain.....	23
4.1.4	Vectors and BAC clones.....	24
4.1.5	Kits .....	24
4.1.6	Oligonucleotides.....	24
4.1.7	Antibodies .....	27
4.2	Methods.....	28
4.2.1	Molecular biology methods.....	28
4.2.1.1	DNA preparation .....	28
4.2.1.2	Determination of nucleic acid concentration .....	29
4.2.1.3	Polymerase chain reaction (PCR) .....	30
4.2.1.4	DNA agarose gel electrophoresis.....	34
4.2.1.5	Real-Time PCR.....	34
4.2.1.6	Generation of the targeting vector DsRedKI .....	36
4.2.2	Microbiological methods.....	38
4.2.2.1	Generation of competent bacteria .....	38
4.2.2.2	Transformation of bacteria.....	38
4.2.3	Cell biological methods.....	39
4.2.3.1	Gene targeting in mouse ES cells .....	39
4.2.3.2	Formation of embryoid bodies.....	39
4.2.3.3	Preparation and cultivation of primary smooth muscle cells.....	39
4.2.3.4	Immunostaining of embryoid bodies and smooth muscle cells .....	40
4.2.3.5	Cell migration assay.....	41
4.2.4	Biochemical methods .....	42

4.2.4.1	Protein preparation.....	42
4.2.4.2	Protein quantification.....	43
4.2.4.3	Protein gel electrophoresis.....	44
4.2.4.4	Coomassie staining.....	46
4.2.4.5	Western blotting.....	46
4.2.4.6	Histology.....	47
4.2.4.7	ELISA.....	48
4.2.4.8	Multiplex bead immunoassay.....	49
4.2.5	Animal procedures.....	49
4.2.5.1	Maintenance of the mouse colony.....	49
4.2.5.2	Generation of chimeric mice.....	50
4.2.5.3	Chimera breeding and generation of the TiEx28DsRed strain.....	50
4.2.5.4	Staging of the estrous cycle.....	50
4.2.5.5	Timed mating.....	51
4.2.5.6	Collection of serum.....	51
4.2.5.7	Tissue harvesting.....	51
4.2.5.8	Counting of blastocysts.....	52
4.2.5.9	Evans Blue staining.....	52
4.2.5.10	Angiogenesis study.....	52
4.2.6	Statistical analysis.....	53
<b>5</b>	<b>Results.....</b>	<b>54</b>
5.1	The DsRedKI mouse model.....	54
5.1.1	Cloning of the targeting vector DsRedKI.....	54
5.1.2	Generation of the titin-DsRed knockin mouse strain TiEx28DsRed.....	56
5.1.3	Verification of the titin-DsRed protein and its localization within the sarcomere ..	59
5.2	Characterization of the smooth muscle specific knockout of titin's kinase region .	63
5.2.1	Establishing the smooth muscle specific mouse model.....	63
5.2.2	Titin's kinase region is essential for embryo implantation.....	66
5.2.2.1	Normal preimplantational embryo development in titin's kinase region deficient mice.....	66
5.2.2.2	Impaired implantation affects embryo positioning, number of implantation sites, and uterine maturation.....	67
5.2.3	Loss of titin's kinase region influences arachidonic acid metabolism.....	71

## Table of Contents

---

5.2.4	Aberrant angiogenesis in knockout animals lacking titin's kinase region.....	72
5.2.5	Alteration of tissue remodeling in titin's kinase region deficient animals .....	74
5.2.5.1	Expression of <i>Murf1</i> and <i>Fhl2</i> depends on titin's kinase region.....	74
5.2.5.2	The transcription level of <i>Cox2</i> and <i>Lpar3</i> is not affected.....	75
5.2.5.3	Alterations of structural and ubiquitin-proteasome related proteins.....	76
<b>6</b>	<b>Discussion .....</b>	<b>78</b>
<b>7</b>	<b>Outlook .....</b>	<b>93</b>
<b>8</b>	<b>Bibliography .....</b>	<b>94</b>
<b>9</b>	<b>Supplement .....</b>	<b>113</b>



## List of Figures

Figure 1: The contractile unit of smooth muscle.....	4
Figure 2: The sarcomere, the contractile unit of striated muscle.....	5
Figure 3: Molecular basis of muscle contraction. ....	7
Figure 4: Titin isoforms and their domain composition. ....	10
Figure 5: Titin's binding partners. ....	11
Figure 6: The murine reproductive system and preimplantational embryonic development. ....	17
Figure 7: Targeting strategy to insert the red fluorescence protein DsRed. ....	55
Figure 8: Verification of the targeting vector DsRedKI. ....	56
Figure 9: ES cell genotyping by PCR.....	56
Figure 10: Proper localization of titin-DsRed in the sarcomere.....	57
Figure 11: Genotyping of TiEx28DsRed animals. ....	58
Figure 12: Titin-DsRed knockin mice did not have an obvious phenotype. ....	59
Figure 13: Detection of titin-DsRed in heart, quadriceps, and soleus.....	60
Figure 14: The DsRed located close to titin's N-terminus did not influence the sarcomeric structure.....	62
Figure 15: Strategy to delete titin's kinase region in smooth muscle.....	63
Figure 16: Activity of the SMMHC cre-recombinase in uterine smooth muscle.....	64
Figure 17: Recombination by the SMMHC cre-recombinase in uterine smooth muscle and the germline.....	65
Figure 18: Normal estrous cycle length and number of blastocysts in knockout females. ....	66
Figure 19: Impaired embryo implantation in knockout females. ....	67
Figure 20: Reduced number of implantation sites in knockout uteri implies a defect during the penetration phase.....	68
Figure 21: Delayed development of knockout uteri during the penetration phase.....	69
Figure 22: The phenotype observed in the knockout females was due to the deletion of titin's kinase region.....	70
Figure 23: Deletion of titin's kinase region affected arachidonic metabolism.....	71

## List of Figures

---

Figure 24: Altered angiogenesis and PDGF-B serum levels in knockout mice. ....	72
Figure 25: Knockout smooth muscle cells did not migrate in response to PDGF-B.....	73
Figure 26: Altered expression of <i>Murfl</i> and <i>Fhl2</i> in knockout uteri.....	74
Figure 27: Loss of titin's kinase region did not alter the expression of <i>Cox2</i> and <i>Lpar3</i> .....	75
Figure 28: Impaired heat shock response and altered cytoskeleton-related proteins in knockout uteri.....	77
Figure 29: Binding partners of titin's kinase region. ....	88
Figure 30: Map of the targeting vector DsRedKI.....	113
Figure 31: Adult smooth muscle knockout animals did not have an obvious phenotype. ....	114
Figure 32: Increase in the PDGF-B serum levels was not accompanied by changes in selected cytokines.....	114
Figure 33: LIF, an important factor of embryo implantation, was unchanged in pregnant E3.5 knockout uteri.....	115
Figure 34: The transcript level of genes encoding selected calcium-related proteins was unchanged.....	115
Figure 35: Dual view of knockout and control 2D-gel.....	116

## List of Tables

Table 1: Enzymes. ....	23
Table 2: Plasmids and BAC clones used for generation of the targeting vector.....	24
Table 3: Kits. ....	24
Table 4: Primers for cloning, sequencing, and genotyping .....	25
Table 5: Primer/probes for Real-Time PCR analysis .....	26
Table 6: Primary antibodies used for immunofluorescence staining (IF) and Western blotting (WB).....	27
Table 7: Secondary antibodies used for immunofluorescence staining (IF) and Western blotting (WB).....	27
Table 8: Primers, template, and expected sizes of the PCR products for cloning. ....	30
Table 9: Primers, PCR conditions, and expected product sizes of the genotyping PCRs. ....	33
Table 10: Knockout mouse models with an implantation phenotype.....	85
Table 11: Differentially regulated proteins in E3.5 pregnant knockout uteri. ....	117

## Abbreviations

12-HETE	12-hydroxyeicosatetraenoic acid
2D-gel electrophoresis	2 dimensional gel electrophoresis
APS	ammonium persulfate
ATP	adenosine triphosphate
BAC	bacterial artificial chromosome
bp	base pair
BSA	bovine serum albumin
bw	body weight
cDNA	complementary DNA
CHAPS	3-((3-cholamidopropyl)dimethylammonio)-1-propanesulfonate
CIP	calf intestinal alkaline phosphatase
CON	control
Cre	causes recombination
C-terminus	carboxy-terminus
Da	dalton
ddH <sub>2</sub> O	double distilled water
DEPC	diethylpyrocarbonate
DMEM	Dulbecco's modified Eagle Medium
DMSO	dimethyl sulfoxide
DNA	deoxyribonucleic acid
DNase	deoxyribonuclease
dNTP	deoxynucleoside triphosphate
DTT	dithiothreitol
E	embryonic day post coitum
ECL	enhanced chemiluminescence
<i>E. coli</i>	<i>Escherichia coli</i>
EDTA	ethylenediamine tetraacetic acid
EGTA	ethylene glycol-bis(2-aminoethylether)N,N,N',N'tetraacetic acid
ELISA	enzyme-linked immunosorbent assay

---

ES cells	embryonic stem cells
FCS	fetal calf serum
FLP	flippase recombination enzyme
FN3	fibronectin-type III
FRT	flippase recognition target
HET	heterozygous
HRP	horseradish peroxidase
ICM	inner cell mass
Ig	immunoglobulin
IgG	immunoglobulin G
IF	immunofluorescence
IPG	immobilized pH gradient
IS	implantation site
IVC	individually ventilated cage
KI	knockin
KO	knockout
LB-A plate	Luria Bertani-ampicillin plate
LPA	lysophosphatic acid
lox-site	locus of crossing-over
mRNA	messenger RNA
MARP family	muscle ankyrin repeat protein family
NP40	nonylphenyl-polyethylenglycol
N-terminus	amino-terminus
PAGE	polyacrylamide gel electrophoresis
PBS	phosphate buffered saline
PCR	polymerase chain reaction
pI	isoelectric point
PIPES	piperazine-N,N'-bis(2-ethanesulphonic acid)
PMSF	phenylmethylsulfonyl fluoride
PVDF	polyvinylidene difluoride

## Abbreviations

---

RNase	ribonuclease
rpm	rotations per minute
RT-PCR	reverse transcription-PCR
S1P	sphingosine-1-phosphate
SDS	sodium dodecyl sulfate
SEM	standard error of the mean
SMCs	smooth muscle cells
SMMHC	smooth muscle myosin heavy chain
SOC	super optimal broth with catabolite repression
TAE	Tris-acetate-EDTA
<i>Taq</i>	<i>Thermus aquaticus</i>
TE	Tris-EDTA
TEMED	N, N, N', N'-tetramethylethylenediamine
TES	n-tris-(hydroxymethyl)-methyl-2-aminomethanesulfonic acid
TESCA	TES with calcium
Tris	tris(hydroxymethyl)-aminomethane
U	unit
uw	uterus weight
VAGE	vertical SDS-agarose gel electrophoresis
WB	Western blotting
WT	wild-type
X-Gal	5-Bromo-4-chloro-3-indolyl- $\beta$ -D-galactopyranoside

## Abbreviations of genes and proteins

Abbreviations are given in *italics* for genes and in **bold letters** for proteins.

<i>Alox12e</i>	E-12/15-LOX	epidermal 12/15-lipoxygenase
<i>Alox15</i>	L-12/15-LOX	leukocyte 12/15-lipoxygenase
<i>Ankrd2</i>	ANKRD2	ankyrin repeat domain protein 2
<i>Anxa2</i>	ANXA2	annexin A2
<i>Arpc2</i>	ARPC2	actin related protein 2/3 complex
<i>Cacna1c</i>	CACN1C	L-type calcium channel
<i>Calb1</i>	CALB1	calbindin 1
<i>Calm1</i>	CALM1	calmodulin 1
<i>Capg</i>	CAPG	capping protein
<i>Car2</i>	CAR2	carbonic anhydrase 2
<i>Carp (Ankrd1)</i>	CARP	cardiac ankyrin repeat protein
<i>Ckb</i>	CKB	brain creatine kinase
<i>Camk2a</i>	CAMK2A	calcium/calmodulin-dependent protein kinase II alpha
<i>Col6A2</i>	COL6A2	collagen type VI alpha 2
<i>Cox2</i>	COX2	cyclooxygenase 2
<i>Cpla2 (Pla2g4a)</i>	cPLA2	cytosolic phospholipase A <sub>2α</sub>
<i>Creb1</i>	CREB1	cAMP responsive element binding protein 1
<i>Darp (Ankrd23)</i>	DARP	diabetes ankyrin repeat protein
<i>Dll4</i>	DLL4	delta-like-4
<i>Dnaja1</i>	DNAJA1	DnaJ (Hsp40) homolog
<i>Etfdh</i>	ETFDH	electron transferring flavoprotein dehydrogenase
<i>Fga</i>	FGA	fibrinogen
<i>Fgf2</i>	FGF basic	fibroblast growth factor basic
<i>Fhl2</i>	FHL2	four and a half LIM domain protein
<i>Gcsf (Csf3)</i>	G-CSF	granulocyte colony-stimulating factor
<i>Hbegf</i>	HB-EGF	heparin binding epidermal-like growth factor

## Abbreviations of genes and proteins

---

<i>Hnrnpab</i>	HNRNPAB	heterogeneous nuclear ribonucleoprotein A/B
<i>Hspb1</i>	HSPB1	heat shock protein 1
<i>Il1b</i>	IL-1 $\beta$	interleukin-1 $\beta$
<i>Il6</i>	IL-6	interleukin-6
<i>Il15</i>	IL-15	interleukin-15
<i>IP10 (CxC110)</i>	IP-10	interferon-inducible protein 10
<i>lacZ</i>	LacZ	$\beta$ -galactosidase
<i>Lif</i>	LIF	leukemia inhibitory factor
<i>Lpar3</i>	LPA3	lysophosphatic acid receptor 3
<i>Mapk13</i>	MAPK 13	mitogen-activated protein kinase 13
<i>Mapk14</i>	MAPK14	mitogen-activated protein kinase 14
<i>Mcp1 (Ccl2)</i>	MCP-1	monocyte chemotactic protein 1
<i>MEx1-2</i>	a titin region	M-band region encoded by M-band exons 1 and 2
<i>MEx6</i>	a titin region	M-band region encoded by M-band exon 6
<i>Mlp (Csrp3)</i>	MLP	muscle LIM protein
<i>Murf1 (Trim63)</i>	MuRF1	muscle-specific RING finger protein 1
<i>Murf2 (Trim55)</i>	MuRF2	muscle-specific RING finger protein 2
<i>Murf3 (Trim54)</i>	MuRF3	muscle-specific RING finger protein 3
<i>Mylk</i>	MLCK	myosin light chain kinase
<i>Myom1</i>	MYOM1	myomesin
<i>N2A</i>	a titin region	N2A region encoded by exon 104
<i>Nbr1</i>	NBR1	neighbor of Brca gene 1
<i>Ndufs3</i>	NDUFS3	NADH dehydrogenase (ubiquinone) Fe-S protein 3
<i>Nrp1</i>	NRP1	neuropilin 1
<i>p62</i>	p62	sequestosome 1
<i>Pcx</i>	PCX	pyruvate carboxylase
<i>Pdgfb</i>	PDGF-B	platelet derived growth factor B
<i>Pdgfrb</i>	PDGFR $\beta$	platelet derived growth factor receptor $\beta$
<i>Pdia4</i>	PDIA4	protein disulfide-isomerase A4
<i>Pparg</i>	PPAR $\gamma$	peroxisome proliferator-activated receptor $\gamma$
<i>Prkaca</i>	PKA	proteinase kinase A
<i>Prkca</i>	PKC	proteinase kinase C
<i>Prkcd</i>	PKC $\delta$	protein kinase C $\delta$
XX		



---

<i>Prkce</i>	PKCε	protein kinase C ε
<i>Prkg1</i>	PKG	protein kinase G
<i>Psmc2</i>	PSMC2	proteasome 26S subunit ATPase 2
<i>Rack1 (Gnb2l1)</i>	RACK1	receptor for activated C kinase 1
<i>S100a1</i>	S100A1	S 100 calcium binding protein A 1
<i>sAnk (Ank1)</i>	sANK1	small ankyrin 1
<i>Sfrs3</i>	SFRS3	splicing factor arginine/serine-rich 3
<i>Srf</i>	SRF	serum response factor
<i>Tagln</i>	TAGLN	transgelin
<i>Tcap</i>	T-cap	Titin-cap
<i>Tek</i>	Tie2	tyrosine kinase with Ig-like and EGF-like domains 2
<i>Tnf</i>	TNF-α	tumor necrosis factor-alpha
<i>Tpi1</i>	TPI1	triosephosphate isomerase 1
<i>Vegf</i>	VEGF	vascular endothelial growth factor
<i>Vegfr1 (Flt1)</i>	VEGFR1	vascular endothelial growth factor receptor 1
<i>Vegfr2 (Flk1)</i>	VEGFR2	vascular endothelial growth factor receptor 2
<i>Vim</i>	VIM	vimentin
<i>ZEx3</i>	a titin region	Z-disc region encoded by Z-disc exon 3



# 1 Abstract

The muscle protein titin is with a molecular weight of up to 3700 kDa the largest protein discovered so far and after actin and myosin the third most abundant protein in vertebrate striated muscle. Titin integrates into the Z-disc and M-band spanning the half sarcomere and forms an elastic scaffold along the myofiber. Titin has been implied in signal transduction, mechanical stability, and maintenance of sarcomere structure in health and disease. While titin in striated muscle has been well studied, its function in smooth muscle remains unclear although smooth muscle titin has been described on transcript as well as on protein level.

To study smooth muscle titin, we established a knockin mouse model, in which titin's N-terminus was labeled using the fluorescence protein DsRed. Striated muscle analysis of titin-DsRed mice confirmed the integration of DsRed within titin at the Z/I-junction of the sarcomere. This modification did not cause any obvious phenotype such as altered viability, heart weight to body weight ratio, or integration of titin into the sarcomere. The use of the DsRed enables live cell imaging as well as DsRed detection and makes the knockin mouse a suitable tool to visualize smooth muscle titin. It is of interest to localize titin in uterus as we were able to address a functional role for smooth muscle titin in early pregnancy. Titin's M-band exons 1 and 2, which encode titin's kinase region, were efficiently removed in uterine smooth muscle of a conditional knockout model using a cre-recombinase. The majority of pregnant knockout animals showed mislocalization and crowding as well as a reduced number of embryo implantation sites. Furthermore, knockout mice had a delayed uterine development in early pregnancy and impaired angiogenesis, which is a hallmark of embryo implantation. The increased PDGF-B serum levels in pregnant knockout animals and the migration failure of knockout smooth muscle cells in response to PDGF-B indicate that impaired angiogenesis is due to a defect in recruiting smooth muscle cells to the site of vessel formation so that newly formed blood vessels were not stabilized properly. Loss of titin's kinase region also affected arachidonic acid metabolism leading to a reduction of its metabolite 12-HETE in pregnant uterus. Our results demonstrate that signaling of titin's kinase region via PDGF-B and 12-HETE influences female fertility most likely by affecting angiogenesis. The increased knowledge of regulatory mechanisms of angiogenesis during implantation enables novel therapeutic advances for select forms of human implantation failure and recurrent spontaneous abortion.

## 2 Zusammenfassung

Das Muskelprotein Titin ist mit einem Molekulargewicht von bis zu 3700 kDa das größte bekannte Polypeptid. Es ist nach Aktin und Myosin das dritthäufigste Protein im quergestreiften Muskel. Titin integriert in die Z-Scheibe und die M-Bande und überspannt damit das halbe Sarkomer. Es formt ein elastisches Gerüst entlang der Muskelfaser und ist sowohl an Signaltransduktion als auch mechanischer Stabilität und Erhaltung der Sarkomerstruktur beteiligt. Während Titin im quergestreiften Muskel bereits eingehend untersucht wurde, ist seine Funktion im glatten Muskel unbekannt, obwohl Titin im glatten Muskel auf Transkriptions- und Proteinebene beschrieben ist.

Um Titin im glatten Muskel zu untersuchen, haben wir ein Knockin-Mausmodell etabliert, in dem der Amino-Terminus von Titin mit Hilfe des Fluoreszenzprotein DsRed markiert wurde. Die Analyse von quergestreiftem Muskel der Titin-DsRed-Mäuse bestätigte die DsRed-Integration in Titin am Übergang von der Z-Scheibe zur I-Bande des Sarkomers. Diese Modifizierung verursachte keinen offensichtlichen Phänotyp hinsichtlich Lebensfähigkeit, Herzgewicht und Einbau von Titin in das Sarkomer. Die Verwendung des DsReds ermöglicht Live-Cell-Imaging und die DsRed-Detektion, so dass unser Knockin-Mausmodell ideal geeignet ist, um Titin im glatten Muskel zu lokalisieren. Von besonderem Interesse ist Titin im Uterus, da wir Titin im glatten Muskel erstmalig eine funktionelle Rolle während der Schwangerschaft zuweisen konnten. Dazu haben wir ein konditionelles Knockout-Modell verwendet. In diesem wurden Titins M-Banden Exons 1 und 2, die die Titin-Kinase-Region codieren, mit Hilfe einer Cre-Rekombinase effizient im glatten Muskel des Uterus entfernt. Die Embryo-Implantationsstellen der meisten schwangeren Knockout-Tiere waren fehllokalisiert, lagen zu dicht oder waren in der Anzahl reduziert. Zudem war die Entwicklung des Uterus zu Beginn der Schwangerschaft bei Knockout-Mäusen verzögert. Angiogenese, die bei der Embryo-Implantation eine wichtige Rolle spielt, war beeinträchtigt und die PDGF-B-Konzentration im Serum von schwangeren Knockout-Tieren war erhöht. Glatte Muskelzellen aus Knockout-Tieren zeigten nicht die erwartete Migration nach PDGF-B-Stimulation. Diese Ergebnisse legen nahe, dass die verminderte Angiogenese durch einen Migrationsdefekt der glatten Muskelzellen zu dem Ort der Gefäßneubildung bedingt ist, so dass neu gebildete Blutgefäße nicht ausreichend stabilisiert werden konnten. Durch den Verlust der Titin-Kinase-Region wurde ebenfalls der Arachidonsäurestoffwechsel beeinträchtigt. Dies führte zu einer verminderten Konzentration des Metaboliten 12-HETE im Uterus während der Schwangerschaft. Unsere Ergebnisse zeigen, dass sich die Signaltransduktion der Titin-Kinase-Region via PDGF-B und 12-HETE auf die

weibliche Fruchtbarkeit auswirkt, vermutlich durch die Beeinflussung von Angiogenese. Das Verständnis von regulatorischen Mechanismen der Angiogenese während der Embryo-Implantation wird neue therapeutische Maßnahmen für einige Arten von Implantationsdefekten und Fehlgeburten ermöglichen.

### 3 Introduction

#### 3.1 Structure and Function of Muscle

Muscles are responsible for contraction that results from thin and thick filaments sliding against each other. Two types of muscles are classified: smooth and striated muscles. The latter is subdivided into skeletal and cardiac muscle.

##### 3.1.1 Smooth Muscle

Smooth muscles surround visceral and vascular organs such as the intestine, blood vessels, and the uterus. The contraction and relaxation of smooth muscles helps to carry food along the gastrointestinal tract, controls the diameter of blood vessels, and is responsible for embryo spacing and parturition during pregnancy.

A smooth muscle consists of elongated spindle-shaped cells that have a single nucleus and are packed with thin and thick filaments (Bagby, 1986). The ratio of thin to thick filaments in smooth muscle (~20:1) is higher than in skeletal muscle (~6:1; Herrera et al., 2004). The thin filaments are composed of actin, tropomyosin, caldesmon, as well as calponin and the thick filaments consist of myosin. Thin filaments are grouped around a thick filament (Figure 1) that is thereby held in the middle of the smooth muscle contractile unit (Draeger et al., 1990; Hodgkinson et al., 1995).

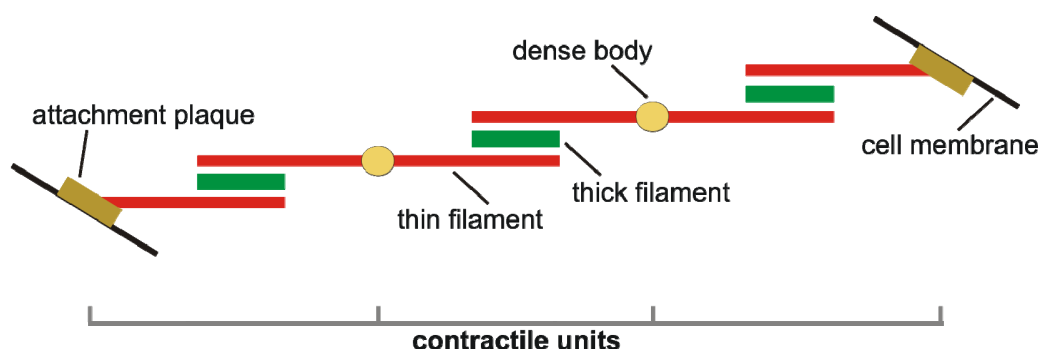


**Figure 1: The contractile unit of smooth muscle.** The schematic representation of three contractile units shows thin filaments (red) that are grouped around a thick filament (green). The thin filaments are anchored in dense bodies (yellow) in the cytoplasm and in attachment plaques (brown) at the cell membrane (black).

The thin filaments are attached to dense bodies in the cytosol or to attachment plaques that are located at the cell membrane of smooth muscle cells (Geiger et al., 1981; Small and Gimona, 1998). Dense bodies and attachment plaques serve the same function as Z-discs in striated muscle and consist mainly of the actin-binding protein  $\alpha$ -actinin. The attachment plaques additionally contain the protein vinculin that binds to  $\alpha$ -actinin. In comparison to striated muscle, in which the contractile units are highly ordered aligned, the contractile units of a smooth muscle cell are oriented in oblique angles. The lack of visible cross striations leads to the name smooth.

### 3.1.2 Striated Muscle

Both skeletal and cardiac muscle cells are striated. Skeletal muscles are attached to the skeleton by tendons and responsible for body movement. Cardiomyocytes are specialized cells within the myocardium of the heart and account for the rhythmic contractions to pump blood through the vessels.

Skeletal and cardiac muscle cells have a similar organization. They are composed of cytoplasmic myofibrils that run in parallel throughout a multinucleated cell and are attached to the cell membrane. The myofibrils are made up of sarcomeres (Figure 2), which comprise thick filaments consisting of myosin and thin filaments consisting of actin, tropomyosin, and troponin.

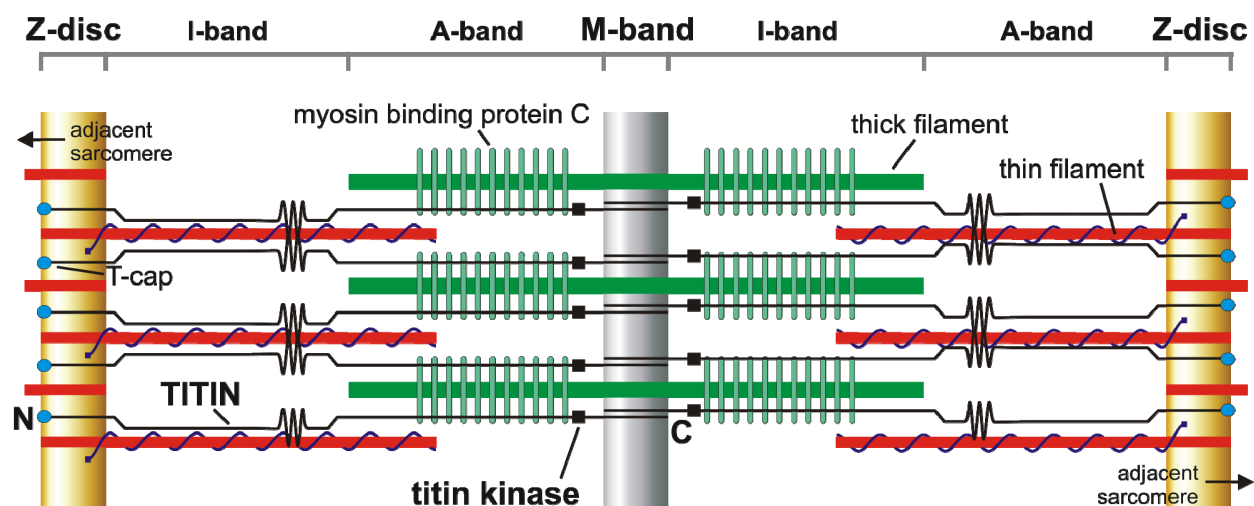


**Figure 2: The sarcomere, the contractile unit of striated muscle.** Schematic representation of the sarcomere that extends between two Z-discs and consists of thin (red) and thick (green) filaments. Titin (black) is integrated with its N-terminus in the Z-disc and with its C-terminus in the M-band spanning the I-band and A-band. It is linked with the myosin binding protein C (light green) to the thick filament. At the Z-disc and M-band, opposite titin molecules overlap so that titin forms a continuous filament along the myofibril. One proposed substrate of the titin kinase (black boxes) is T-cap (blue circles). Adapted from Gregorio et al., 1999.

The sarcomere is the contractile unit of striated muscle and defined as the region between two neighboring Z-discs. Z-discs are the attachment sites for thin filaments of adjacent sarcomeres that are cross-linked by  $\alpha$ -actinin. In the middle of the sarcomere is the M-band, in which myomesin as well as the M-protein cross-link the overlapping thick filament system. The area nearby the Z-discs, which contains thin filaments, is called the I-band. The thin filaments extend into the A-band, the region where thick filaments are present. I- and A-band are named for their properties under polarizing light. The I-band is isotropic leading to a bright appearance whereas the A-band is anisotropic leading to a dark appearance. The highly ordered structure and the parallel arrangement of the filaments in the sarcomeres lead to the striated appearance of skeletal and cardiac muscle.

### 3.1.3 Muscle contraction

Contraction of smooth as well as striated muscle depends on ATP-dependent cyclic interactions between thick filaments and thin filaments under influence of cytosolic calcium. This is described as the sliding-filament model (Hanson and Huxley, 1953; Huxley and Niedergerke, 1954; Huxley, 1957; Guilford and Warshaw, 1998).

In both striated and smooth muscle, ATP is hydrolyzed to ADP by the ATPase activity of the myosin head. The released energy leads to a conformational change in myosin displacing the myosin head (Figure 3). Afterwards, the myosin head binds to the actin filament resulting in the release of ADP and  $P_i$  that triggers a power stroke, in which myosin returns to the initial conformation by the released energy. Thereby, the actin filaments are pulled along the thick filaments towards the center of the sarcomere and the contractile unit shortens. Binding of ATP to the myosin head leads to its detachment from actin and the cross-bridge cycle starts again. Muscle contraction ends if the intracellular calcium concentration is returned to the resting value by transporting calcium with the help of  $Ca^{2+}$ -ATPases and sodium-calcium exchangers back into the sarcoplasmic reticulum and outside of the cells, respectively. As a result, tropomyosin blocks again the binding sites of myosin at the actin filaments in striated muscle. In smooth muscle, the myosin light chain kinase (MLCK) is deactivated and the myosin regulatory light chain is dephosphorylated by the myosin light chain phosphatase.



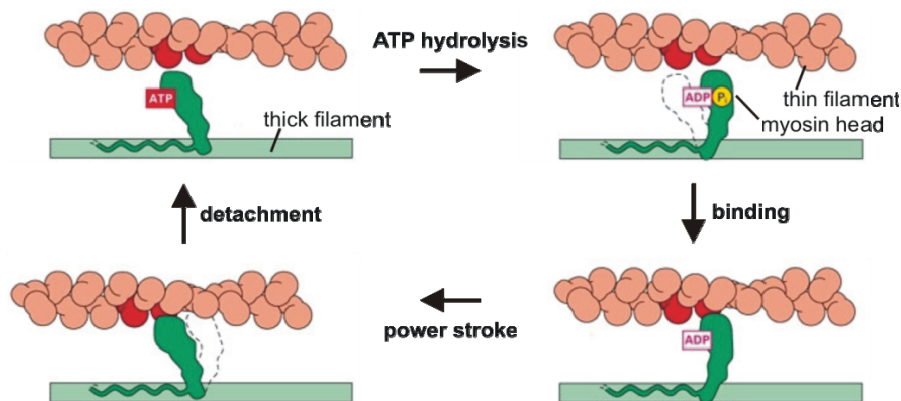


**Figure 3: Molecular basis of muscle contraction.** If the intracellular calcium concentration is high and the myosin-binding sites on actin are exposed, ATP is hydrolyzed by the ATPase activity of the myosin head (top left) leading to a displacement of the myosin head (top right). Binding of the myosin head to actin (bottom right) results in ADP and P<sub>i</sub> release that triggers a power stroke, in which myosin turns to the initial conformation (bottom left). Thereby, the actin filaments are pulled along the thick filament so that the contractile unit shortens. Binding of ATP to the myosin head leads to the detachment of the myosin head and the cross-bridge cycle starts again. Modified from Alberts et al., 2002.

Contraction is controlled by the somatic nervous system in skeletal muscle and by the autonomic nervous system in heart and smooth muscle. In addition, receptor activation by growth factors and hormones, which is independent of membrane potential change, also leads to smooth muscle contraction. The action potential triggers the opening of calcium channels in the muscle cell membrane and in the sarcoplasmic reticulum so that calcium is released into the cytosol. In smooth muscle cells, the sarcoplasmic reticulum is only poorly developed so that the increase in cytosolic calcium in response to an action potential mainly depends on the membrane calcium channels. As a consequence, change in cytosolic calcium level occur much slower in smooth muscle than in striated muscle allowing the smooth muscle to produce slow and steady contractile tension. In striated muscle, binding of calcium to troponin leads to a slight movement of tropomyosin so that the myosin-binding sites on actin are exposed. This makes binding of the myosin heads of the thick filament possible. Smooth muscle lacks the tropomyosin-troponin system that is necessary for rapid response. Instead, intracellular calcium together with calmodulin binds to the MLCK, which is then able to phosphorylate the myosin regulatory light chain resulting in myosin head ATPase activity. In contrast, myosin regulatory light chain phosphorylation only modulates the contractility in striated muscle (Persechini and Stull, 1984).

## 3.2 Titin

Titin was first described in 1977 as an elastic muscle protein by the name of connectin (Maruyama et al., 1977). Two years later, a protein of striated muscle with a megadalton size was accumulated by electrophoresis (Wang et al., 1979). Because of its large size, the protein was named titin after the Titans from the Greek mythology. Later it was discovered that titin and connectin are identical (Maruyama et al., 1981).

### 3.2.1 Titin's structure and localization within the sarcomere

Titin is with a molecular weight of up to 3700 kDa the largest protein in mammals and forms beside actin and myosin the third filament system in striated muscle (Labeit et al., 1992; Labeit and Kolmerer, 1995). One titin molecule with a length of  $>1\ \mu\text{m}$  spans over a half sarcomere (Nave et al., 1989) integrating its N-terminus into the Z-disc and its C-terminus into the M-band (Figure 2). Opposite titin molecules overlap in the Z-disc as well as in the M-band forming a continuous filament system along the myofibril (Figure 2; Gregorio et al., 1998; Obermann et al., 1997).

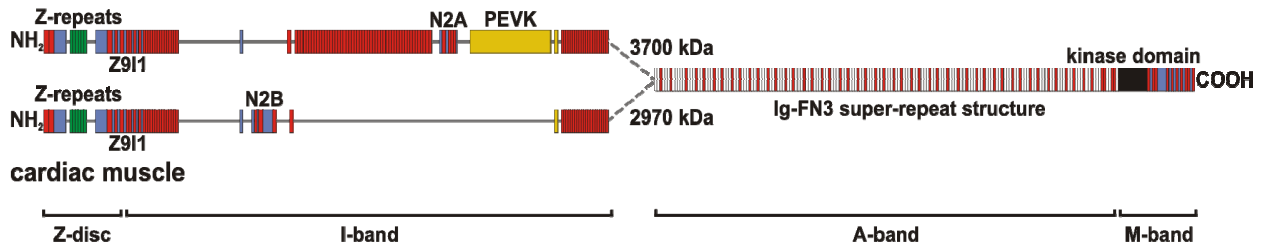
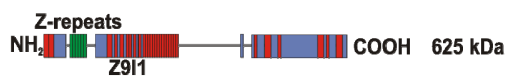
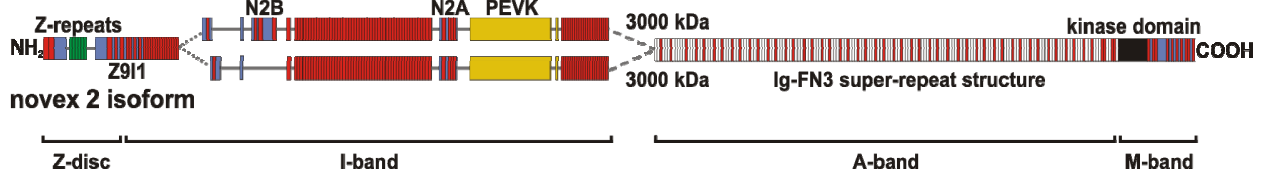
~90% of titin's protein mass comprises of immunoglobulin (Ig) and fibronectin-type III (FN3) domains and ~10% are 17 unique domains (Figure 4; Labeit et al., 1990; Labeit and Kolmerer, 1995). ~80 kDa of titin's N-terminus is integrated into the Z-disc of the sarcomere (Gregorio et al., 1998). This Z-disc region of titin contains nine Ig domains (Z1-Z9) separated by unique sequences and up to seven Z-repeats (Labeit and Kolmerer, 1995; Gautel et al., 1996). The I-band region of titin is 800 to 1500 kDa long depending on the isoform. It consists of tandem arranged Ig domains and a PEVK region that is rich in prolin (P), glutamate (E), valin (V), and lysine (K). Furthermore, the I-band region of titin contains the N2A region and the cardiac N2B region (Labeit and Kolmerer, 1995). The Ig domain regions, the PEVK, and the N2B region are responsible for titin's elastic properties. During muscle stretch, first the Ig domain regions are extended at lower forces by straightening their inter-domain linkers followed by extension of the PEVK region as well as the N2B region that extends at higher forces (Trombitas et al., 1998; Helmes et al., 1999; Kellermayer et al., 1997). Since titin forms an elastic connection between the Z-disc and the M-band, it is responsible for the elasticity of the sarcomere and muscle passive tension by acting as a molecular spring (Linke et al., 1996, 1999; Granzier et al., 1997; Trombitas et al., 1999; Watanabe et al., 2002). The A-band of titin accounts for a mass of ~2000 kDa. It has a regular Ig-FN3 super-repeat structure that causes stiffness (Labeit et al.,

1992; Labeit and Kolmerer, 1995). The ~200 kDa C-terminus of titin is located within the M-band of the sarcomere and designated as titin's M-band region (Labeit and Kolmerer, 1995). It contains a kinase domain and 10 repetitive Ig domains (M1-M10), which are separated by intervening sequence (is) stretches of varying length (is1-is7; Gautel et al., 1993).

### 3.2.2 Titin isoforms

The gene locus of titin was mapped for human and mouse to chromosome 2 (Muller-Seitz et al., 1993; Pelin et al., 1997). The human titin gene consists of 363 exons predicted to code for a polypeptide with a maximum molecular weight of 4200 kDa (Bang et al., 2001a).

Titin's A- and M-band domains are constitutively expressed except for M-band exon 5, which is alternatively spliced (Kolmerer et al., 1996). In contrast, titin's elastic elements of the I-band segment are alternatively spliced to determine the elasticity of sarcomeres thereby modulating passive muscle stiffness (Cazorla et al., 2000; Freiburg et al., 2000). The three major titin isoforms N2A, N2B, and N2BA (Figure 4) are differently expressed during muscle development and in different muscles (Labeit and Kolmerer, 1995; Warren et al., 2004; Ottenheijm et al., 2009b). N2A isoforms are the longest titin molecules with a molecular weight up to 3700 kDa. One N2A isoform, such as in the soleus, or two N2A isoforms, such as in quadriceps, can exist in a skeletal muscle type (Ottenheijm et al., 2009b). They contain a large PEVK region and depending on the muscle type up to 90 tandem Ig domains to increase muscle elasticity (Labeit and Kolmerer, 1995; Freiburg et al., 2000). Compared to the N2A isoform, the two cardiac titin N2B and N2BA isoforms are less elastic and shorter with 2970 kDa and 3300 kDa, respectively. The main titin isoform in the heart is with ~70% N2B (Neagoe et al., 2002). It contains 37 tandem Ig domains and a short PEVK region, which makes the heart the stiffest striated muscle. The N2B and the N2BA isoforms contain the heart specific N2B domain. The N2BA isoform, which is predominantly expressed during embryogenesis, contains structural elements of both the N2B and the N2A isoform varying in the length of the tandem Ig domains and the PEVK region. Since the N2BA isoform is more elastic than the N2B isoform, the elasticity of the sarcomeres in the heart can be determined by variation of the N2B:N2BA isoform ratio (Labeit and Kolmerer, 1995; Cazorla et al., 2000; Freiburg et al., 2000; Bang et al., 2001a).

**A)****skeletal muscle****B)****novex 3 isoform****novex 1 isoform**

**Figure 4: Titin isoforms and their domain composition.** Titin isoforms spanning over the Z-disc, I-band, A-band, and M-band of the sarcomere contain Ig domains (red), FN3 domains (white), Z-repeats (green), the PEVK region (yellow), unique sequences (blue), and the kinase domain (black). The Ig domains Z9 and I1 of titin's Z-disc to I-band junction are indicated. A) Splicing of the I-band leads to the N2A isoform with the N2A region in skeletal muscle and to the shorter N2B isoform with the N2B region in the heart, in which additional the N2BA isoform is expressed (not shown). B) The novex isoforms 1, 2, and 3 are also obtained by splicing of the I-band in heart and skeletal muscle, whereas novex 3 contains an alternative titin C-terminus. Adapted from Bang et al., 2001a.

In heart and skeletal muscle additional isoforms are produced by alternative splicing of the Z-disc and I-band region of titin. Splicing of titin's central Z-disc region determines the Z-repeat number (Gautel et al., 1996). Since this Z-repeat is responsible for the titin- $\alpha$ -actinin cross bridges, the mechanical properties of the Z-disc are influenced by variation of titin's Z-repeat number (Sorimachi et al., 1997). Titin's Z-disc region is not only expressed differentially in skeletal and cardiac muscle, but also during embryonic development (Sorimachi et al., 1997). Titin's I-band region is also spliced resulting in the novex isoforms 1, 2, and 3 (Figure 4). The short novex 3 isoform (700 kDa), which contains an alternative titin C-terminus, mediates the insertion of the long titin isoforms into the sarcomere. The function of the novex isoforms 1 and 2 that contain unique exons located N-terminal to the N2B region is still unknown (Bang et al., 2001a).

### 3.2.3 Titin binding partners

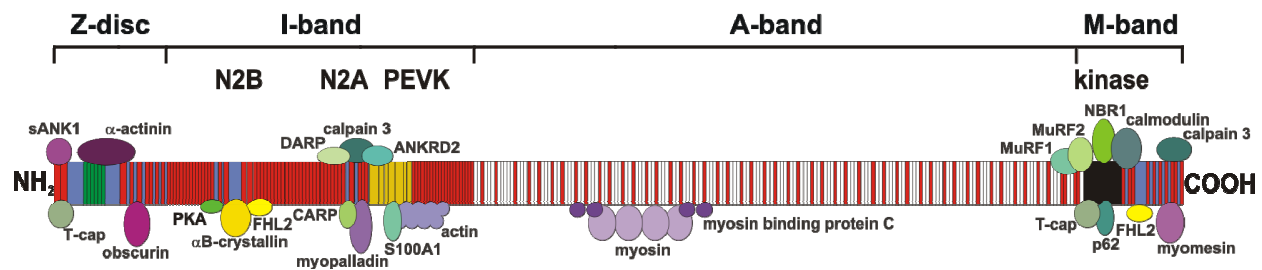


**Figure 5: Titin's binding partners.** Proteins that bind to titin's Z-disc ( $\alpha$ -actinin, obscurin, sANK1, T-cap), I-band (N2B region:  $\alpha$ B-crystallin, FHL2, PKA; N2A region: ANKRD2, CARP, calpain 3, DARP, myopalladin; PEVK region: actin, S100A1), A-band (myosin, myosin binding protein C), and M-band region (calmodulin, calpain 3, FHL2, MuRF1, MuRF2, myomesin, NBR1, p62, T-cap) are depicted (structural proteins: purple; adapter proteins: yellow; signaling proteins green). For the titin molecule the Ig domains (red), FN3 domains (white), Z-repeats (green), the PEVK region (yellow), unique sequences (blue), and the kinase domain (black) are shown. Modified from Bang et al., 2001a.

#### 3.2.3.1 Z-disc region proteins

Titin's N-terminus, which is integrated into the Z-disc of the sarcomere, forms cross bridges with  $\alpha$ -actinin that links titin to the thin filament system (Ohtsuka et al., 1997a, b; Gregorio et al., 1998). The protein sANK1 (small ankyrin 1) as well as T-cap (Titin-cap, telethonin, Figure 2) interact with titin's Ig domains Z1 and Z2 (Kontrogianni-Konstantopoulos and Bloch, 2003; Gregorio et al., 1998; Mues et al., 1998). The binding of sANK to titin suggests a role in organizing the sarcoplasmic reticulum at the Z-disc of the sarcomere. T-cap together with its binding partner MLP (muscle LIM protein) has been proposed to play a role as stretch sensor (Knoll et al., 2002), in muscle growth (Nicholas et al., 2002), and in differentiation of myocytes (Kong et al., 1997). Another binding partner of titin's Z-disc region is obscurin that interacts with titin's Ig domains Z8 and Z9 (Bang et al., 2001a; Young et al., 2001). Obscurin plays a role in signal transduction and co-assembles with titin during myofibrillogenesis (Sanger and Sanger, 2001; Young et al., 2001).

#### 3.2.3.2 I-band region proteins

Within titin's I-band region, the PEVK, N2A, and N2B region contain multiple protein binding sites. FHL2 (four and a half LIM domain protein), which mediates protein-protein interactions, binds to titin's heart specific N2B region. FHL2 targets the metabolic enzymes phosphofructokinase, creatine kinase, and adenylate kinase to titin to ensure energy supply at the

site of high energy consumption (Lange et al., 2002). In addition to FHL, the small heat shock protein  $\alpha$ B-crystallin interacts with the N2B region (Bullard et al., 2004). In response to adrenergic stimulation, the N2B region can also be phosphorylated by the PKA (protein kinase A) leading to the decrease of passive tension (Yamasaki et al., 2002). The N2A region provides a binding site for the protease calpain 3 (Sorimachi et al., 1995), which is involved in myofibrillogenesis, sarcomere assembly, and the proteolysis of different muscle proteins such as titin, talin, and ezrin (Taveau et al., 2003; Kramerova et al., 2004). CARP (cardiac ankyrin repeat protein), DARP (diabetes ankyrin repeat protein), and ANKRD2 (ankyrin repeat domain protein) that are members of the MARP (muscle ankyrin repeat protein) protein family also bind to titin's N2A region (Bang et al., 2001b). They are involved in the modulation of gene expression during development (Jeyaseelan et al., 1997; Baumeister et al., 1997; Bang et al., 2001b). Another binding partner of titin's N2A region is the protein myopalladin that influences sarcomere integrity (Bang et al., 2001b). The PEVK region interacts with actin and the calcium-binding protein S100A1 (S 100 calcium binding protein A 1). It has been speculated that this titin-actin interaction contributes to muscle passive tension, which can be modulated by S100A1 (Yamasaki et al., 2001).

### **3.2.3.3 A-band region proteins**

The FN3 and Ig domains that form the super-repeat structure within titin's A-band region interact with myosin and the myosin binding protein C (Figure 2), which also binds to myosin (Okagaki et al., 1993), so that titin is linked to the thick filament (Wang et al., 1992; Houmeida et al., 1995; Freiburg and Gautel, 1996). These interactions specify amount and location of myosin and myosin binding protein C molecules that are incorporated into the thick filament system. This it is believed to control the assembly and exact length of myosin filaments and to act as a molecular scaffold maintaining the integrity of the sarcomere.

### **3.2.3.4 M-band region proteins**

Titin's C-terminal M-band region that is integrated into the M-band of the sarcomere provides at its Ig domain M4 a binding site for the protein myomesin that forms antiparallel dimers (Obermann et al., 1996). The additional interaction of myomesin with myosin and the direct interaction of myosin with titin connect the titin molecules tightly to the thick filament to compensate force imbalance in the sarcomere (Bähler et al., 1985; Nave et al., 1989; Obermann et al., 1996). Furthermore titin's M-band region binds MuRF1 (muscle-specific RING finger

protein 1) as well as calpain 3 (Kinbara et al., 1997) and FHL2 (Lange et al., 2002), which both also interact with titin's I-band region (Gregorio et al., 1999). MuRF1 binds with its central region to titin's Ig domains A168 and A169 N-terminal to titin's kinase region (Centner et al., 2001). It has been shown that the interaction of MuRF1 with titin maintains the stability of the filament's structure (McElhinny et al., 2002). The binding sites for MuRF1 and calpain 3 from opposing titin molecules are in close proximity. The functional relevance is unknown, but both proteins have been implicated in ubiquitination and degradation processes (Bodine et al., 2001). Cleavage of muscle proteins by the protease calpain 3 leads to ubiquitination and degradation via the 26S proteasome (Hasselgren and Fischer, 2001). The ubiquitin ligase MuRF1 binds to various muscle proteins including myosin light chain, T-cap, and nebulin suggesting a function in controlling proteasome-dependent degradation (Witt et al., 2005). MuRF1 forms heterodimers with the homologous proteins MuRF2 and MuRF3 (Centner et al., 2001; Gregorio et al., 2006), which are involved in the stabilization of microtubules (Spencer et al., 2000; Pizon et al., 2002). MuRF2 also interacts with titin's domains A168-170 and other muscle proteins such as T-cap and nebulin (Witt et al., 2005). MuRF1 interacts with enzymes that are involved in ATP-production and with proteins that have nuclear function implicating a role in signal transduction (Witt et al., 2005). Recent work shows that MuRF1 associates with SRF (serum response factor) and interacts with RACK1 (receptor for activated C kinase 1) to regulate PKC (proteinase kinase C) activity (Arya et al., 2004; Willis et al., 2007).

### 3.2.4 Titin's kinase

Titin's M-band region is encoded by six exons termed M-band exon 1-6, of which the M-band exon 1 encodes a kinase domain (Labeit et al., 1992; Obermann et al., 1996). It is a serine/threonine kinase that is highly conserved in vertebrates and invertebrates suggesting an important function in signal transduction (Gautel et al., 1995). The kinase shows homology to the myosin light chain kinase (MLCK) family and the invertebrate muscle proteins twitchin and stretchin-MLCK (Heierhorst et al., 1994; Gautel et al., 1995). It consists of a catalytic domain and a regulatory tail that blocks the ATP binding site. The activation of the kinase has been proposed to base on a dual mechanism at the regulatory tail, in which the inhibiting tyrosine residue Y170 is phosphorylated and  $\text{Ca}^{2+}$ /calmodulin binds (Mayans et al., 1998). In contrast to other kinases, which turn upon activation from a closed into an open conformation, titin's kinase already has the open conformation in the auto-inhibited form.

The proteins T-cap, NBR1 (neighbor of Brca gene 1), and p62 (sequestosome 1) are suggested substrates of titin's kinase (Mayans et al., 1998; Lange et al., 2005). It has been shown that titin's kinase phosphorylates T-cap in differentiating cardiomyocytes indicating a role in myofibrillogenesis (Mayans et al., 1998). Controversial, investigations *in vivo* have found that T-cap expression starts after myofibrillogenesis at embryonic day 15.5 and that the loss of titin's kinase region does not affect sarcomere assembly until embryonic day 10.5 (Weinert et al., 2006). Titin's kinase has been implicated in responding to mechanical stress by force-induced conformational changes (Grater et al., 2005). It has been shown that activation of the kinase by stretch leads to a conformation that allows the interaction with NBR1, which targets the ubiquitin-associated p62 to sarcomeres. The protein p62 interacts with MuRF2, which translocates in response to mechanical inactivity to the nucleus, where it inhibits the transcription activity of the SRF and reduces the amount of the SRF (Lange et al., 2005). A point mutation in the human titin kinase domain causing myopathy was linked to this pathway (Lange et al., 2005). Hence titin's kinase has been implicated in the regulation of gene expression and protein turnover. In contrast, results obtained with MuRF2-deficient mice suggest that titin-MuRF2 signaling is dispensable for normal cardiac response to stress so that a molecular mechanism by which titin's kinase is involved in stress-sensing remains unclear (Willis et al., 2007).

### 3.3 Smooth muscle titin

The first evidence for the existence of smooth muscle titin arose from the isolation of a protein from chicken gizzard smooth muscle with an amino acid sequence similar to titin (Maruyama et al., 1977). This protein has remained uncharacterized. Keller and colleagues have identified and characterized a titin-like ~2000 kDa protein referred to as smitin (smooth muscle titin-like protein) from chicken gizzard smooth muscle. They showed its localization within the smooth muscle contractile apparatus as well as *in vitro* interactions with smooth muscle myosin (Keller et al., 2000; Kim and Keller, 2002) and smooth muscle  $\alpha$ -actinin (Chi et al., 2005). Therefore it is possible that smitin links dense bodies to thick filaments in avian smooth muscle. However, smitin failed to cross-react with a tested titin antibody (Kim and Keller, 2002). Mahler and colleagues have discovered in chicken the protein zeugmatin localizing at Z-discs of cardiac muscle as well as dense bodies and attachment plaques of gizzard smooth muscle (Maher et al., 1985). Later studies suggested that zeugmatin is the N-terminal region of titin (Turnacioglu et al., 1996, 1997).



The first investigation of titin in mammals revealed the expression of titin's Z-disc region in rabbit uterus using reverse transcription-PCR (RT-PCR; Sorimachi et al., 1997). Later it was shown that human uterus, bladder, and carotid artery RNA contains titin transcripts encoding the N-terminus including  $\alpha$ -actinin binding domains. Accordingly the binding of vertebrate smooth muscle titin to smooth muscle  $\alpha$ -actinin *in vitro* has been demonstrated (Chi et al., 2008). Furthermore, transcripts of titin's exons 1 to 7 were amplified from the human smooth muscle tissues aorta, stomach, carotids, and uterus by RT-PCR (Labeit et al., 2006). The expression of titin isoforms in smooth muscle has been confirmed by a titin exon array, in which human aorta, bladder, carotid, and stomach were investigated (Labeit et al., 2006). Alternatively spliced titin isoforms were identified, which contain 80 to about 100 exons at a transcriptional level of ~100-fold less abundant than in skeletal muscle. These exons encode parts of titin's Z-disc, I-band, and A-band regions. Consistent with the exon array data, a ~1000 kDa titin was detected by titin Z-disc, I-band, and A-band antibodies in porcine aorta and stomach. Smooth muscle titin was located in the cytoplasm of cultured human aortic smooth muscle cells and in the tunica media of bovine aorta. As in avian smooth muscle, it has also been shown *in vitro* that vertebrate smooth muscle titin contains binding sites for  $\alpha$ -actinin and filamins at its N-terminus and binding sites for myosin at its C-terminus. Thus it has been suggested that smooth muscle titin links thick filaments with dense bodies to provide passive elasticity and structural integrity to smooth muscle.

### **3.4 Embryo spacing and implantation**

#### **3.4.1 The female reproductive system**

The female reproductive system consists of vagina, uterus, oviduct, and ovaries. In the uterus (corpus uteri) embryos implant and develop during pregnancy. It is a hollow organ located in the pelvic cavity of female mammals. In higher primates the uterus is fused to a single organ, the simplex form. In rodents such as mice the uterus consists of two separate uteri horns that are dorsally combined, the duplex form (Figure 6). The uterus extends down into the cervix uteri that leads into the vagina. On the top of the uterus two tubular oviducts, which are called Fallopian tubes in woman, are connected. They link the uterus to the periovarian space and the ovaries. In the duplex form, each uterine horn is associated with one oviduct.

The wall of the uterus is made up of the three layers endometrium (tunica mucosa), myometrium (tunica muscularis), and perimetrium (tunica serosa). The endometrium lines the lumen of the

uterus and consists of the lamina epithelialis mucosae and the lamina propria mucosae (stroma endometrialis), which both undergo morphologic and functional changes in response to ovarian hormones during the menstrual cycle in great apes and humans or estrous cycle in most other mammals. The part of the endometrium that experiences changes (pars functionalis) is reconstituted by the basal part (pars basalis; Hoffmeister and Schulz, 1961). The lamina epithelialis mucosae is a single-layered prismatic epithelium with secretory and ciliated cells and an underlying basal lamina. The lamina propria mucosae comprises of connective tissue that encloses tubular glands (glandulae uterinae) and blood vessels. Next to the endometrium is the myometrium that consists of an internal circular and an external longitudinal smooth muscle layer, which are separated by highly vascularized connective tissue (stratum vasculosum). The uterus is covered by a serous membrane, the perimetrium.

### 3.4.2 Embryo implantation

Mammalian embryo implantation ensures the firm connection of the embryo in the maternal uterine tissue and involves the synchronizing of embryonic development until blastocyst state with the uterine differentiation into the receptive state.

During ovulation unfertilized eggs (Figure 6 red) are released from the ovary into the infundibulum of the oviduct. If mating occurs, the oocytes are fertilized leading to zygotes (Figure 6 green). In mice, this time point is called embryonic day 0.5 (E0.5). The zygotes undergo mitotic cell divisions leading to the formation of a morula until embryonic day 3.0 (E3.0). Thereby, the embryos travel along the oviduct by cilia transport that is amended by smooth muscle contraction (Halbert et al., 1976, 1989; Vizza et al., 1995; Perez Martinez et al., 2000). At embryonic day 3.5 (E3.5), embryos in the late morula stage consisting of totipotent cells enter the uterine lumen and transform by lineage differentiation to an early blastocyst. They are composed of a fluid filled cavity (blastocoel) as well as the trophectoderm and the inner cell mass (ICM), which is pluripotent and generates the cell lineages of the embryo. Before implantation, the blastocysts distribute equally among both uterine horns with evenly spacing so that the implantation sites are equidistant independent of the blastocyst number. It has been shown that this process of spacing involves smooth muscle contraction. Myometrial contractions are higher during the preimplantation period and relaxin, an inhibitor of myometrial activity, disrupts the blastocyst distribution in rats (Pusey et al., 1980; Rogers et al., 1983; Crane and Martin, 1991). Recent findings indicate that lysophosphatic acid (LPA) signaling mediated by its receptor LPA3 regulates embryo spacing by effecting uterine contraction (Hama et al., 2007).

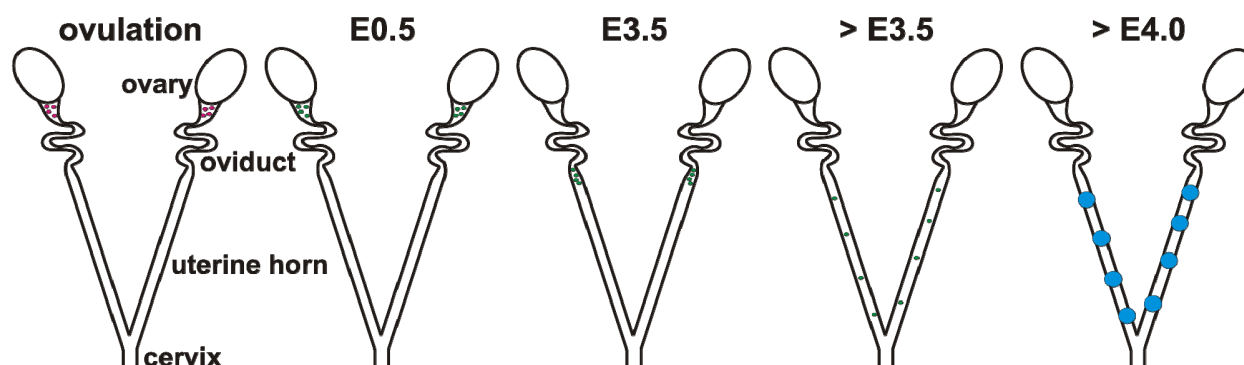


**Figure 6: The murine reproductive system and preimplantational embryonic development.** During ovulation unfertilized eggs (red) are released into the oviduct, which are fertilized at embryonic day 0.5 (E0.5). Afterwards the zygotes (green) develop thereby traveling along the oviduct to enter the uterine horns at embryonic day 3.5 (E3.5) as blastocysts. Before implantation at embryonic day 4.0 (E4.0), the blastocysts are evenly distributed along both uterine horns with evenly spacing (> E3.5). After embryonic day 4.0 (> E4.0), it is possible to make implantation sites visible with the help of the dye Evans Blue (blue).

After hatching of the blastocysts from their outer shell (zona pellucida) and differentiation of the ICM into the epiblast and primitive endoderm, implantation initiates. It is classified into apposition, attachment, and penetration. During apposition at embryonic day 4.0 (E4.0), a fluid accumulation in the intercellular tissue spaces of the uterus (edema) leads to uterine luminal closure resulting in interaction of the embryonic trophectoderm with the luminal epithelium of the maternal uteri endometrium. This is followed by the attachment phase at embryonic day 4.25 (E4.25), in which the trophectoderm associates tightly with the luminal epithelium. Apposition and attachment depend on the synchronized differentiation and proliferation of the uterus to the receptive state that occurs under the direction of the ovarian steroid hormones progesterone and estrogen acting through their nuclear receptors (Carson et al., 2000; Dey et al., 2004). It has been shown that the signaling pathway initiated by HB-EGF (heparin binding epidermal-like growth factor) is crucial for blastocyst-uterine crosstalk (Paria et al., 1993; Raab et al., 1996). Growth factors, adhesion molecules such as integrins, cytokines such as LIF (leukemia inhibitory factor), and vasoactive mediators are also involved (Carson et al., 2000; Stewart et al., 1992; Fouladi-Nashta et al., 2005). The attachment reaction involves a localized increase in stromal vascular permeability of the uterus (Psychoyos, 1986), which is possible to visualize with the help of the dye Evans Blue (Figure 6 blue). This vascular permeability is extended during the penetration phase, when the embryo invades through the luminal epithelium and basal lamina into the stroma. Thereby the superficial endometrial vessels are also penetrated by the embryo to establish a vascular relationship (Schlafke and Enders, 1975) that requires uterine angiogenesis as well (3.5.2). The stromal cells differentiate into decidual cells (decidualization) leading to the loss of the luminal epithelium at the site of the implanting blastocyst (Parr and Parr, 1989). The

deciduum provides nutritional support to the developing embryo before a functional placenta is established.

### 3.5 Angiogenesis

During angiogenesis, new blood vessels develop from pre-existing vessels to ensure sufficient blood transport, for example during pregnancy, wound healing, and inflammation. The newly formed microvasculature consists of endothelial cells forming the inner vessel lining that is covered by pericytes or vascular smooth muscle cells.

#### 3.5.1 Sprouting angiogenesis

Angiogenesis by endothelial sprouting initiates with an increase in vascular permeability in response to VEGF (vascular endothelial growth factor), a key regulator for vasculogenesis and angiogenesis (Carmeliet et al., 1996; Fong et al., 1995). This allows leakage of plasma proteins that provide a scaffold for migrating endothelial cells. Before endothelial cells migrate, their interendothelial as well as the periendothelial cell contact are modulated to destabilize the vessel. It has been shown that angiopoietin 2 is involved in detaching smooth muscle cells and loosening the extracellular matrix (Maisonpierre et al., 1997; Gale and Yancopoulos, 1999). Some endothelial cells within the capillary vessel are the tip cells that lead the growing sprout. Notch receptors and their ligand DLL4 (delta-like-4) are essential for discriminating between tip and the neighboring cells, which involves also VEGF (Sainson et al., 2005; Hellström et al., 2007; Lobov et al., 2007; Suchting et al., 2007). The migration and proliferation of endothelial tip cells is promoted by a spatial VEGF concentration gradient (Ruhrberg et al., 2002; Gerhardt et al., 2003). The effects of VEGF are complemented by angiopoietin 1. This angiogenic factor promotes remodeling including vessel maturation, stabilization, and leakiness by interaction with the receptor Tie2 (tyrosine kinase with immunoglobulin-like and EGF-like domains 2; Suri et al., 1996; Thurston et al., 1999; Sato et al., 1995; Wakui et al., 2006).

To form functional blood-carrying vessels, the endothelial sprouts need to suppress the motile behavior and form endothelial-endothelial junctions with tip cells of other sprouts or with existing capillaries. The generation of the vascular lumen stabilizes the new vessel by improved oxygen delivery that lowers the *Vegf* expression. Vascular maturation requires also pericytes and vascular smooth muscle cells. These mural cells are derived from neural crest cells, undifferentiated mesenchymal cells, or vascular stem cells and have common molecular markers

such as  $\alpha$ -smooth muscle actin, desmin, and the neuro-glial proteoglycan 2 (Armulik et al., 2005; Bergers and Song, 2005). The endothelial sprout generates a concentration gradient of PDGF-B (platelet derived growth factor B) that promotes the recruitment of mural cells (Lindahl et al., 1997; Hellström et al., 1999). The tyrosine kinase receptor PDGF $\beta$  (PDGFR $\beta$ ) that is expressed in mesenchymal precursor cells, pericytes, and vascular smooth muscle cells mediates the PDGF-B guided migration and is also required for mural cell proliferation and integration into the vessel wall. PDGFR $\beta$  action involves cooperation with a family of G-protein coupled sphingolipid receptors that bind the sphingolipid sphingosine-1-phosphate (S1P), which is secreted by endothelial cells (Liu et al., 2000; Allende and Proia, 2002; Spiegel and Milstien, 2003). Mural cells that cover the endothelium of growing vessels inhibit endothelial cell proliferation as well as migration and stimulate the formation of extracellular matrix proteins thereby leading to vascular maturation (Gerhardt et al., 2003; Jain, 2003; Cleaver and Melton, 2003). Pericytes that are embedded in a basal lamina establish direct contact with endothelial cells and cover immature blood vessels and capillaries. In contrast, vascular smooth muscle cells are separated from the endothelium by a basement membrane layer consisting of fibers such as collagen and cover mature and larger diameter vessels.

### 3.5.2 Uterine angiogenesis during embryo implantation

Angiogenesis takes place in the ovary and uterus of adult mammals during the reproductive cycle and pregnancy (Gordon et al., 1995; Torry and Torry, 1997; Abulafia and Sherer, 1999). In the preimplantation period, increased uterine permeability as well as angiogenesis occurs at the site of blastocyst apposition to provide sufficient vascularized uterine tissue for successful implantation (Plaks et al., 2006). A number of studies show that VEGF and its receptors VEGFR1, VEGFR2, and NRP1 (neuropilin 1) are differentially expressed in mouse uterus in a spatiotemporal manner before and during the attachment phase (Hyder and Stancel, 1999; Halder et al., 2000; Chakraborty et al., 1995). Furthermore, it has been shown in uterine samples of women with recurrent miscarriage that the expression of the receptors for VEGF and angiopoietins was reduced (Vuorela et al., 2000; Vuorela and Halmesmäki, 2006). Inhibition of angiogenesis before or after implantation by an antiangiogenic compound results in resorption of all embryos in mice (Klauber et al., 1997) suggesting that the formation of new blood vessels from pre-existing vessels is important for implantation and development of the placenta.

During the preimplantation period, *Vegf* expression and uterine vascular permeability, which is required for angiogenesis, occurs in mouse in response to the ovarian steroid hormones estrogen

and progesterone (Chakraborty et al., 1995; Hyder et al., 2000; Ma et al., 2001). Furthermore, it has been shown that VEGF is mainly responsible for the estrogen-induced increase in vascular permeability, which is essential for successful embryo implantation (Rockwell et al., 2002). Results obtained from mice carrying a null mutation for *Cox2*, the gene encoding the rate-limiting enzyme in prostaglandin biosynthesis cyclooxygenase 2 (COX2), indicate that prostaglandins influence uterine vascular permeability and angiogenesis during implantation and decidualization via VEGF and angiopoietin signaling (Matsumoto et al., 2002). It was shown that HB-EGF produced by embryo and uterus induces *Cox2* expression in the luminal epithelium and underlying stromal cells at the site of blastocyst attachment (Lim et al., 1997).

### 3.6 Knockout and knockin technology

Knockout and knockin mice are genetically engineered so that a gene is turned off or modified by an insertion, respectively. The technology is based on the usage of pluripotent embryonic stem (ES) cells as first described by Evans and Kaufmann (Evans and Kaufman, 1981). Differentiation of the ES cells in cell culture is inhibited to allow contribution to germline cells of chimeras. Therefore, ES cells are grown on mitotic inactivated primary embryonic fibroblasts (feeder cells) and the protein LIF is added to the culture medium (Smith et al., 1988).

To modify the gene of interest by homologous recombination, a recombinant targeting vector is cloned *in vitro*, which contains a long and a short arm as well as a middle part. The long and the short arm consist of DNA sequences that are homologous to the gene of interest. The middle part contains a neomycin resistance cassette flanked by two FRT-sites (flippase recognition target-sites) and the modified gene. The targeting vector enters ES cells by electroporation, in which a short current pulse opens the cell membrane (Piedrahita et al., 1992; Austin et al., 2004), and integrates in a few cells stably in the genome. The integration occurs either randomly or into the gene locus of interest by homologous recombination due to homologous sequences of the targeting vector (Doetschman et al., 1987; Thomas and Capecchi, 1987). The antibiotic G418 that inhibits protein translation is added to the cell medium to select the ES cells, which integrated the targeting vector stably into the genome. Only these cells contain the neomycin resistance cassette encoding the bacteria gene for the neomycin phosphotransferase under the control of a ubiquitous promoter. This enzyme degrades the antibiotic so that the ES cells can grow in the presence of G418. Antibiotic-resistant cells are isolated and investigated by PCR or Southern Blot for homologous recombination of the targeting vector into the genome (Piedrahita et al., 1992; Austin et al., 2004). Homologously recombined ES cells are injected into

blastocysts that are obtained from superovulated female mice. The injected blastocysts are transferred into the uteri of pseudopregnant mice, in which they implant so that embryos can develop. Offspring of the recipient mice are called chimeras because they are arisen from cell populations of both blastocyst and recombined ES cells. In contrast to ES cells, which have been generated from a mouse strain with a brown (agouti) coat color (129), the blastocysts have been obtained from a mouse strain with a black coat color (C57BL/6) so that chimeric animals show a black and brown coat color mixture (Bradley et al., 1984). Chimeras are bred with the mouse strain C57BL/6. This breeding results in brown offspring if germline cells of the chimeras have been developed from the heterozygously recombined ES cells. Half of these animals should be heterozygous for the modified gene.

Since the neomycin resistance cassette has the potential to affect the phenotype of genetically engineered animals (Kaul et al., 2000), heterozygous animals carrying the targeting vector are mated to transgenic mice that express the FLP-recombinase in their germline (Rodriguez et al., 2000). This enzyme catalyzes the recombination between two FRT-sites thereby cutting out any DNA stretch between. Offspring from this mating, in which the neomycin cassette has been removed by FLP-mediated excision, is used to generate a colony of homozygous mice that only contain the modified gene and one residual FRT-site.

### 3.7 Aim of the study

Human infertility is a global problem. ~12% of women have difficulties in getting pregnant or carrying a baby to term (NSFG, 2002). Today conception can be improved by *in vitro* fertilization and embryo transfer techniques. Nevertheless, implantation failure and pregnancy loss are not only common problems after assisted reproduction, but also after natural conception. Furthermore, fetal as well as maternal health is endangered by ectopic pregnancies as well as placenta previa, which are associated with mislocalization of the embryo. The mechanisms of smooth muscle contraction that contribute to the localization of the embryo within the uterus are not well understood. Cellular events of implantation have been described, but only little is known about the molecular pathways. A hallmark of implantation is uterine vascular development and remodeling at the fetal-maternal interface triggered by angiogenic factors. The importance of vessel formation has been demonstrated because disruption of angiogenesis at the site of implantation is associated with poor reproduction in humans (Meegdes et al., 1988; Vuorela et al., 2000). It is necessary to define the mechanism by which defects in angiogenesis

contribute to human implantation failure and early miscarriage. This will help to improve fetal health and female fertility.

Smooth muscle cells are involved in angiogenesis and responsible for uterine contraction. In contrast to striated muscle, in which sarcomeres have been well characterized, structure and signaling of the smooth muscle contractile unit need to be investigated in more detail. The actin-myosin based structural and functional analogy between the smooth and striated muscle contractile apparatus suggests that smooth muscle also contains a titin-like protein involved in structure, biomechanics, and signal transduction. Although smooth muscle titin has been described on transcript and protein level, it is not included in the current models of smooth muscle structure and a function has not been assigned. Aim of our research was the morphological and functional characterization of titin in smooth muscle. A knockin mouse model should be established to visualize and thereby localize titin *in situ* and *in vivo* using the red fluorescence protein DsRed. To address a role for smooth muscle titin, we used a loss of function approach of titin's kinase region. We hypothesized that titin's kinase region in smooth muscle has essential functions regarding muscle contractility and signaling as it has been shown for embryonic as well as mature striated muscle (Gotthardt et al., 2003; Weinert et al., 2006; Peng et al., 2006, 2007). Furthermore, it is possible that titin's kinase in smooth muscle converts mechanical input to biochemical signals by interacting with signal transduction proteins in a strain-dependent manner similar to its proposed function in striated muscle (Tskhovrebova and Trinick, 2003; Granzier and Labeit, 2004; Lange et al., 2005). The clinical relevance of titin's M-band region has been demonstrated by a point mutation in the human titin kinase domain that causes myopathy (Lange et al., 2005). For our study, the conditional knockout model of titin's M-band exons 1 and 2 (Gotthardt et al., 2003), which encode titin's kinase region, was available to generate a smooth muscle knockout mouse strain. We used this mouse model to assess, whether the deletion of titin's kinase region affects embryo spacing and implantation as well as angiogenesis. Furthermore, insights into signaling pathways involving titin's kinase region during early pregnancy should be gained with the help of Real-Time PCR, 2D-gel analysis, and immunoassays.



## 4 Materials and Methods

### 4.1 Materials

#### 4.1.1 Chemicals

If not stated otherwise, all chemicals were purchased from Sigma-Aldrich, Roth, Invitrogen, and GE Healthcare.

#### 4.1.2 Enzymes

Table 1: Enzymes.

Name	Manufacturer
Calf intestinal alkaline phosphatase (CIP)	Roche
Collagenase type I	Sigma-Aldrich
Collagenase type II	Invitrogen
Dispace II	Sigma-Aldrich
Elastase type IV	Sigma-Aldrich
Expand Long Template PCR System	Roche
Phusion High-Fidelity DNA Polymerase	New England BioLabs
Proteinase K	Roche
Restriction endonucleases	New England BioLabs and MBI Fermentas
RNase A from bovine pancreas (type III-A)	Sigma-Aldrich
<i>Taq</i> DNA polymerase	Invitrogen

#### 4.1.3 Bacterial strain

For transformation of plasmid DNA, the *Escherichia coli* (*E. coli*) strain DH5 $\alpha$  (Bethesda Research Laboratories, 1986) was used.

#### 4.1.4 Vectors and BAC clones

For cloning of the targeting vector, the plasmids and bacterial artificial chromosome (BAC) clones listed in Table 2 were used.

**Table 2: Plasmids and BAC clones used for generation of the targeting vector.**

Name	Manufacturer
BAC clone 96022	CITB Mouse BAC Library, Incyte Genomics
BAC clone RP23-436E5	BACPAC Resource Center
pDsRed-Monomer-C1	Clontech
pGemFRTloxNeo	Prof. Dr. med. Gotthardt

#### 4.1.5 Kits

**Table 3: Kits.**

Name	Manufacturer
12(S)-HETE EIA Kit	Assay Designs
Agilent RNA 6000 Nano Kit	Agilent
BigDye Terminator v3.1 Cycle Sequencing Kit	Applied Biosystems
DNA Ligation Kit Ver.1	TAKARA BIO INC.
EasyPure DNA Purification Kit	Biozym
FAST qPCR MasterMix Plus	Eurogentec
Growth Factor Mouse 4-Plex Panel	Invitrogen
MILLIPLEX Mouse Cytokine/Chemokine Panel-7-Plex	Millipore
NucleoBond BAC 100	Macherey-Nagel
peqGOLD Plasmid Miniprep Kit I	PEQLAB
pGEM-T Easy Vector System	Promega
Plasmid Maxi Kit	Qiagen
RNase-Free DNase Set	Qiagen
RNA UltraSense One-Step Quantitative RT-PCR System	Invitrogen
RNeasy Mini Kit	Qiagen
ThermoScript RT-PCR System for First-Strand Synthesis	Invitrogen

#### 4.1.6 Oligonucleotides

Primers for cloning, sequencing, and genotyping (Table 4) were designed using the online software Primer3. Oligonucleotides for cloning were synthesized by TIB MOLBIOL and oligonucleotides for sequencing and genotyping were synthesized by BioTeZ. Primer and probes

for Real-Time PCR analysis were purchased from Applied Biosystems as gene expression assays (*Alox15*, *Cacna1c*, *Calb1*, *Calm1*, *Camk2a*, *Cox2*, *Creb1*, *Fhl2*, *Lpar3*, *Mapk13*, *Myom1*, *Nbr1*, *p62*, *Pparg*, *Prkcd*, *Prkce*, *Sl00a1*, *T-cap*) or designed using the Software Primer Express 1.5 (Applied Biosystems) to be synthesized by BioTeZ or Eurogentec. The double labeled probes for Real-Time PCR analysis carried the fluorescence reporter dye 6-carboxyfluorescein (6-FAM) at the 5'-end and the quencher dye 6-carboxytetramethylrhodamine (TAMRA) at the 3'-end (Table 5). The sequences of the oligonucleotides that were custom made are provided in 5'→3' orientation in the following tables.

**Table 4: Primers for cloning, sequencing, and genotyping provided in 5'→3' orientation.**

Name	Sequence	Application
3'neoflox	TCGACTAGAGGATCAGCTTGGGCTG	genotyping
Cre800fw	GCTGCCACGACCAAGTGACAGCAATG	genotyping
Cre1200rev	GTAGTTATTCGGATCATCAGCTACAC	genotyping
lacZ1080fw	CCTCTGCATGGTCAGGTCATGGATG	genotyping
lacZ10620rev	GTGGGCGTATTCGCAAAGGATCAGC	genotyping
MG-FLP1	GTCACTGCAGTTTAAATACAAGACG	genotyping
MG-FLP2	GTTGCGCTAAAGAAGTATATGTGCC	genotyping
MG-Ti-FRTr2	AAGTTCGCTATACAAGTGGCTAAG	genotyping
MG-Ti-SL1fw	GTGTCTGGCACTGCTTCCTTGGAAAGTG	genotyping
MG-Ti-SL2rev	ACCGCTCCCATGCCTTCGAGAGTCTTG	genotyping
MR-GK2Prom5'r	AAAGCGCATGCTCCAGACTGCCTTG	sequencing
MR-neor	AGCCATGATGGATACTTTCTCG	sequencing
NB-DsRedmf	CTCCACCGAGAAGCTGTACC	sequencing
NB-DsRedmr	CTTGGAGCCGTAAGGAACT	sequencing
NB-fDsRedI	GGTACCCTCGAGATGGACAACACCGAGGACGTCA	cloning
NB-fDsRedII	CTCGAGATGGACAACACCGAGGACGTCA	genotyping
NB-fDsRedrecF	CAGCATCATGGTAAAGGCCATCAA	genotyping
NB-fLA	CTCGAGAGTTCCCCACACTTTGAAGAAAG	cloning
NB-fMA	TGTACAGTGAAGCTGAAAAGGGCTGAAAGG	cloning
NB-fSA	GGATCCATATTTAAATGTTTCTTTACCTATTATTCAAG	cloning
NB-GKFRTTr	GGGGGAACTTCCTGACTAG	sequencing
NB-LOXFRTf	CTGGGGCTCGACTAGAGGAT	sequencing
NB-rDsRedI	GGTACCCTGGGAGCCGGAGTGGCG	cloning
NB-rDsRedII	CTGGGAGCCGGAGTGGCG	genotyping
NB-DsRedGeno	ATAGAGACCTTGCTTTGCCTGTG	genotyping
NB-rDsRedrecF	CATTCAAATGTTGCCATGGTGTCC	genotyping

NB-rLA	CTCGAGCACTTCTTTGGTTTCGCTGGT	cloning
NB-rMA	AAGCTTGATAAGGGATAGTCTTGGGCATAC	cloning
NB-rSA	CCCGGGTCACTCTTTTCAGACACACCAGA	cloning
NB-rSAc	CCCGGGCTGCAAAAGAAGACACACAGAAAG	cloning
NB-ttnEx18f	GGGTATTTTGTGCCAAGCTC	sequencing
NB-ttnEx19r	TCCTCTGTGATGCTGGTGTC	sequencing
NB-ttnEx20f	CCACCGAAGAGAAACGGTAA	sequencing
NB-ttnEx21f	GAGCTTAGATGTGGGCCGTA	sequencing
NB-ttnEx22f	TTTGGAATCTGGGTTTGG	sequencing
NB-ttnEx23f	TCAATAAGCCTATAACACTGGAAC	sequencing
NB-ttnEx24r	ATTGCTCTTGGGATGTTTCG	sequencing
NB-ttnEx25f	TCATTCTAAAACATGCAGAAGCA	sequencing
NB-ttnEx26f	CCATGAGTCCCTGAACACAG	sequencing
NB-ttnEx27f	GGTAAAAACAAGAGTTTATTGAAATG	sequencing
NB-ttnEx27r	TGGTGGTAGCACTTTCTGCTT	sequencing
NB-ttnEx28f	TACCCAAGGATCAGGCATGT	sequencing
NB-ttnEx28mf	CAACTGCCTGATGGGAAAAA	sequencing
NB-ttnEx28mr	GCTGAGGGTAGCCTGTCAT	sequencing
NB-ttnEx30mr	TCCCATCAACAACAAAGCTG	sequencing
Sp6	GGATCCCTATACTTCAGAGTCTTCT	sequencing
T7	TAATACGACTCACTATAGG	sequencing

**Table 5: Primer/probes for Real-Time PCR analysis provided in 5'→3'orientation (fw: forward; rev: reverse; FAM: 6-carboxyfluorescein; TAMRA: 6-carboxytetramethylrhodamine).**

Name	Sequence
18S RNA fw	CGCCGCTAGAGGTGAAATTC
18S RNA rev	TGGGCAAATGCTTTCGCTC
18S RNA probe	6-FAM-TGGACCGGCGCAAGACGGAC-TAMRA
MEx1-2 fw	CCGATGGACTCAAGTACAGGATT
MEx1-2 rev	CCCATGCCTTCGAGAGTCTT
MEx1-2 probe	6-FAM-TCCTTGGAAGTGGAAGTTCCAGCTAAGATACAC-TAMRA
MEx6 fw	GCCTTGTGTGGTAGTTCTAAATTCAA
MEx6 rev	TTTGCTGTGGCTCATTGCTT
MEx6 probe	6-FAM-TTTCACCGGGAAGTGGGCAA-TAMRA
MuRF1 fw	CCGAGTGCAGACGATCATCTC
MuRF1 rev	CCTTCACCTGGTGGCTATTCTC
MuRF1 probe	6-FAM-AGCTGGAGGACTCGTGCAGAGTGACC-TAMRA

MuRF2 fw	TGGAGAACGTATCCAAGTTGGT
MuRF2 rev	CCTTTGATGCTTCCACGATCT
MuRF2 probe	6-FAM-CATGGATGAGCCCGAAATGGCA-TAMRA
N2A fw	AAAATGTGGATCCTAAAGAGTATGAGAAG
N2A rev	GAGGAGGCCCGGAAGT
N2A probe	6-FAM-TGCGCGCATGTACGGAATCACC-TAMRA
ZEx3 fw	CGATGGCCGCGCTAGA
ZEx3 rev	CTCAGGGAGTATCGTCCACTGTT
ZEx3 probe	6-FAM-TGATGATCCCCGCCGTGACTAAAGC-TAMRA

#### 4.1.7 Antibodies

Primary and secondary antibodies, which were used for immunofluorescence staining and Western blotting, including the host species, dilutions, and manufacturer are provided in the tables below.

**Table 6: Primary antibodies used for immunofluorescence staining (IF) and Western blotting (WB).**

Name	Species	Dilution IF	Dilution WB	Manufacturer
$\alpha$ -actinin (EA53)	mouse	1:500		Sigma-Aldrich
DsRed	rabbit	1:200	1:500	Clontech
smooth muscle actin	rabbit	1:100		Lab Vision
titin M8/M9	rabbit	1:200	1:500	Prof. Dr. Siegfried Labeit

**Table 7: Secondary antibodies used for immunofluorescence staining (IF) and Western blotting (WB).**

Name	Species	Dilution IF	Dilution WB	Manufacturer
anti-mouse Alexa Fluor 488	goat	1:500		Invitrogen
anti-rabbit Cy3	goat	1:500		Jackson Research
anti-rabbit IgG HRP-conjugated	goat		1:2000	GE Healthcare
anti-rabbit IgG biotin-conjugated	goat	1:500		Jackson Research

## **4.2 Methods**

### **4.2.1 Molecular biology methods**

#### **4.2.1.1 DNA preparation**

##### **4.2.1.1.1 Preparation of plasmid DNA**

Bacteria colonies generated by transformation (4.2.2.2) were used to inoculate overnight cultures. Small amounts of recombinant plasmid DNA for cloning were isolated from 3 ml cultures with the peqGOLD Plasmid Miniprep Kit I. Higher yield of plasmid DNA of the initial cloning vectors pDsRed-Monomer-C1 and pGemFRTloxNeo as well as the targeting vector DsRedKI was obtained by processing 200 ml cultures using the Plasmid Maxi Kit. Both kits were used according to the protocol given by the companies. The DNA concentration was determined (4.2.1.2) and the DNA was stored at -20°C.

##### **4.2.1.1.2 Preparation of BAC DNA**

BACs were isolated from 500 ml overnight cultures of the BAC clones 96022 and RP23-436E5 using the NucleoBond BAC 100 Kit according to the “Low-copy plasmid purification (Maxi/BAC, Mega)” protocol provided by the manufacturer. Before storage at -20°C, the concentration was determined (4.2.1.2).

##### **4.2.1.1.3 Purification of DNA from agarose gels**

For cloning, DNA fragments were extracted from agarose gels (4.2.1.4) using the EasyPure DNA Purification Kit according to manufacturer's instructions. DNA was eluted in 15 µl double distilled water (ddH<sub>2</sub>O). Afterwards, the concentration was measured and storage was carried out at -20°C.

##### **4.2.1.1.4 Preparation of genomic DNA from ES cells**

96-well cell culture plates, in which ES cells were grown to confluence, were obtained from the MDC Transgenic Core Facility (4.2.3.1) and used for preparation of genomic DNA. Cell culture

medium was removed and the ES cells were washed twice with 100  $\mu$ l phosphate buffered saline (PBS; 137 mM NaCl, 2.7 mM KCl, 4.3 mM  $\text{Na}_2\text{HPO}_4 \times 2 \text{ H}_2\text{O}$ , 1.4 mM  $\text{KH}_2\text{PO}_4$ , pH 7.4). 100  $\mu$ l ES cell lysis buffer (0.1% sodium dodecyl sulfate (SDS)) supplemented with 2  $\mu$ l proteinase K (14 mg/ml) and 0.5  $\mu$ l RNase A (10 mg/ml) was added to each well for digestion of the cells overnight at 55°C in a wet chamber. DNA was precipitated overnight using 10  $\mu$ l 8 M LiCl and 100  $\mu$ l isopropanol and subsequent centrifugation for 30 min at 3500 rpm and 4°C. DNA pellets were washed with 70% ethanol, air-dried and dissolved in 50  $\mu$ l TE (Tris-EDTA) buffer (10 mM Tris-HCl, 1 mM  $\text{Na}_2\text{EDTA}$ , pH 8.0) at 55°C in a wet chamber overnight. After measuring of the concentration (4.2.1.2), the DNA was stored at 4°C.

#### 4.2.1.1.5 Preparation of genomic DNA from mouse tail

For genotyping with PCR products exceeding 600 bp, genomic DNA was purified from the tail tip. Therefore, ~2 mm of the tail tip (4.2.5.1) was digested in 725  $\mu$ l tail buffer (20 mM Tris-base pH 8.0, 5 mM  $\text{Na}_2\text{EDTA}$  pH 8.0, 0.2% SDS, 4.3 mM NaCl) supplemented with 25  $\mu$ l proteinase K (10 mg/ml) at 52°C with 750 rpm shaking overnight. DNA was extracted with phenol/chloroform/isoamyl alcohol (25:24:1) and precipitated by the addition of 0.1 volume 8 M LiCl and 2.5 volumes 99% ethanol. After centrifugation at 13,000 rpm and 4°C for 30 min, the pellet was washed twice with 70% ethanol, air-dried and resuspended in 100  $\mu$ l TE buffer (4.2.1.1.4). The concentration was determined (4.2.1.2) and samples were stored at 4°C.

#### 4.2.1.1.6 Preparation of short DNA fragments from mouse tissue

Mouse genomic DNA for PCR genotyping was prepared following the HotSHOT method (Truett et al., 2000), if the expected PCR fragments had a size of less than 600 bp. ~1 mm of mouse tail snips (4.2.5.1) or uterine tissue in estrous stage (4.2.5.7) were heated at 95°C for 30 min in 75  $\mu$ l alkali lysis buffer (25 mM NaOH, 0.2 mM  $\text{Na}_2\text{EDTA}$ ). After cooling on ice, 75  $\mu$ l neutralization buffer (40 mM Tris-HCl) was added and 1  $\mu$ l was directly used for PCR. DNA preparations were stored at 4°C for short term or at -20°C for long term.

#### 4.2.1.2 Determination of nucleic acid concentration

The concentration of DNA and RNA samples were measured spectrophotometrically at 260 nm using the NanoDrop ND-1000 (Thermo Scientific) according to manufacturer's instructions.

#### 4.2.1.3 Polymerase chain reaction (PCR)

All polymerase chain reactions (PCRs) were carried out in the Hybaid Px2 Thermal Cycler (Thermo Scientific) or in the PTC-200 and PTC-225 Thermo Cycler (MJ Research) using primers as listed in Table 4 and dNTPs from Invitrogen or a Kit for 4.2.1.3.1 and 4.2.1.3.2.

##### 4.2.1.3.1 Amplification of DNA for cloning

DNA fragments for cloning were amplified from plasmids or BAC clones. Table 8 shows the primer pairs, the template, and the expected product size for each PCR.

**Table 8: Primers, template, and expected sizes of the PCR products for cloning.**

PCR	Primer	Template	Product Size
DsRed	NB-fDsRedI, NB-rDsRedI	5 ng pDsRed-Monomer-C1	693 bp
long arm (LA)	NB-fLA, NB-rLA	1 ng BAC clone RP23-436E5	7838 bp
middle arm (MA)	NB-fMA, NB-rMA	1 ng BAC clone 96022	654 bp
short arm (SA)	NB-fSA, NB-rSA	1 ng BAC clone 96022	1592 bp
short arm control (SAc)	NB-fSA, NB-rSAc	1 ng BAC clone 96022	1871 bp

The PCRs DsRed, middle arm, short arm, and short arm control were performed using the Expand Long Template PCR System preparing the reaction mix according to manufacturer's instructions with 1 or 5 ng template (Table 8). The PCR products were amplified using the following cycle conditions, whereas the elongation time was for the DsRed and MA PCR 45 s and for the SA and SAc PCR 75 s:

1. initial denaturation	94°C	120 s	
2. denaturation	94°C	15 s	
3. annealing	55°C	30 s	
4. elongation	72°C	45 or 75 s	10 x step 2-4
5. denaturation	60°C	45 s	
6. annealing	65°C	15 s	
7. elongation	65°C	45 or 75 s + 5 s/cycle	20 x step 4-6
8. final elongation	72°C	7 min	
9. storage	4°C	∞	



The LA PCR to amplify the long arm was done with the Phusion High-Fidelity DNA Polymerase utilizing the pipetting instruction as given by the company with 1 ng of template (Table 8). The PCR reaction was done according to the program:

1. initial denaturation	98°C	30 s	
2. denaturation	98°C	10 s	
3. annealing	60°C	30 s	
4. elongation	72°C	150 s	29 x step 2-4
5. final elongation	72°C	10 min	
6. storage	4°C	∞	

After PCR, DNA fragments were loaded on an agarose gel (4.2.1.4), purified (4.2.1.1.3) and subcloned into the pGEM-T Easy Vector (4.2.1.6.2.4). Before subcloning, the LA PCR product was A-tailed (4.2.1.6.2.1).

#### 4.2.1.3.2 DNA sequencing

The PCR products used for cloning and the targeting vector DsRedKI were verified by DNA sequencing using the chain termination method. The BigDye Terminator v3.1 Cycle Sequencing Kit was utilized for the sequencing reactions with the primers as listed in Table 4 according to a protocol modified from manufacturer's instructions. The PCR fragments short arm, DsRed, middle arm, long arm, and short arm control inserted into the pGEM-T Easy vector were sequenced with the primers Sp6 and T7, whereas the long arm was additionally sequenced with primers covering titin's exons 18 to 28 (Table 4). The complete targeting vector DsRedKI was sequenced with all primers for sequencing that are listed in Table 4, except Sp6. As template, 300 ng of purified plasmid DNA (4.2.1.1.1) was used in the following reaction mixture:

	<b>final concentration</b>	<b>volume</b>
5 x BigDye sequencing buffer	1 x	2 µl
10 µM primer	250 nM	0.25 µl
DNA template	300 ng/10 µl	X µl
2.5 x BigDye Ready Reaction Premix	0.25 x	1 µl
ddH <sub>2</sub> O		add to 10 µl

The PCR cycling conditions were chosen:

1. denaturation	96°C	10 s	
2. annealing	50°C	5 s	
3. elongation	60°C	4 min	30 x step 1-3
4. storage	4°C	∞	

PCR products were purified by gel filtration using Sephadex G50 superfine (GE Healthcare) in MultiScreen Filter Plates (Millipore) following the guidelines of the company. 10 µl Hi-Di Formamide (Applied Biosystems) was added to each purified sample. The sequencing was done with a 3100 Genetic Analyzer (Applied Biosystems) that was operated by the group of Professor Dr. Norbert Hübner. The sequence data were analyzed with the help of the software SeqMan II 4.03 (DNASTAR Inc.).

### 4.2.1.3.3 Soriano PCR for Es cell and mouse genotyping

An adapted Soriano protocol (Nagy et al., 2003a) was used for the neo PCR to screen ES cells for homologous recombination of the targeting vector and to verify the integration of the targeting vector into the titin locus of chimeras and their offspring. 10 x Gittschier buffer (166 mM (NH<sub>4</sub>)<sub>2</sub>SO<sub>4</sub>, 670 mM Tris-HCl, 67 mM MgCl<sub>2</sub>, 50 mM β-mercaptoethanol, 67 µM Na<sub>2</sub>EDTA, pH 8.8), the primers 3'neoflox and NB-DsRedGeno, and 300 ng ES cell DNA (4.2.1.1.4) or 100 ng mouse genomic DNA (4.2.1.1.5) as template were utilized leading to a PCR product with a size of 1971 bp. The following PCR reaction mix was used:

	<b>final concentration</b>	<b>volume</b>
10 x Gittschier buffer	1 x	2.5 µl
DMSO	10 %	2.5 µl
10 mg/ml BSA	80 µg/ml	0.2 µl
10 mM dNTP mix	1 mM	2.5 µl
10 µM primer forward	0.4 µM	1 µl
10 µM primer reverse	0.4 µM	1 µl
DNA template	100 or 300 ng/25 µl	X µl
5 U/µl <i>Taq</i> DNA polymerase	0.05 U/µl	0.25 µl
ddH <sub>2</sub> O		add to 25 µl

The PCR cycle profile was:

1. initial denaturation	94°C	80 s	
2. initial annealing	58°C	120 s	
3. initial elongation	65°C	5 min	
4. denaturation	94°C	30 s	
5. annealing	58°C	30 s	
6. elongation	65°C	180 s	40 x step 4-6
7. final elongation	65°C	10 min	
8. storage	10°C	∞	

The PCR reactions were loaded on an agarose gel for detection of the products (4.2.1.4).

#### 4.2.1.3.4 PCR for mouse genotyping

For mouse genotyping the PCRs as listed in Table 9 were used.

**Table 9: Primers, PCR conditions, and expected product sizes of the genotyping PCRs.**

PCR	Primer	MgCl <sub>2</sub>	Annealing	Product Size
cre	Cre800fw, Cre1200rev	1.5 mM	55°C	400 bp
DsRed	NB-fDsRedII, NB-rDsRedII	1.5 mM	57°C	693 bp
FLP	MG-FLP1, MG-FLP2	3 mM	55°C	480 bp
lacZ	lacZ1080fw, lacZ10620rev	1.5 mM	55°C	550 bp
lox	MG-Ti-SL1fw, MG-Ti-SL2rev	3 mM	55°C	WT 200 bp/ lox 300 bp
rec	MG-Ti-SL1fw, MG-Ti-FRTr2	2 mM	55°C	370 bp
recF	NB-fDsRedrecF, NB-rDsRedrecF	1.5 mM	57°C	WT 282 bp/ recF 369 bp

The following protocol was used with 1 µl of HotSHOT DNA (4.2.1.1.6) and final MgCl<sub>2</sub> concentrations as indicated in Table 9:

	final concentration	volume
10 x <i>Taq</i> DNA polymerase Buffer	1 x	2.5 µl
50 mM MgCl <sub>2</sub>	1.5 or 2 or 3 mM	0.75 or 1 or 1.5 µl
10 mM dNTP mix	0.2 mM	0.5 µl
10 µM primer forward	0.4 µM	1 µl
10 µM primer reverse	0.4 µM	1 µl
DNA template		1 µl
5 U/µl <i>Taq</i> DNA polymerase	0.03 U/µl	0.15 µl
ddH <sub>2</sub> O		add to 25 µl

The following PCR amplification conditions were chosen with annealing temperatures as given in Table 9:

1. initial denaturation	94°C	120 s	
2. denaturation	94°C	15 s	
3. annealing	55 or 57°C	45 s	
4. elongation	72°C	180 s	35 x step 2-4
5. final elongation	72°C	8 min	
6. storage	10°C	$\infty$	

The PCR reactions were analyzed using agarose gels (4.2.1.4).

### **4.2.1.4 DNA agarose gel electrophoresis**

Size dependent separation and visualization of DNA fragments after PCR and restriction digest was done using agarose gels. Depending on the expected DNA fragment sizes, 0.5-2% agarose gels were prepared using UltraPure Agarose (Invitrogen) in 0.5 x Tris-acetate-EDTA (TAE) buffer (20 mM Tris-HCl, 5 mM Na-acetate, 0.5 mM Na<sub>2</sub>EDTA, pH 8.0) supplemented with ethidium bromide solution to a final concentration of 0.5 µg/ml. Samples were mixed with 0.1 volume of DNA loading buffer (50% glycerol, 0.5% orange G, 25 mM Na<sub>2</sub>EDTA) and loaded on a gel to separate DNA fragments in 0.5% TAE buffer using a Mupid-21 Mini-Gel Electrophoresis Unit (Cosmo Bio Co.) at 100 V. DNA fragments were visualized at 312 nm and photographed with the Gel Doc 2000 Gel Documentation System (Bio-Rad) and their size was determined using the 1 Kb DNA Ladder (Invitrogen).

DNA fragments, which were used for cloning of the targeting vector, were cut out with a scalpel under UV light and purified (4.2.1.1.3).

### **4.2.1.5 Real-Time PCR**

#### **4.2.1.5.1 Preparation of RNA**

Tissue of non-pregnant (estrous stage) and E3.5 pregnant SMcTiMEx1-2 mice (4.2.5.7) was transferred into 1 ml Trizol (Invitrogen) to isolate total RNA according to the manufacturer's recommendations. The tissue was homogenized 3 x 20 s using an Ultra-Turrax T-25 (IKA-Werk) followed by the optional centrifugation step. Isolated RNA was dissolved in 89 µl RNase-free water (Qiagen) and stored at -80°C.

Isolated total RNA was thawed on ice and the RNA concentration was determined (4.2.1.2). 100 µg of RNA were digested with the RNase-Free DNase Set to remove genomic DNA according to the protocol “DNase Digestion of RNA before RNA Cleanup” of the Qiagen RNeasy Mini Handbook. Afterwards the RNA was purified using the RNeasy Mini Kit according to manufacturer’s protocol for RNA Cleanup. RNA was eluted with 2 x 30 µl of RNase-free water. The concentration of the RNA was again determined (4.2.1.2) and the RNA quality was assessed using the Bioanalyzer (4.2.1.5.2).

#### 4.2.1.5.2 Bioanalyzer

RNA quality was determined using the 2100 Bioanalyzer (Agilent). This method is based upon on-chip gel electrophoresis and detection by laser-induced fluorescence of dye labeled RNA. RNA was processed using the Agilent RNA 6000 Nano Kit together with the Agilent RNA 6000 Ladder following the given protocol. Only samples with a RNA integrity number (RIN) of over 8 were used for cDNA synthesis (4.2.1.5.3) or Real-Time PCR analysis (4.2.1.5.4).

#### 4.2.1.5.3 cDNA synthesis

To convert RNA into complementary DNA (cDNA), a reversed transcription PCR with a viral RNA-dependent DNA polymerase was performed using the ThermoScript RT-PCR System for First-Strand Synthesis Kit. According to manufacturer’s specifications, cDNA was synthesized from 3 µg RNA (4.2.1.5.1) with random hexamer primers at 50°C for 50 min in a PTC-225 Thermo Cycler (MJ Research).

#### 4.2.1.5.4 Real-Time PCR reaction

TaqMan was used as a Real-Time PCR system to quantify the transcriptional mRNA level of genes of interest. The quantification is based on the fluorescence of a reporter dye, whose signal increases in direct proportion to the amount of amplified PCR product in a sample, that was detected and quantified.

Quantitative Real-Time PCR was carried out using gene expression assays (4.1.6) or self-designed primer/probe sets (Table 5) with 900 nM each primer and 250 nM probe. 10 ng cDNA (4.2.1.5.3) per reaction was used with the FAST qPCR MasterMix Plus following manufacturer’s instructions scaling the reaction mix down to a total volume of 10 µl. To detect

low abundant titin mRNA with the primer/probe sets MEx1-2, MEx6, N2A, and ZEx3, TaqMan was carried out with the RNA UltraSense One-Step Quantitative RT-PCR System. The provided manual was adapted to a 10 µl reaction including the ROX Reference Dye and 20 ng RNA (4.2.1.5.1). Amplification reaction for each sample was run in triplicates for 40 cycles using a 7900HT Fast Real-Time PCR System (Applied Biosystems) operating in a 384-well format with 10 µl reaction volume.

Data were collected with the Sequence Detection System 2.3 software (Applied Biosystems) and analyzed using the Comparative CT Method ( $\Delta\Delta C_T$  Method) as described in the User Bulletin 2 of the ABI PRISM 7700 Sequence Detection System. For this relative quantification, data were normalized to 18S cDNA and displayed as fold change relative to the control.

### **4.2.1.6 Generation of the targeting vector *DsRedKI***

#### **4.2.1.6.1 Cloning strategy**

The targeting vector *DsRedKI* was designed with the computer program Clone Manager 6 (Sci Ed Central) spanning the 5' region of the mouse titin gene around the exon 28. Backbone of the targeting vector was the vector pGemFRTloxNeo containing the neomycin resistance cassette, in which the PCR fragments short arm, *DsRed*, middle arm and long arm (4.2.1.3.1) were consecutively cloned.

To construct the targeting vector, first the middle arm was cut out from the pGEM-T Easy vector with the help of the restriction endonucleases Bsp1407I and HindIII. Then the middle arm was ligated into the vector pGemFRTloxNeo, which was previously linearized with the same enzymes, leading to MApGemFRTloxNeo. The *DsRed* fragment subcloned into the pGEM-T Easy was cut out with Acc65I and cloned into the plasmid MApGemFRTloxNeo opened with Bsp1407I, to obtain the plasmid *DsRedMApGemFRTloxNeo*. The short arm of the targeting vector was gained from the pGEM-T Easy vector by digestion with BamHI and SmaI. The same enzymes were utilized for digestion of the plasmid *DsRedMApGemFRTloxNeo* to ligate the short arm inside resulting in the plasmid *DsRedMApGemFRTloxNeoSA*. After cutting the long arm from the pGEM-T Easy vector by XhoI, the final targeting vector *DsRedKI* was assembled by ligation of the long arm into the plasmid *DsRedMApGemFRTloxNeoSA* that was linearized by XhoI. Before electroporating into ES cells (4.2.3.1), the targeting vector was linearized with the enzyme ScaI.

A control vector was also cloned as a positive test for the ES cell genotyping PCR (4.2.1.3.3). Therefore, the DNA fragment short arm control was cut out from the pGEM-T Easy vector by BamHI and SmaI and ligated into the pGemFRTloxNeo that had been digested with the same enzymes.

#### 4.2.1.6.2 Enzymatic modifications of DNA

##### 4.2.1.6.2.1 *A-tailing*

The long arm of the targeting vector was amplified with the Phusion High-Fidelity DNA Polymerase leading to blunt-ended fragments. To ligate this PCR fragment into the pGEM-T Easy vector, it was modified using the A-tailing procedure as outlined in the Technical Manual of the pGEM-T and pGEM-T Easy vector systems. 5.7 µl purified long arm PCR fragments (4.2.1.1.3) were processed for 30 min at 70°C and used afterwards directly for ligation (4.2.1.6.2.4).

##### 4.2.1.6.2.2 *Restriction digest of DNA*

For vector linearization and excision of specific DNA fragments, single and double restriction digests were performed, whereas the amount of restriction endonuclease and buffer as well as the reaction conditions were set up according to manufacturer's recommendations. After 2 h of digestion at 37°C in a volume of 20 µl, the linearized vectors were dephosphorylated (4.2.1.6.2.3) and the DNA fragments were isolated by agarose gel electrophoresis (4.2.1.4).

##### 4.2.1.6.2.3 *Dephosphorylation of DNA fragments*

To minimize the re-ligation of a vector after digestion with a single enzyme (4.2.1.6.2.2), the vector was dephosphorylated. 3 U calf intestinal alkaline phosphatase was added to the linearized vector after the restriction digest and incubated for 30 min at 37°C. The reaction was stopped by accomplishing agarose gel electrophoresis (4.2.1.4).

##### 4.2.1.6.2.4 *Ligation of DNA fragments*

PCR products, which were purified (4.2.1.1.3) or purified and A-tailed (4.2.1.6.2.1), were subcloned into the pGEM-T Easy vector following the instructions of the manufacturer. The

molar ratio of 1:3 for vector to insert was chosen and samples were incubated for 90 min at room temperature.

For cloning of the targeting vector, DNA fragments were ligated into the vector using the DNA Ligation Kit according to the protocol provided by the manufacturer. Typically, 20 µl buffer A was combined with 5 µl of linearized plasmid vector and DNA insert that were mixed in the molar ratio of 1:4. 5 µl buffer B was added to start the ligation reaction, which was performed at 16°C for 2 h. After the incubation time, DNA ligation mixtures were used directly for transformation (4.2.2.2).

### **4.2.2 Microbiological methods**

#### **4.2.2.1 Generation of competent bacteria**

Competent *E.coli* DH5α were generated according to a modified “TFB-Based Chemical Transformation Protocol” published by Hanahan et al. (Hanahan et al., 1991). In step 9 of this protocol, only DMSO was added to the cell suspension and afterwards 100 µl aliquots were generated, which were stored at -80°C.

#### **4.2.2.2 Transformation of bacteria**

Transformation was used to incorporate plasmids into competent *E. coli* for amplification of plasmids after ligation. A modified protocol of Hanahan et al. (Hanahan et al., 1991) was utilized. 200 µl of competent bacteria (4.2.2.1) were thawed on ice, mixed with 5 µl of ligation reaction (4.2.1.6.2.4), and incubated for 30 min on ice. Transformation was performed for 45 s at 42°C and afterwards cells were shaken for 40 min at 37°C in 1 ml SOC medium (2% bacto tryptone, 0.5% yeast extract, 10 mM NaCl, 10 mM MgCl<sub>2</sub>, 10 mM MgSO<sub>4</sub>, 2.5 mM KCl, 20 mM glucose, pH 7.0). 100 µl of this cell suspension was transferred to a LB-A plate (1% bacto tryptone, 0.5% yeast extract, 171 mM NaCl, 1.5% agar, 50 µg/ml ampicillin, pH 7.0) or to a LB-A plate coated with 20 µl of 2.5 mM X-gal (MBI Fermentas) to identify recombinant clones by blue-white selection, if the plasmid had the pGEM-T Easy vector as a backbone. Plates were incubated overnight at 37°C.



### **4.2.3 Cell biological methods**

#### **4.2.3.1 Gene targeting in mouse ES cells**

The ES cell targeting was necessary to incorporate the targeting vector DsRedKI into the genome of mouse ES cells. It was done by the Transgenic Core Facility of the MDC-Berlin using the cell line 14.1. This service included culture, storage, and electroporation of ES cells as well as drug selection, isolation, and passaging of ES cell colonies that were resistant against the antibiotic G418. These clones were grown in 96-well plates for verification of the targeting vector within the genome (4.2.1.3.3) and cryopreservation. Homologously recombined ES cells were expanded and used for formation of embryoid bodies (4.2.3.2) and injection into blastocysts (4.2.5.2).

#### **4.2.3.2 Formation of embryoid bodies**

Embryoid bodies (embryo-like aggregates) were formed from undifferentiated ES cells and differentiated into beating cardiomyocytes to confirm the integration of the DsRedKI targeting vector into the titin locus after targeting. The method used was previously described by Wobus et al. (Wobus et al., 1991). Briefly, ES cells (4.2.3.1), which were positive for the insertion of the targeting vector tested by PCR, were cultivated in a cell culture incubator at 37°C and 5% CO<sub>2</sub> in hanging drops that consisted of 400-600 cells in 20 µl differentiation medium (6.7 g DMEM powder (with L-Glutamine and 4500 mg/l D-Glucose, Invitrogen) and 1.2 g NaHCO<sub>3</sub> in 540 ml ddH<sub>2</sub>O, after sterile filtration addition of 20% fetal calf serum (FCS, Sigma-Aldrich), 1 x non-essential amino acids (100x, Invitrogen), 100 U/ml penicillin and 100 µg/ml streptomycin (Invitrogen) and 4.2 µl β-mercaptoethanol). The ES cells aggregated to embryoid bodies within three days and were then cultivated for five days in suspension using differentiation medium. Subsequently, single embryoid bodies were picked and transferred to a 24-well plate containing coverslips that were previously coated with gelatin. The embryoid bodies were allowed to attach and beating cell clusters were used for immunostaining (4.2.3.4).

#### **4.2.3.3 Preparation and cultivation of primary smooth muscle cells**

Smooth muscle cells were isolated from murine aorta by dissection and subsequent enzymatic treatment of the vascular tissue according to a modified protocol of Ray et al. (Ray et al., 2001). 90 d old control and knockout SMcTiME<sub>x1-2</sub> females were sacrificed by cervical dislocation to

prepare the aorta. The aorta was transferred to medium (DMEM (4.5 g/l Glucose with UltraGlutamine I, Lonza) supplemented with 100 U/ml penicillin and 100 µg/ml streptomycin (Invitrogen) and 10% FCS (Sigma-Aldrich)). Using the stereomicroscope Leica MZ7.5, the adherent fat as well as the tunica adventitia was removed to uncover the tunica media containing the smooth muscle cells. The tunica media was placed into an enzymatic solution consisting of 1.36 mg collagenase type II and 1 mg elastase type IV dissolved in 1 ml prewarmed medium and digested for 1.5 h at 37°C and 5% CO<sub>2</sub> in a cell culture incubator to release the smooth muscle cells. After centrifugation for 3 min at 800 rpm, the enzymatic solution was removed and each cell pellet was resuspended in 500 µl medium and transferred to a 48-well plate coated with gelatin. In order to allow the cells to attach to wells, the plate was placed into the cell culture incubator and left undisturbed for five days. For re-plating, cells were washed with PBS (Cambrex) and treated for 3 min with 0.05% trypsin-EDTA (Invitrogen). After addition of medium and centrifugation for 3 min at 800 rpm, the cell pellet was resuspended in medium and seeded. Until usage for immunostaining (4.2.3.4) or the migration assay (4.2.3.5), smooth muscle cells were allowed to grow to confluence and further passaged.

#### **4.2.3.4 Immunostaining of embryoid bodies and smooth muscle cells**

Cell culture medium was removed and embryoid bodies (4.2.3.2) and smooth muscle cells (4.2.3.3) grown on coverslips were washed once with PBS-azide (0.02% NaN<sub>3</sub> in PBS) and fixed with ice-cold methanol for 15 min. After washing the cells 3 x for 5 min with PBS, they were permeabilized with 0.2% Triton X-100 in PBS-azide for 15 min and incubated with blocking solution for 50 min (1% goat serum, 2% BSA in PBS-azide) to stain embryoid bodies with DsRed as well as α-actinin and smooth muscle cells with smooth muscle actin (Table 6) in PBS-azide overnight at 4°C. Afterwards the cells were washed 2 x 15 min with PBS and incubated with the secondary antibody (Table 7) diluted in PBS-azide for 1 h. Anti-rabbit Cy3 as well as anti-mouse Alexa Fluor 488 for the embryoid bodies and anti-rabbit Cy3 for the smooth muscle cells was used. Subsequently, cells were washed 2 x 15 min with PBS. Nucleus staining of smooth muscle cells was performed for 30 min with DAPI (1 mg/ml) that was 1:2000 diluted in PBS. Before the cells, which have attached to coverslips, were placed in Fluorescence Mounting Medium (Dako) on glass slides, they were washed 2 x for 15 min with PBS and rinsed 3 x with ddH<sub>2</sub>O. Images were taken using the laser scanning confocal microscope Leica TSP SP2 and analyzed using Adobe Photoshop CS2.

#### **4.2.3.5 Cell migration assay**

Migration assays were performed using a modified Boyden chamber as described earlier (Natarajan et al., 1996). This is a filter assay with a cell culture insert that forms two compartments, which are separated by a porous membrane. Cells can be induced to migrate from the upper chamber through the membrane into the lower compartment following the gradient of a chemoattractant.

Primary smooth muscle cells (4.2.3.3) were starved for 24 h in normal medium (DMEM (4.5 g/l Glucose with UltraGlutamine I, Lonza) supplemented with 100 U/ml penicillin and 100 µg/ml streptomycin (Invitrogen), 0.2% BSA and 0.4% FCS (Sigma-Aldrich)), harvested, washed with PBS, and resuspended in serum-free medium (normal medium without FCS) to a final concentration of  $10^6$  cells/ml. 400 µl of cell suspension was plated on coverslips to document the presence of smooth muscle cells by immunostaining (4.2.3.4). Additionally, 200 µl of each cell suspension was added to the upper compartment of a cell culture insert containing a polycarbonate filter with 8 µm pores (Corning Incorporated) that was coated with 20 µg/ml type 1 collagen (Invitrogen) and placed in a 24-well. The lower compartment of each 24-well was filled with 600 µl serum-free medium supplemented with no or  $10^{-10}$  M PDGF-B (Reddy et al., 2003). After 4 h, cells that migrated to the lower side of the filter were fluorescently labeled by incubation in 450 µl serum-free medium with 8 µM calcein-AM for 45 min at 37°C and 5% CO<sub>2</sub>. Afterwards the cell culture inserts were transferred into 500 µl prewarmed 0.05% trypsin-EDTA (Invitrogen) and incubated for 10 min to detach the migratory cells from the underside of the membrane. 200 µl trypsin-EDTA solution was transferred in duplicates into a flat-bottom black 96-well plate (Greiner Bio-One GmbH) to quantify the cell count of each sample by reading the fluorescence at an excitation of 485 nm and an emission of 520 nm in a Synergy HT Multi-Mode Microplate Reader (BioTek).

## **4.2.4 Biochemical methods**

### **4.2.4.1 Protein preparation**

#### **4.2.4.1.1 Protein lysates for 2D-gel electrophoresis**

Uterine tissue of E3.5 pregnant SMcTiMEx1-2 mice (4.2.5.7) was ground under liquid nitrogen and mixed with 4 x volume of 2D-lysis buffer (8 M urea, 2 M thiourea, 4% chaps, 0.5% pharmalyte, 10 mM DTT, 1 mM PMSF, 100 nM Calyculin A). After sonication using the sonopuls sonicator SH70G (Brandelin electronic GmbH) with 70% power for 2 min on ice, the cell debris was spun down at 50,000 rpm at 4°C for 30 min. The protein concentration of the supernatant was determined by the Bradford assay (4.2.4.2.1) and the protein lysates were stored in aliquots at -80°C.

#### **4.2.4.1.2 Protein lysates for VAGE**

Protein lysates of heart, quadriceps, and soleus of TiEx28DsRed mice in estrous stage (4.2.5.7) were prepared according to a modified protocol of Warren et al. (Warren et al., 2003). Tissues were pulverized under liquid nitrogen and transferred with the help of 40 x volume titin sample buffer (8 M urea, 2 M thiourea, 3% SDS, 0.05 M Tris-HCl, 0.03% bromophenol blue, 75 mM DTT, pH 6.8) into a Dounce homogenizer (Wheaton). After 3 min of homogenization, samples were vortexed thoroughly, left at room temperature for 25 min, and centrifuged for 5 min at 13,000 rpm. Supernatants were removed and their protein concentration was measured using the amido black method (4.2.4.2.2). Afterwards, supernatants were aliquoted and stored at -80°C.

#### **4.2.4.1.3 Protein lysates for multiplex bead immunoassay**

Tissue Extraction Reagent I (Invitrogen) was supplemented with protease inhibitor cocktail (Sigma-Aldrich) according to manufacturer's manual. Uteri of E3.5 pregnant SMcTiMEx1-2 mice (4.2.5.7) were homogenized in 1 ml buffer per 100 mg tissue with the help of an Ultra-Turrax T-8 (IKA-Werk). Afterwards, samples were centrifuged for 5 min at 10,000 rpm and 4°C to pellet the tissue debris. Before aliquoting and storing at -80°C, the protein concentration of the supernatant was analyzed using the Bradford method (4.2.4.2.1).

#### 4.2.4.1.4 Protein lysates for ELISA

Uterine horns of SMcTiMEx1-2 mice pregnant at E3.5 (4.2.5.7) were homogenized in 0.5 ml of 50 mM phosphate buffer (0.16%  $\text{KH}_2\text{PO}_4$ , 1.04%  $\text{Na}_2\text{HPO}_4 \times 7 \text{ H}_2\text{O}$  in ddH<sub>2</sub>O, pH 7.4) using an Ultra-Turrax T-8 (IKA-Werk). After centrifugation of the homogenates at 10,000 g for 20 min at 4°C, the supernatant was stored in aliquots at -80°C until assayed directly using ELISA (Li et al., 2004).

#### 4.2.4.2 Protein quantification

##### 4.2.4.2.1 Bradford assay

Protein amount was quantified with the method of Bradford (Bradford, 1976), which is based on the absorbance maximum shift of Coomassie Brilliant Blue G-250 from 465 nm to 595 nm in response to protein binding. The Bradford protein assay (Bio-Rad) was carried out according to manufacturer's instruction using the Ultrospec 2100 *pro* UV/Visible Spectrophotometer (GE Healthcare).

##### 4.2.4.2.2 Amido black method

Protein concentration of VAGE samples was determined with the amido black method because SDS in the lysis buffer impairs the Bradford method (Schaffner and Weissmann, 1973). This quantification is predicated on the binding of the dye amido black to protein that is bound on a membrane. BSA (bovine serum albumin) dilutions in VAGE lysis buffer, which were used to generate a standard curve, and 1 µl of each protein sample were spotted on a nitrocellulose membrane (GE Healthcare) in duplicates. On an orbital shaker, the membrane was incubated for 1 min in amido black staining solution (45% methanol, 10% acetic acid, 0.1% amido black) followed by destaining (90% methanol, 2% acetic acid) until the background staining of the membrane was removed. The membrane was cut to separate the protein spots and to transfer each protein spot to an individual reaction tube containing 800 µl elution buffer (50% ethanol, 0.05 mM  $\text{Na}_2\text{EDTA}$ , 25 mM NaOH). During 30 min incubation on a shaker, the protein spots were discolored releasing the bound amido black into the elution buffer. The absorbance of amido black in the elution buffer was measured at 630 nm using the Ultrospec 2100 *pro* UV/Visible Spectrophotometer (GE Healthcare). The protein concentration in each sample was determined with the help of the BSA standard curve.

#### **4.2.4.3 Protein gel electrophoresis**

##### **4.2.4.3.1 2D-gel electrophoresis**

###### **4.2.4.3.1.1 First dimension**

In the first dimension, proteins of a lysate were separated according to their isoelectric point. 18 cm immobilized pH gradient (IPG) strips with a pH-gradient of 3 to 10 (GE Healthcare) were rehydrated overnight at room temperature in 340 µl rehydration solution (8 M urea, 2 M thiourea, 2% chaps, 0.5% Pharmalyte pH 3-10 (GE Healthcare), 12 µl/1ml DeStreak-reagent (GE Healthcare), 0.03% bromophenol blue). 125 µg protein lysate (4.2.4.1.1) were replenished with rehydration solution to a total volume of 50 µl and applied to IPG strips by cup-loading. The samples were isoelectric focused under DryStip Cover Fluid (GE Healthcare) at 20°C using the MultiphorII (GE Healthcare) with the following profile:

1. gradient	300 V	30 min
2. step	300 V	30 min
3. gradient	500 V	1 h
4. step	500 V	1 h
5. gradient	3500 V	1.5 h
6. step	3500 V	5.5 h

After focusing, the strips were immediately used for the second dimension.

###### **4.2.4.3.1.2 Second dimension**

After isoelectric focusing, the second dimension was used to separate proteins dependent on their molecular weight using continuous sodium dodecyl sulfate-polyacrylamide gel electrophoresis (SDS-PAGE). Each IPG strip was incubated for 15 min at room temperature in 10 ml equilibration buffer A (6 M urea, 50 mM Tris-HCl, 30% glycerol, 2% SDS, 22 mM DTT) and afterwards for 15 min at room temperature in 10 ml equilibration buffer B (6 M urea, 50 mM Tris-HCl, 30% glycerol, 2% SDS, 0.135 M iodoacetamide, 0.03% bromophenol blue) on an orbital shaker. Then the IPG strips were placed on SDS-gels (T=12.5%, C=2.6%; 133 ml ddH<sub>2</sub>O, 152 ml 40% acrylamide, 85 ml 2% bisacrylamide, 125 ml 1.5 M Tris-base pH 8.8, 5 ml 10% SDS, 1.25 ml 10% ammonium persulfate, 0.25 ml TEMED) and overlaid with 0.5 % agarose in 1 x SDS running buffer (25 mM Tris-base, 192 mM glycine, 0.1% SDS). For SDS-

PAGE, 1 x SDS running buffer in the lower chamber and 2 x SDS running buffer in the upper chamber of an Ettan Dalt Twelve Electrophoresis Unit (GE Healthcare) was used. Electrophoresis was performed at 16°C with 2 W/gel for 30 min followed by 15 W/gel. Afterwards, the gels were stained with Coomassie (4.2.4.4).

#### 4.2.4.3.1.3 *Quantification*

To visualize protein differences in uteri of knockout compared to control mice, gels were analyzed with the Delta2D Version 3.4 software (DECODON). The percent volume value (% V) of each protein spot for six knockout and six control samples was averaged and the quotient of average % V knockout and average % V control was calculated for each spot. The resulting ratio values were filtered to obtain the proteins that were downregulated (ratio < 0.8) and upregulated (ratio > 1.3) in knockout compared to control uteri. Weak protein spots with an average % V of lower than 0.03 in knockout and control gels were excluded.

#### 4.2.4.3.1.4 *Mass spectrometry*

To identify proteins by mass spectrometry according to a published procedure (Raddatz et al., 2008), protein spots of 2D-gels stained with Coomassie Brilliant Blue were cut out and send to the Ernst-Moritz-Arndt-University of Greifswald (group of Professor Dr. Hecker).

#### 4.2.4.3.2 Vertical SDS-agarose gel electrophoresis (VAGE)

Proteins with a high molecular weight can only be poorly separated using SDS-PAGE. Hence a vertical SDS-agarose gel electrophoresis (VAGE) with a 1% agarose gel was performed to separate titin isoforms of heart, quadriceps, and soleus protein lysates (4.2.4.1.2). VAGE was adapted from a published protocol (Warren et al., 2003). A SE 600 Vertical Gel Unit (GE Healthcare) with VAGE running buffer (50 mM Tris-base, 0.384 M glycine, 1% SDS) in the lower chamber and VAGE running buffer supplemented with 10 mM  $\beta$ -mercaptoethanol in the upper chamber was used. SDS-agarose gels (1% SeaKem Gold Agarose (Cambrex), 30% glycerol, 50 mM Tris-base, 0.384 M glycine, 1% SDS) were run at 15 mA constant current in a 4°C cold room. After electrophoretic separation, gels were stained with Coomassie Brilliant Blue (4.2.4.4) or transferred to a membrane (4.2.4.5.1).

#### **4.2.4.4 Coomassie staining**

Each step of the staining procedure was conducted on an orbital shaker. 2D-gels were fixed (50% ethanol, 10% acetic acid) for 1 h and gels from VAGE were first fixed (50% methanol, 12% acetic acid, 5% glycerol) for 1 h and then dried at 37°C overnight to minimize background staining. Afterwards both gel types were washed 3 x for 10 min with ddH<sub>2</sub>O followed by overnight staining with a Coomassie Brilliant Blue G-250 (Sigma-Aldrich) solution prepared according to Neuhoff et al. (Neuhoff et al., 1988). Excess dye was removed by ddH<sub>2</sub>O washing and gel images were taken using the Camilla or Stella 8300 imaging system (Raytest). VAGE gels were processed using the Aida Image Analyzer v. 4.24 software (Raytest) and 2D-electrophoresis gels were analyzed using the Delta2D software (4.2.4.3.1.3).

#### **4.2.4.5 Western blotting**

##### **4.2.4.5.1 Semi-dry blotting**

The semi-dry electroblotting was used to transfer titin for immunological detection to a PVDF (polyvinylidene difluoride) membrane (GE Healthcare). The membrane was incubated 10 s in 100% methanol, 2 min in ddH<sub>2</sub>O and 15 min in anode buffer II (25 mM Tris-base, 0.05% SDS, 10% methanol, pH 10.4). VAGE-gels (4.2.4.3.2) were equilibrated for 10 min in cathode buffer (25 mM Tris-base, 0.05% SDS, 10% methanol, 40 mM caproic acid, 10 mM  $\beta$ -mercaptoethanol, pH 10.4) and then assembled with the membrane and Whatman 3MM Chr paper (Schleicher & Schuell). Previously, the blotting paper towards the cathode was wet in cathode buffer and the blotting paper towards the anode was soaked in anode buffer I (300 mM Tris-base, 0.05% SDS, 10% methanol, pH 10.4) and anode buffer II. The transfer was performed at constant 250 mA for 90 min in the PerfectBlue Semi-Dry Electrobloetter SEDEC M (PEQLAB).

The blot transfer efficiency was controlled by incubation for 3 min with Ponceau S staining solution (Sigma-Aldrich). Excessive dye was removed with ddH<sub>2</sub>O to make the protein bands visible. Then the membrane was destained with PBS-T (0.1% Tween 20 in PBS).

##### **4.2.4.5.2 Immunological detection of proteins**

The detection of specific proteins after semi-dry Western blotting was done by an immunological reaction using antibodies. Unspecific binding sites on the membrane were blocked with 5% milk powder in PBS-T for 1 h followed by incubation of the membrane with



the primary antibody (Table 6) in 5 % protease free BSA (SERVA) in PBS at 4°C overnight. After washing the membrane 3 x 15 min with PBS-T, it was incubated with the secondary antibody (Table 7) in 5% milk powder in PBS for 1 h and washed 2 x 15 min with PBS-T and 1 x 15 min with PBS. The secondary antibody was conjugated with horseradish peroxidase and imaged with the ECL-system (enhanced chemiluminescence) using the SuperSignal West Femto Maximum Sensitivity Substrate (Thermo Scientific) according to manufacturer's instruction. Chemiluminescence was detected with the Stella 8300 Imaging system (Raytest).

#### **4.2.4.6 Histology**

##### **4.2.4.6.1 Immunostaining**

Heart and quadriceps of TiEx28DsRed animals in estrous stage (4.2.5.7) were fixed overnight at 4°C in formalin. Then the tissue was dehydrated in 30% sucrose in PBS overnight at 4°C and embedded in Tissue-Tek O.C.T. Compound (Sakura). 10 µm thick longitudinal sections were cut using the Cryostat HM 560 Cryo-Star (Thermo Scientific) with a specimen temperature of -25°C and a knife temperature of -35°C and placed on HistoBond slides (Marienfeld). Cryosections were stored at -20°C.

For immunostaining, sections were air-dried, fixed for 15 min with 2% paraformaldehyde in PBS-azide (0.02% NaN<sub>3</sub> in PBS), and washed 2 x for 5 min with PBS. After permeabilization and blocking for 1 h (10% goat serum, 0.3% Triton X-100, 0.2% BSA in PBS) samples were washed 4 x with PBS for 5 min and incubated with the primary antibody titin M8/M9 (Table 6) in PBS at 4°C in a wet chamber overnight. Excess primary antibodies were removed by a 6 x PBS wash each for 10 min. Sections were stained with an anti-rabbit IgG biotin-conjugated antibody (Table 7) in PBS for 1 h followed by 6 x PBS washing. Then the signal of the titin M8/M9 antibody was amplified by incubation with streptavidin conjugated to Alexa Fluor 647 (1:1000; Invitrogen) in PBS for 1 h. Finally, sections were washed 4 x for 5 min with PBS and 2 x for 1 min with ddH<sub>2</sub>O and mounted in Fluorescence Mounting Medium (Dako). Protein localization was documented using the laser scanning confocal microscope Leica TSP SP2 and images were analyzed using Adobe Photoshop CS2.

##### **4.2.4.6.2 LacZ staining**

LacZ staining was performed to monitor the activity of the SMMHC cre-recombinase in uteri of SMcGtROSA26 reporter mice. These mice contain a lox-flanked DNA stop element followed by

the *lacZ* gene knocked into the ROSA26 locus. Only if the floxed stop segment is excised by cre-recombinase activity, the *lacZ* is expressed. The ability of the  $\beta$ -galactosidase to cleave X-gal leading to a blue insoluble product is used to monitor the presence of this enzyme. The staining procedure for uteri of SMcGtROSA26 mice in estrus stage (4.2.5.7) was adapted from the protocol “Staining Frozen Sections” (Nagy et al., 2003b). After consecutive incubation in fixative (0.2% paraformaldehyde, 2 mM MgCl<sub>2</sub>, 5 mM EGTA, 0.1 M PIPES, pH 6.9) and 30% sucrose in PBS-M (2 mM MgCl<sub>2</sub> in PBS) at 4°C overnight, the tissue was embedded in Tissue-Tek O.C.T. Compound (Sakura) to cut cross sections as described before (4.2.4.6.1).

The samples were air-dried and fixed for 5 min with 2% paraformaldehyde and 0.125% glutaraldehyde in PBS followed by a 3 x PBS-M wash for 1 min. Afterwards the slides were incubated 3 x for 2 min in detergent solution (2 mM MgCl<sub>2</sub>, 0.01% Na-deoxycholate, 0.02% NP40 in PBS) and 2 min in staining solution (2 mM MgCl<sub>2</sub>, 5 mM potassium ferricyanide, 5 mM potassium ferrocyanide in PBS). Sections were stained overnight at 37°C with 2.5 mM X-gal (MBI Fermentas) in staining solution. For the counterstain with eosin, the samples were rinsed in ddH<sub>2</sub>O for 2 min and stained for 1 min with eosin solution (1% eosin, 0.05% acetic acid in ddH<sub>2</sub>O). Before embedding in Roti-Histokitt (Roth), dehydration of the sections was performed with increasing alcohol concentrations (70%, 90%, and 100%) each for 30 s. Pictures were taken using the BX51 Research Microscope (Olympus).

#### **4.2.4.7 ELISA**

An enzyme-linked immunosorbent assay (ELISA) kit was used to measure the metabolite 12-hydroxyeicosatetraenoic acid (12-HETE) in homogenates of uterine samples (4.2.4.1.4) according to the manufacturer's instructions. The principle of this method is based on the competitive binding of 12-HETE, which is conjugated to alkaline phosphatase, and the metabolite in the sample to an antibody that is immobilized on wells. The obtained signal read at 405 nm in a Synergy HT Multi-Mode Microplate Reader (BioTek) was indirectly proportional to the amount of 12-HETE in the sample. Data acquired for the standards were displayed as logit-log plot and a linear regression fit was performed to obtain a standard curve, which was used to calculate the concentrations of 12-HETE in the sample. Metabolite concentration was normalized to the total protein concentration of the sample that was measured using the Bradford method (4.2.4.2.1).

#### **4.2.4.8 Multiplex bead immunoassay**

Multiplex bead immunoassay is an immunoassay on the surface of fluorescent-coded beads, which allows the investigation of several analytes in a single sample at the same time. With the help of this method, the growth factors G-CSF (granulocyte colony-stimulating factor), FGF (fibroblast growth factor) basic, PDGF-B, and VEGF (Growth Factor Mouse 4-Plex Panel) as well as IL-1 $\beta$  (interleukin-1 $\beta$ ), IL-6, IL-15, IP-10 (interferon-inducible protein 10), LIF, MCP-1 (monocyte chemotactic protein-1), and TNF- $\alpha$  (tumor necrosis factor-alpha; Mouse Cytokine/Chemokine Panel-7-Plex) were quantitatively determined in serum (4.2.5.6) and uterine tissue lysate of E3.5 pregnant mice (4.2.4.1.3). Prior to immunoassay analysis, all tissue lysates were normalized against their total protein concentration. The kits were carried out following the protocol given by the companies utilizing the Luminex 200<sup>TM</sup> instrument with the software xPONENT 3.0 (Luminex Corporation). The concentrations of the analytes in the sera or lysates were calculated from the standard curve using as curve fitting software xPONENT 3.0. Thereby the four parameter algorithm for the Invitrogen kit and the 5-parameter logistic for the Millipore kit was used.

### **4.2.5 Animal procedures**

#### **4.2.5.1 Maintenance of the mouse colony**

TiEx28DsRed, FLP-transgene, SMMHCcre, SMcGtROSA26, TiMex1-2, and SMcTiMex1-2 mice were derived from own breeding. The founder of the transgenic mouse lines FLP-recombinase (FLP-transgene) and smooth muscle myosin heavy chain (SMMHC) cre-recombinase (SMMHCcre) were kindly provided (Rodriguez et al., 2000; Xin et al., 2002). SMMHCcre males were bred with 129S-Gt(ROSA)26Sor<sup>tm1Sor</sup>/J reporter mice, which were purchased from The Jackson Laboratory, to obtain the double heterozygous strain SMcGtROSA26. The conditional knockout strain of titin's M-band exons 1 and 2 (TiMex1-2) was available in the group (Gotthardt et al., 2003), so that the smooth muscle specific TiMex1-2 (SMcTiMex1-2) strain was obtained by breeding the SMMHCcre strain with TiMex1-2 mice. The TiEx28DsRed mouse strain was newly generated (4.2.5.3). All mice were numbered by ear marks and tail biopsies were taken for genotyping (4.2.1.3.3 and 4.2.1.3.4).

All mice used in the studies were of 129/S6 (Taconic) and C57Bl/6 (Charles River) mixed background. They were housed in the animal facility of the MDC-Berlin in a 12 h light/dark, 20°C temperature controlled environment with free access to food and water using individually ventilated cages (IVCs). The animal procedures were performed in accordance to the regulatory rules for Animal Welfare of the German Society for Laboratory Animal Science.

### **4.2.5.2 Generation of chimeric mice**

The generation of mouse chimera was done by the Transgenic Core Facility of the MDC-Berlin. This process included the microinjection of ES cells from one clone (4.2.3.1), which incorporated the targeting vector DsRedKI within the titin locus, into blastocysts obtained from superovulated C57Bl/6 mice. These blastocysts were surgically transferred into pseudopregnant recipient mice leading to chimeric offspring. After weaning, the chimeras were transferred to the animal colony for breeding (4.2.5.3).

### **4.2.5.3 Chimera breeding and generation of the *TiEx28DsRed* strain**

Chimeras (4.2.5.2) were mated with C57Bl/6 (Charles River) mice to obtain offspring that carries the DsRedKI targeted gene. Offspring with brown coat color (agouti) that contained the targeted allele was bred with FLP-transgene mice (Rodriguez et al., 2000) to delete the neomycin resistance cassette. Afterwards the FLP-transgene was removed from double heterozygous mice by crossing them with 129/S6 (Taconic) animals. Mice heterozygous for the altered titin locus were used to generate the colony of the *TiEx28DsRed* strain.

### **4.2.5.4 Staging of the estrous cycle**

Induced by ovarian hormones, the murine reproductive system undergoes periodic physiological changes, which are classified into the four stages metestrus, diestrus, proestrus and estrus (Allen, 1922; Snell, 1941). Each stage shows a distinct uterine and vaginal cytology. To collect non-pregnant uteri in the estrous stage of the estrous cycle and to determine the estrous cycle length, it was necessary to monitor changes in vaginal epithelial cells at 24 h intervals by vaginal lavage (Frick and Berger-Sweeney, 2001). Therefore, the vagina of 90 d old wild-type, heterozygous, and homozygous *TiEx28DsRed*, double heterozygous and heterozygous *SMcGtROSA26* mice, *SMMHCcre* mice, and control, heterozygous, and knockout *SMcTiMEx1-2* female mice was rinsed with ddH<sub>2</sub>O to extract vaginal cells and the fluid was placed onto a microscope slide.

After evaporation of the water, the sample was examined under the inverted light microscope Olympus CK40 applying the guidelines of Allen and Snell (Allen, 1922; Snell, 1941). At least, two continuous cycles were observed before sacrificing the mice.

#### **4.2.5.5 Timed mating**

90 d old control, heterozygous and knockout females of the SMcTiMEx1-2 strain as well as SMMHCcre mice were mated. Thereby knockout males were used for control females and control males were used for heterozygous and knockout females to get embryos with similar genotypes. SMMHCcre females were bred with 129/S6 males. Mating was set up at 6 pm and the morning of detecting a vaginal plug was designated as E0.5.

#### **4.2.5.6 Collection of serum**

The retrobulbar venous plexus puncture was used to obtain blood samples from E3.5 pregnant control and knockout SMcTiMEx1-2 mice (4.2.5.5). Mice were anesthetized with ether and blood was withdrawn using a capillary tube that was directed towards the major venous structure of the eye. For serum collection, blood was allow to coagulate for 5 min at room temperature and then 55 min on ice before it was centrifuged for 15 min at 3000 rpm. The upper serum phase was taken, frozen in liquid nitrogen and stored at -80°C until investigation by multiplex bead immunoassay (4.2.4.8).

#### **4.2.5.7 Tissue harvesting**

The body weight of mice in estrous stage (4.2.5.4) and of E3.5 pregnant control and knockout SMcTiMEx1-2 mice (4.2.5.5) was measured. Animals were killed by cervical dislocation to dissect uterus from SMcGtROSA26, SMMHCcre as well as SMcTiMEx1-2 mice and heart, quadriceps, and soleus from TiEx28DsRed mice. The tissue weight of uterus and heart was determined and if applicable the left uterine horn was flushed with DEPC-PBS to confirm the pregnancy day E3.5 by the presence of blastocysts. Then, the tissue was used for cryosections (4.2.4.6) or quick frozen in liquid nitrogen and stored at -80°C until RNA or protein preparation.

#### **4.2.5.8 Counting of blastocysts**

Control and knockout SMcTiMEx1-2 mice pregnant at E3.5 (4.2.5.5) were killed by cervical dislocation to take out the uteri. Blastocysts were flushed from both uterine horns with PBS and counted using the stereomicroscope Leica MZ7.5 (Ye et al., 2005).

#### **4.2.5.9 Evans Blue staining**

To determine the number and localization of embryo implantation sites at E4.5 and E5.5, they were stained by Evans Blue. This is an azo compound dye that binds to serum albumin in the blood thereby making areas of vascular permeability, such as implantation sites, visible. Timed mated SMMHCcre as well as control, heterozygous and knockout SMcTiMEx1-2 females (4.2.5.5) were intravenously injected with 150  $\mu$ l Evans Blue (1% in PBS) solution (Ye et al., 2005). 5 min after injection, mice were killed by cervical dislocation and uterus and heart were dissected. Their weight was determined and pictures of the uteri were taken using an Olympus  $\mu$  720 SW camera. Afterwards uteri horns of E4.5 pregnant females were investigated for the presence of blastocysts as described (4.2.5.8).

#### **4.2.5.10 Angiogenesis study**

A standard method to investigate angiogenesis *in vivo* is the injection of matrigel. This is a solubilized basement membrane preparation extracted from Engelbreth-Holm-Swarm mouse sarcoma that is a tumor rich in extracellular matrix proteins. The matrigel plug assay was carried out as described previously with modifications (Isaji et al., 1997). Matrigel Phenol Red-free (BD Biosciences) was thawed overnight at 4°C and mixed with 30ng/ml VEGF and 64 units/ml heparin. 0.5 ml of this mixture was injected subcutaneously in one site at the abdominal midline of 90 d old male and female control and knockout SMcTiMEx1-2 mice. Upon injection, the matrigel hardened to form a plug. After seven days, mice were euthanized by ether and the matrigel was harvested, weighted, and frozen in liquid nitrogen. Afterwards 150  $\mu$ l blood was taken by cardiac puncture, mixed with 7.53  $\mu$ l heparin (64 units/ml) and frozen in liquid nitrogen. Matrigel as well as the blood were stored at -80°C until analyzing for the formation of blood vessels by determination of hemoglobin content. Therefore, matrigel plugs were digested with 2 mg/ml collagenase type I and 2 mg/ml dispase II in TESCA buffer (50 mM TES, 0.36 mM CaCl<sub>2</sub>, pH 7.4 at 37°C) for 2 h at 37°C and 750 rpm and afterwards the quantity of

hemoglobin was measured using Drabkin's reagent (Sigma-Aldrich) according to manufacturer's instructions. Blood hemoglobin content was also determined with Drabkin's reagent to express the results as blood volume per unit weight of matrigel (Bandyopadhyay et al., 2002).

#### **4.2.6 Statistical analysis**

Evaluation of data was done using the GraphPad Prism 5 software (GraphPad Software). Data of one group were displayed as mean with standard error of the mean (SEM). The t-test was applied to compare the means of two groups. The comparison of the means of three and more unmatched groups was done with the help of the one-way ANOVA. The two-way ANOVA was used to determine how experimental data are affected by two factors, both individually and together. For the 2D-gel analysis, a P-value of  $P < 0.1$  \* fulfilled the significance criteria and for the other experiments a P-value of  $P < 0.05$  \*,  $P < 0.01$  \*\*, and  $P < 0.001$  \*\*\* was considered to be significant.

## 5 Results

To investigate titin in smooth muscle, we used a morphological and a functional approach. A knockin mouse model was established to visualize smooth muscle titin with the help of the red fluorescence protein DsRed. Mice expressing the titin-DsRed were viable and fluorescence emitted by the DsRed was detected in muscle tissue. Furthermore, a loss of function approach was used to analyze the role of titin's kinase region, which is encoded by titin's M-band exons 1 and 2, in smooth muscle. Deletion of titin's kinase region in uterine tissue led to an embryo implantation phenotype with impaired angiogenesis and tissue remodeling.

### 5.1 The DsRedKI mouse model

#### 5.1.1 Cloning of the targeting vector DsRedKI

We cloned a targeting vector to insert the red fluorescence protein DsRed into titin. The DsRed should be present close to titin's N-terminus but not interfere with titin's integration into the Z-disc of the sarcomere and with the protein binding sites of T-cap, sANK,  $\alpha$ -actinin, and obscurin (Figure 5). Hence the DsRed coding sequence was incorporated into the exon 28 of titin considering its domain composition. This exon encodes unique sequences and Ig-domains (Bang et al., 2001a), which are located at titin's Z-disc to I-band junction (Figure 4). In the targeting vector DsRedKI, the coding sequence of the DsRed was inserted between the coding sequence of the Ig-domain Z9 and the Ig-domain I1 of titin's Z/I-band junction preserving the reading frame (Figure 7). The whole targeting vector spanned the genomic region from titin's exon 18 to exon 31. It consisted of the long arm from exon 18 to exon 28 until the DsRed insertion, the DsRed, the middle arm, the neomycin resistance cassette flanked by two FRT-sites, and the short arm. The middle arm included remains of exon 28 and intron sequence and the short arm contained intron sequence as well as exon 29 to exon 31. The targeting strategy included insertion of the targeting vector, which was linearized with the enzyme ScaI, into ES cells using electroporation. The integration of the targeting vector into the titin wild-type allele of ES cells by homologous recombination led to the targeted allele. After germline transmission, the neomycin resistance cassette was removed by the enzyme FLP-recombinase resulting in mice carrying the knockin allele (recF). Compared to the wild-type allele, the KI allele contained one



FRT-site in an intron and the coding sequencing of the DsRed in exon 28 within the reading frame.

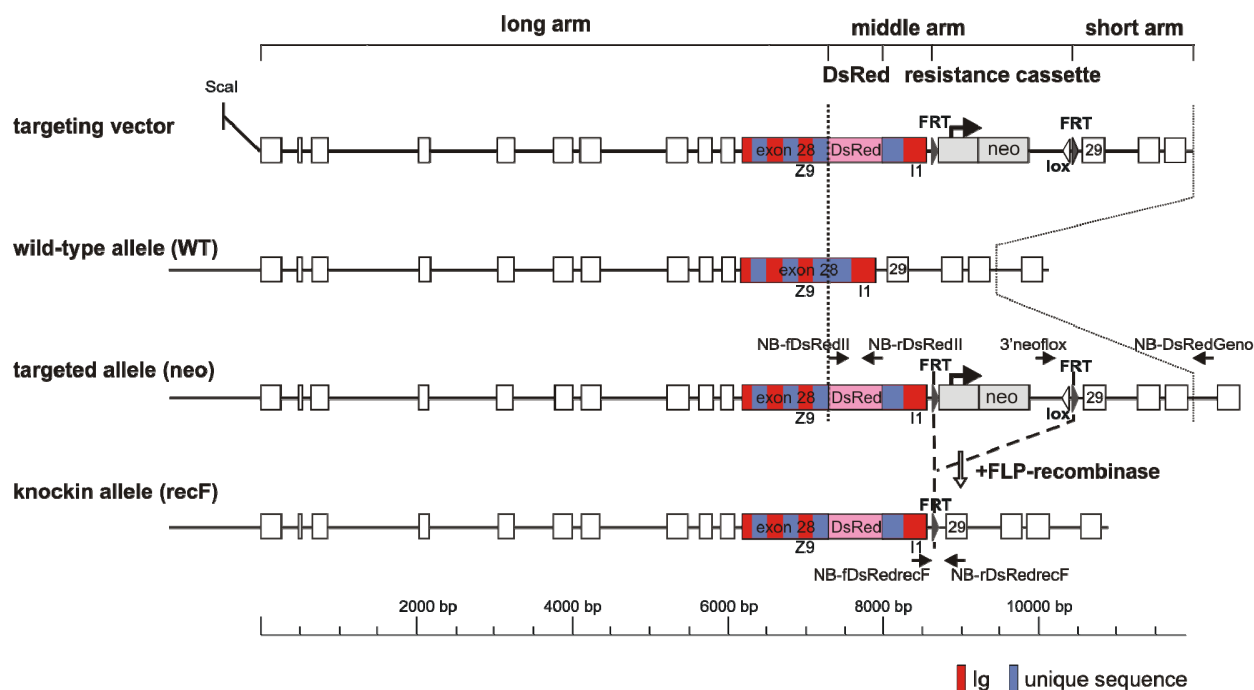


**Figure 7: Targeting strategy to insert the red fluorescence protein DsRed.** The illustration shows the exon/intron (boxes/lines) structure of the titin gene at the Z/I-junction of the sarcomere spanning the region from exon 18 to exon 31. In the targeting vector, the DsRed coding sequence was inserted into the exon 28. Homologous recombination of the targeting vector, which was linearized with the enzyme ScaI, into the wild-type (WT) allele in ES cells led to the targeted allele (neo). After germline transmission, the neomycin resistance cassette (neo) flanked by two FRT-sites (FRT) was removed by the FLP-recombinase leading to mice carrying the knockin allele (recF) including the DsRed and one FRT-site. Primers for genotyping are indicated as arrows. The coding regions for the Ig domains (red) and the unique sequences (blue) are shown for the exon 28 and the Ig domains Z9 and I1 are specified.

The targeting vector DsRedKI was assembled using a PCR-based strategy, in which the PCR fragments were cloned into a vector containing the neomycin resistance cassette (supplement Figure 30). Verification of the targeting vector was done by restriction digest with BamHI, Bsp1407I, NcoI, and ScaI leading to DNA fragments in the predicted sizes (Figure 8; BamHI 8108 bp, 4618 bp, 2621 bp; Bsp1407I 10346 bp, 4378 bp, 623 bp; NcoI 11301 bp, 3223 bp, 823 bp; ScaI 15347 bp).

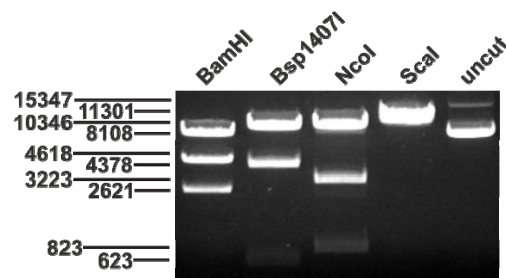


**Figure 8: Verification of the targeting vector DsRedKI.** Restriction digest with BamHI, Bsp1407I, NcoI, and ScaI show the predicted fragment sizes (BamHI 8108 bp, 4618 bp, 2621 bp; Bsp1407I 10346 bp, 4378 bp, 623 bp; NcoI 11301 bp, 3223 bp, 823 bp; ScaI 15347 bp) on a DNA-agarose gel. Uncut targeting vector was used as control.

The coding regions and the neomycin resistance cassette including the FRT-sites were sequenced to ensure that no mutations have occurred. The unique ScaI restriction site within targeting vector and was used for linearization before the ES cell targeting.

### 5.1.2 Generation of the titin-DsRed knockin mouse strain TiEx28DsRed

Two gene targeting experiments were done to insert the targeting vector by homologous recombination into the genome of mouse ES cells resulting in 384 clones that were screened by PCR for the integration of the targeting vector into the titin locus. This ES cell genotyping PCR was established with the help of the cloned control vector, which was used as template in different amounts (Figure 9A). The sensitivity of the ES cell genotyping PCR reached 100 fg with plasmid DNA, but a very weak signal was also noticeable at 15 fg.

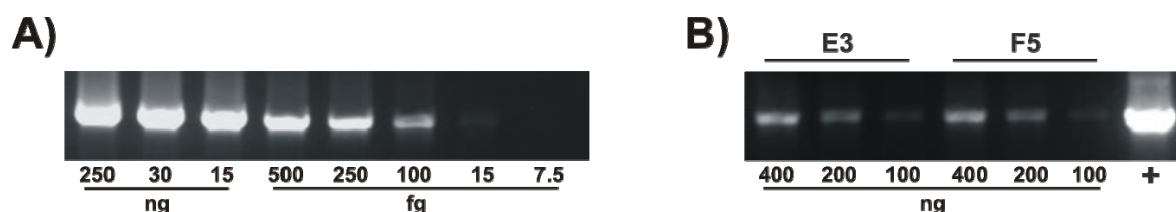


**Figure 9: ES cell genotyping by PCR.** A) Establishing the PCR using the control vector in different amounts as indicated. This PCR is sensitive to detect 100 fg of plasmid DNA as visible by the 1971 bp PCR product of the expected size on an agarose-gel. A very weak PCR-signal was also noticeable at 15 fg. B) The ES cell clones E3 and F5 were identified out of 384 clones by PCR for having incorporated the targeting vector into the titin gene by homologous recombination. Thereby, three different concentrations of DNA as indicated as well as the control vector as positive control (+) were used for the PCR.

The ES cell genotyping PCR indentified the targeted ES cell clones E3 and F5 for having incorporated the targeting vector into the titin gene (Figure 9B). To test the expression of the

DsRed within the titin gene and the proper incorporation of the titin-DsRed into the sarcomere, ES cells from the clones E3 and F5 were differentiated into cardiomyocytes via embryoid bodies. 17 days after forming aggregates, cell clusters beat indicating the presence of cardiomyocytes in the culture. Since it was not possible to detect fluorescence emitted by the DsRed, the cells were stained using an antibody against DsRed. Additionally, a  $\alpha$ -actinin antibody was used to confirm the localization of the red fluorescence protein close to the Z-disc of the sarcomere (Figure 10).

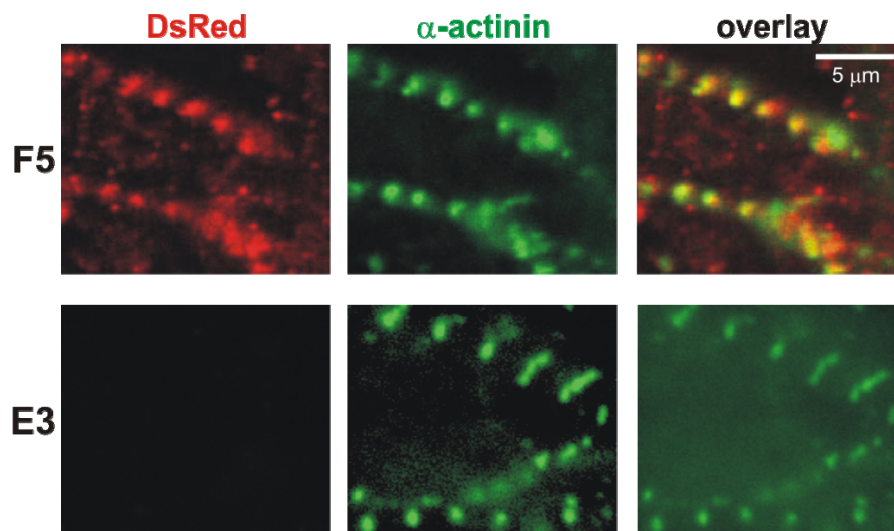


**Figure 10: Proper localization of titin-DsRed in the sarcomere.** Immunostaining using an antibody against DsRed (red) and  $\alpha$ -actinin (green) of embryoid bodies obtained from the ES cell clones F5 and E3 that were differentiated into beating cardiomyocytes (n=3). For clone F5, DsRed colocalized with  $\alpha$ -actinin (yellow, overlay) indicating that DsRed is present at the Z-disc close to titin's N-terminus, which is incorporated properly into the sarcomere leading to a striated pattern. The presence of cardiomyocytes obtained from clone E3 was confirmed by the  $\alpha$ -actinin staining, but it was not possible to detect the DsRed.

The striated pattern of the DsRed staining (red) showed the proper incorporation of the titin-DsRed into the sarcomere of cardiomyocytes derived from the ES cell clone F5. The presence of the DsRed at the Z-disc was demonstrated by its colocalization (yellow, overlay) with the Z-disc protein  $\alpha$ -actinin (green). It was not possible to detect DsRed antibody staining in cells of the ES cell clone E3, although the striated pattern of  $\alpha$ -actinin confirmed the presence of cardiomyocytes. Since cardiomyocytes derived from the clone F5 expressed titin-DsRed, ES cells from this clone were injected into blastocysts to generate chimeric mice. Two blastocyst injections resulted in nine chimeras. Five chimeric animals had a brown coat color of more than 70% indicating a high contribution from the ES cell clone and a low contribution of the host C57BL/6 blastocyst, which would lead to a black fur. All chimeras were bred with C57BL/6 mice and thereby germline transmission of the targeted allele was obtained. Genotyping of mice,

which were used to establish and maintain the TiEx28DsRed strain, was done by PCR (Figure 11) with primers as indicated in Figure 7. Mice that show PCR products in the expected sizes were used for further breeding.

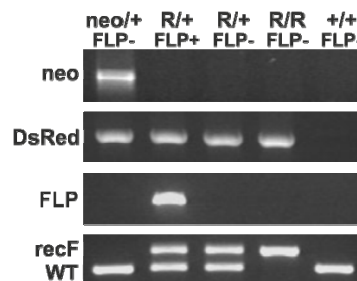


**Figure 11: Genotyping of TiEx28DsRed animals.** PCR-analysis of the possible genotypes (wild-type +/+ FLP-; heterozygous neo/+ FLP- and R/+ FLP+ or FLP-; homozygous R/R FLP-; neo: neomycin resistance cassette; R: DsRed) revealed, that neo/+ FLP- mice incorporated the targeting vector with neomycin resistance cassette in the titin gene (neo-PCR 1971 bp) including the coding sequence for the DsRed (DsRed-PCR 693 bp). To remove the neomycin resistance cassette, these animals were mated with FLP-transgene mice leading to double heterozygous R/+ FLP+ mice. They contain the FLP-transgene (FLP-PCR 480 bp) as well as a recombined targeted allele (recF 369 bp) and a titin wild-type allele (WT 282 bp). In the next generation, the FLP-transgene was crossed out leading to R/+ FLP- mice, which were used for breeding to establish the TiEx28DsRed strain colony resulting also in homozygous knockin (R/R FLP-) and wild-type control mice (+/+ FLP-).

The first sign of germline transmission was the appearance of pups with brown coat color, which were investigated for the presence of the DsRedKI targeting construct in the titin gene. This was done with one primer binding within the neomycin resistance cassette and the other binding in the titin gene outside of the genomic region present in the targeting vector (neo-PCR). These animals were additionally genotyped for the presence of the DsRed coding sequence (DsRed-PCR). Since the neomycin resistance cassette can affect the phenotype of genetically engineered mice (Kaul et al., 2000), heterozygous animals carrying the targeting vector (neo/+ FLP-) were bred with FLP-transgene mice leading to double heterozygous mice (R/+ FLP+; DsRed and FLP-PCR). The deletion of the neomycin resistance cassette by the FLP-recombinase was controlled by the recF-PCR resulting in a recF as well as a wild-type (WT) band. Both PCR products were formed because recombination had occurred in heterozygous animals that carry also one wild-type allele. Animals carrying heterozygous the targeting vector (neo/+ FLP-) show a wild-type signal in the recF-PCR as well. In the next generation, the FLP-transgene was crossed out to obtain heterozygous animals (R/+ FLP-; DsRed and recF-PCR). They were used to generate the colony of the TiEx28DsRed strain. Thereby, also homozygous knockin animals (R/R FLP-) that show only the recF PCR product as well as wild-type controls (+/+ FLP-) that show only the wild-type PCR product were born (DsRed and recF-PCR). Animals obtained by heterozygous breeding were used for analysis.

### 5.1.3 Verification of the titin-DsRed protein and its localization within the sarcomere

Since introducing of the DsRed coding sequence altered the titin gene, we had to exclude that expression of titin-DsRed results in an obvious phenotype regarding viability and fertility. Therefore, offspring from breeding of heterozygous male and female mice was investigated for the distribution of the genotype. We found normal Mendelian ratios of 23.25% (n=10) wild-type, 53.5% (n=23) heterozygous knockin, and 23.25% (n=10) homozygous knockin mice examining in total 43 animals. Also the distribution of 46.5% (n=20) males and 53.5% (n=23) females were as expected and mice of all genotypes had a normal lifespan. Figure 12 shows that the body weight with ~24.5 g and the ratio of heart weight to body weight (corrected heart weight) with ~4.8 mg/g for wild-type (+/+), heterozygous (R/+) and homozygous (R/R) female mice were unchanged. These data indicate that the integration of the DsRed into the titin protein did not affect apparently the structure and function of the heart and skeletal muscle.

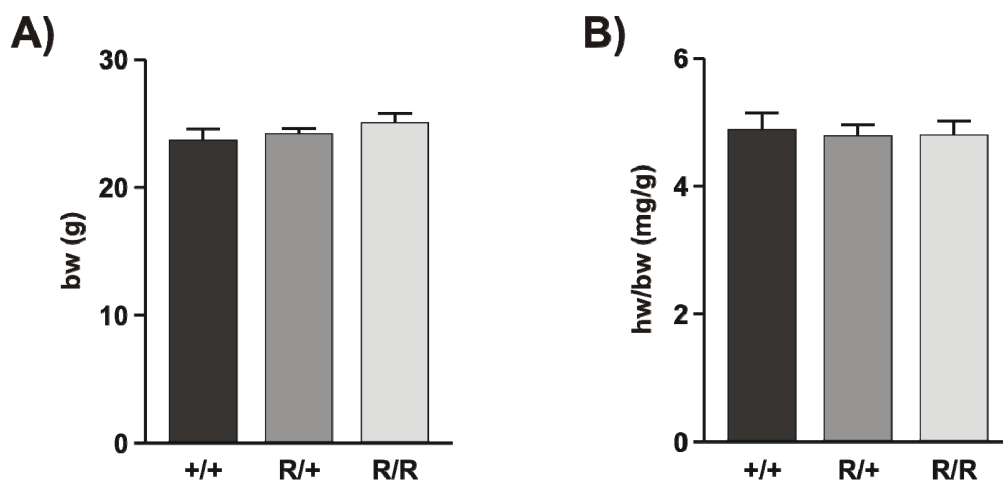


**Figure 12: Titin-DsRed knockin mice did not have an obvious phenotype.** Heterozygous (+/R; n=6) and homozygous (R/R; n=5) female animals had an equal body weight (A) as well as heart weight to body weight ratio (B) compared to the littermate wild-type control (+/+; n=7; mean with SEM; One-way ANOVA  $P > 0.5$ ).

TiEx28DsRed mice did not have an obvious phenotype so that it was possible to further investigate the mouse model on protein level. Therefore, we used a SDS-agarose gel to separate the titin-isoforms and Western blotting (Figure 13) using samples of the striated muscles heart, quadriceps, and soleus, in which titin is well studied.

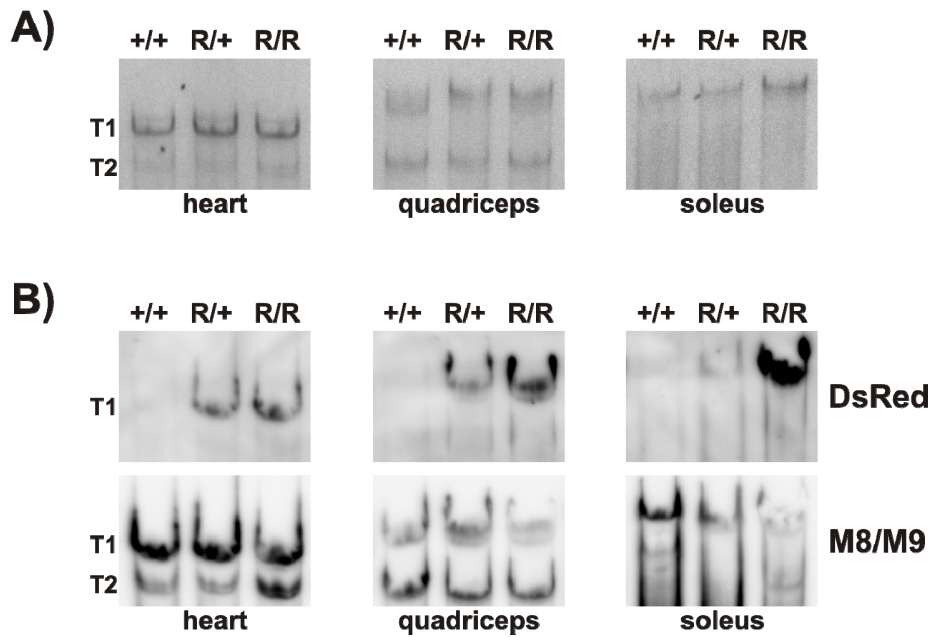


**Figure 13: Detection of titin-DsRed in heart, quadriceps, and soleus.** A) Coomassie stained SDS-agarose gel shows separation of the T1 N2B (2970 kDa) and N2BA (3300 kDa) isoforms of the heart, the two N2A isoforms of the quadriceps and the long N2A isoform (3700 kDa) in the soleus as well as the T2 degradation product (~2000 kDa) in samples from wild-type (+/+; n=3), heterozygous (R/+; n=3) and homozygous (R/R; n=3) mice. B) Western blot using a DsRed antibody verified the presence of DsRed in T1 full-length titin of heterozygous (n=3) and homozygous knockin mice (n=3). The M8/M9 antibody used in Western blot detected T1 and T2 titin demonstrating the translation of titin's C-terminus in striated muscle samples of all genotypes (n=3).

The SDS-agarose gel shows that it was possible to separate the T1 N2B (2970 kDa) and N2BA (3300 kDa) isoforms of the heart and the two T1 N2A isoforms of the quadriceps as well as the T2 degradation products (Figure 13A). In the soleus, the longest T1 N2A isoform (3700 kDa) was observed. All titin isoforms and the corresponding smaller T2 degradation products (~2000 kDa) were present in wild-type (+/+), heterozygous (R/+), and homozygous (R/R) mice demonstrating that the DsRed did not affect the expression and translation of full length titin in striated muscle. Furthermore, the existence of the same amount of titin isoforms in the three genotypes in the heart, quadriceps, and soleus indicates that the DsRed insertion did not affect protein stability. Since the DsRed has a calculated molecular weight of 26.8 kDa, which is small compared to titin isoforms of up to 3700 kDa in striated muscle, it was not possible to separate in heterozygous knockin mice the titin-DsRed from the wild-type titin molecules. To ensure, that the DsRed was present within titin, Western blot was performed using a DsRed antibody (Figure 13B). We detected a strong signal from the T1 isoforms in the heart, quadriceps, and soleus samples of homozygous mice and a weaker signal in the samples of heterozygous mice because homozygous knockin mice carry only the titin-DsRed and the heterozygous knockin mice expressed titin-DsRed as well as wild-type titin. The titin isoforms in the samples from wild-

type littermate controls served as a negative control. Figure 13B confirms with the help of the M8/M9 antibody, which is reacting against titin's C-terminal region, that full length titin was translated in wild-type, heterozygous, and homozygous mice. In contrast to the DsRed-antibody, which did not detect the degradation product T2, the M8/M9 antibody identified T1 and T2.

As intended by the targeting strategy, DsRed was expressed and translated within full length titin in knockin mice of the TiEx28DsRed strain. To investigate the DsRed localization and its influence on titin's integration into the sarcomere, fluorescence microscopy of cryosections was performed using quadriceps as an example of skeletal muscle and heart (Figure 14). It was possible to monitor the fluorescence emitted by the DsRed (red) in heterozygous (R/+) and homozygous (R/R) knockin mice in both heart (A) and quadriceps (B). A weaker signal was detected in heterozygous mice because they carry titin-DsRed as well as wild-type titin. No signal was detected in control wild-type mice (+/+). The DsRed fluorescence appeared as striated pattern indicating that the incorporation of titin into the sarcomere and thereby also sarcomere assembly was normal. The localization of the DsRed close to titin's N-terminus was confirmed using an M8/M9-antibody (green) that marks the M-band. This immunostaining led to a striated pattern for all genotypes in heart and quadriceps due to the highly ordered arrangement of the sarcomeres in striated muscle. Overlay with the DsRed fluorescence (overlay) shows an alternating striated pattern. This demonstrates the constant series of Z-discs and M-bands in the striated muscle of heterozygous and homozygous knockin mice confirming the presence of DsRed at the Z-disc. Thus, titin-DsRed integrated into the Z-disc and M-band so that the sarcomeric structure was not influenced by the insertion of the DsRed into the titin's Z/I-junction. The targeting strategy was successful and we were able to establish the new titin-DsRed knockin mouse model TiEx28DsRed, which will help to visualize and analyze titin in smooth muscle.



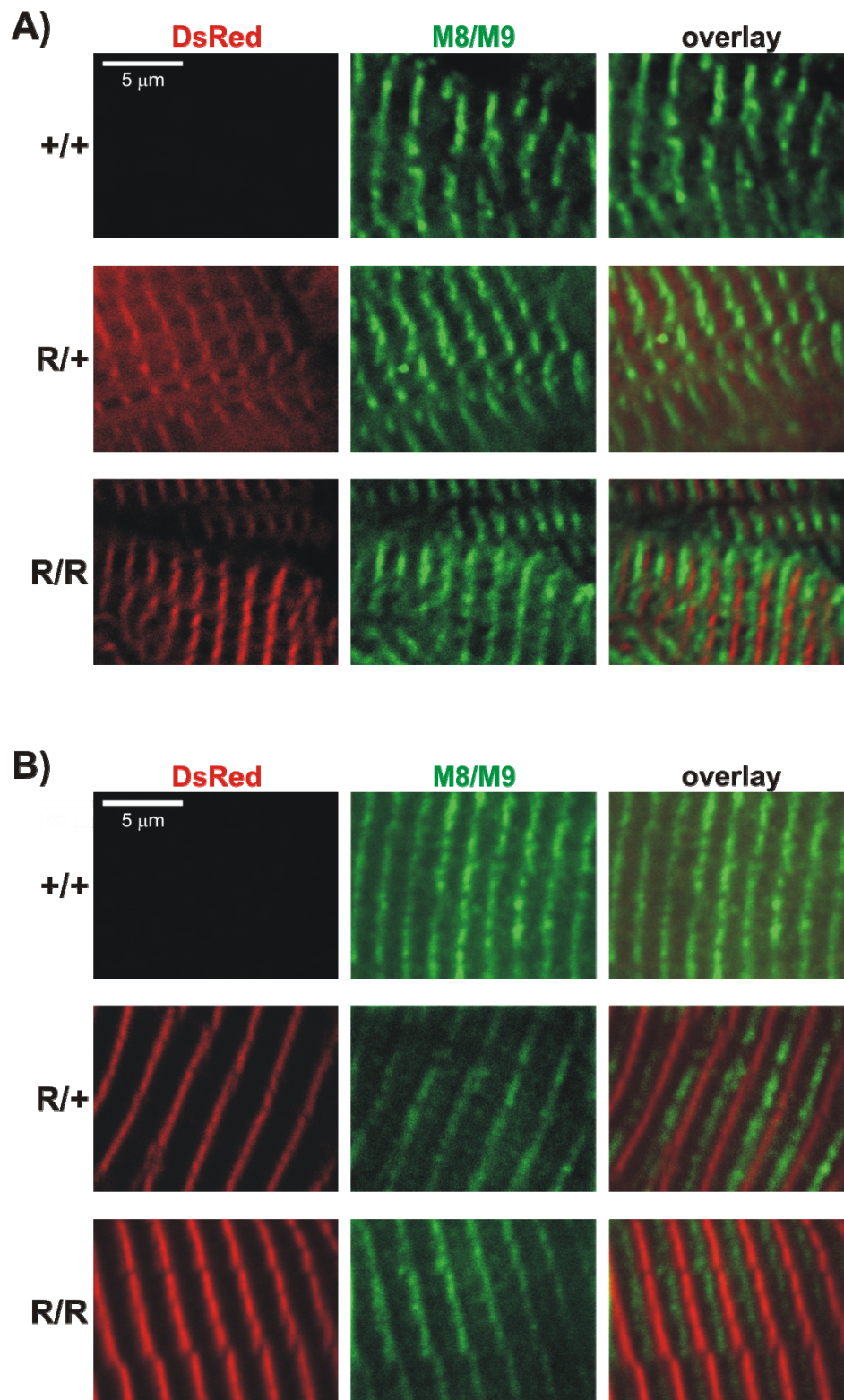


**Figure 14: The DsRed located close to titin's N-terminus did not influence the sarcomeric structure.** Fluorescence microscopy of (A) heart and (B) quadriceps cryosections obtained from wild-type (+/+; n=3), heterozygous (R/+; n=3) and homozygous (R/R; n=3) mice. Fluorescence was emitted by the DsRed (red) in heterozygous and homozygous knockin animals and appeared as striated pattern demonstrating that the sarcomere assembly was normal. Immunostaining with an antibody against the immunoglobulin domains M8 and M9 at titin's C-terminus marking the M-band resulted in a striated pattern for all genotypes (green). The overlay of the M8/M9 staining with the DsRed fluorescence shows an alternating striated pattern (overlay) demonstrating a constant series of Z-discs and M-bands in striated muscle of heterozygous and homozygous mice. This indicates the presence of the DsRed close to titin's N- terminus. Bar: 5 μm.



## 5.2 Characterization of the smooth muscle specific knockout of titin's kinase region

### 5.2.1 Establishing the smooth muscle specific mouse model

For analysis of the titin's kinase region in smooth muscle, the conditional knockout mouse model TiMEx1-2 (Gotthardt et al., 2003) was used, in which titin's M-band exons 1 and 2 that correspond to titin's exons 358 and 359, are flanked by two lox-sites (Figure 15 floxed allele). The conditional mouse model was bred with a transgenic mouse strain (SMMHCcre), which expresses the cre-recombinase under the control of the smooth muscle myosin heavy chain promoter, mediating the deletion of titin's M-band exons 1 and 2 by recombination of the lox-sites in the generated SMcTiMEx1-2 mouse strain (Figure 15 deleted allele).

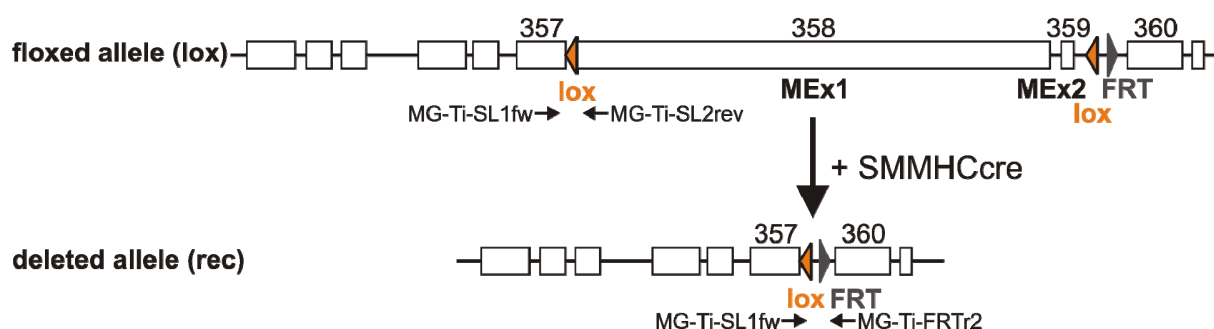


**Figure 15: Strategy to delete titin's kinase region in smooth muscle.** Exon/intron (boxes/lines) structure of the titin gene close to its 3'end as present in the conditional knockout model TiMEx1-2. Titin's M-band exons 1 and 2 (titin exons 358 and 359) encoding the kinase region, which are flanked by two lox-sites (floxed allele), are deleted (deleted allele) by breeding with transgene animals expressing the cre-recombinase under the control of the smooth muscle myosin heavy chain promoter (SMMHCcre) leading to the SMcTiMEx1-2 mouse strain. Primers for genotyping the titin alleles are indicated as arrows. Modified from Gotthardt et al., 2003.

Our aim was to study the effect of the deletion of titin's kinase region in smooth muscle on uterus, because pregnancy involves contraction as well as tissue remodeling. It has been shown, that the SMMHC cre-recombinase is present from E12.5 in smooth muscle (Xin et al., 2002), but its recombination activity in uterine tissue has not been confirmed. Therefore, SMMHCcre mice were crossed with GtROSA26 reporter mice to monitor cre-recombinase activity in the generated SMcGtROSA26 strain. Figure 16 shows the lacZ staining of cryosections obtained from uteri in the estrous stage of 90 d old adult females. The sections were counterstained with eosin so that the cytoplasm and connective tissue appears red.



**Figure 16: Activity of the SMMHC cre-recombinase in uterine smooth muscle.** LacZ staining (blue) counterstained with eosin (red) of uterine cross sections shows that the SMMHCcre was active leading to recombination in circular and longitudinal smooth muscle cells in the uterus of animals that contain the lacZ reporter gene as well as the cre-recombinase transgene (lacZ<sup>+</sup> cre<sup>+</sup>; n=3). The negative controls, either the lacZ reporter gene (lacZ<sup>+</sup>, cre<sup>-</sup>; n=3) or the cre-recombinase transgene (lacZ<sup>-</sup>, cre<sup>+</sup>; n=3), did not give a signal in the LacZ staining. cSMCs: circular smooth muscle cells; ge: glandular epithelium; l: lumen; le: luminal epithelium; ISMCs: longitudinal smooth muscle cells; myo: myometrium; s: stroma ; bar: 100  $\mu$ m.

In animals that carried the *lacZ* reporter gene (lacZ<sup>+</sup>) as well as the cre-recombinase transgene (cre<sup>+</sup>) recombination mediated by the cre-recombinase has occurred in myometrial circular and longitudinal smooth muscle cells. This cre-recombinase activity led to *lacZ* expression and the presence of the  $\beta$ -galactosidase, which is visible by the blue lacZ staining. The negative staining controls of mice containing either the *lacZ* reporter gene (lacZ<sup>+</sup>, cre<sup>-</sup>) or the cre-recombinase transgene (lacZ<sup>-</sup>, cre<sup>+</sup>) did not show *lacZ* expression indicating that endogenous  $\beta$ -galactosidase is not sufficient for recombination and the cre-recombinase alone cannot cause lacZ staining. Since we could show that the cre-recombinase under the control of the smooth muscle myosin heavy chain promoter is active in the uterine smooth muscle, we investigated recombination in uterus and tail of SMcTiMEx1-2 and SMMHCcre animals in estrous stage by PCR (Figure 17A).

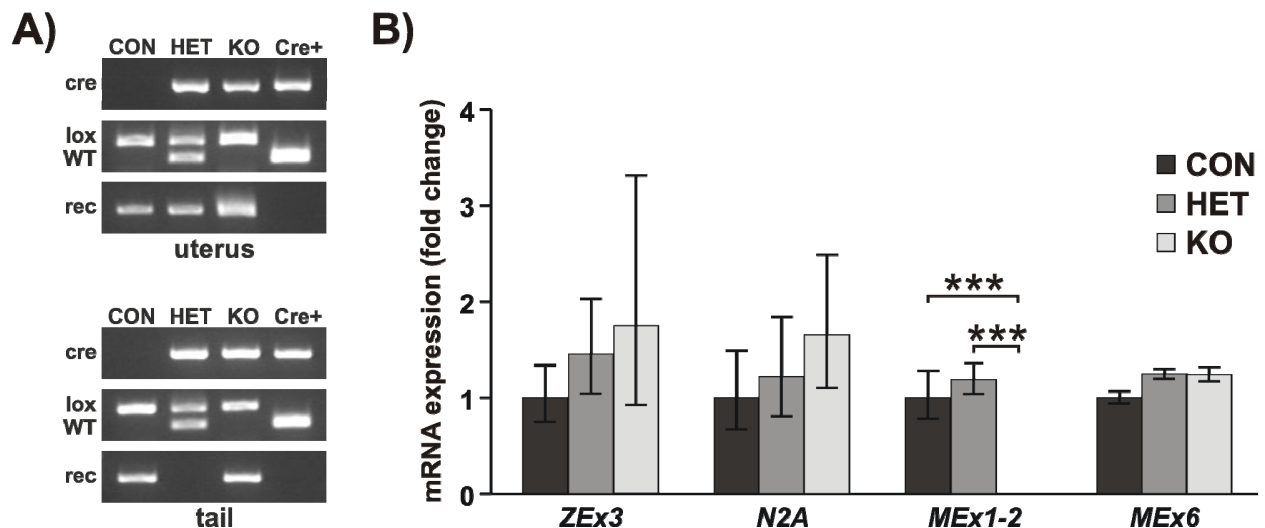


**Figure 17: Recombination by the SMMHC cre-recombinase in uterine smooth muscle and the germline.** A) PCR-analysis of uterine and tail tissues obtained from control (CON), heterozygous (HET), and knockout (KO) mice of the SMcTiMEx1-2 strain and animals of the SMMHCcre strain containing the transgene (Cre+) in estrous stage. The tissues were genotyped for the presence of the floxed titin allele (lox) or the corresponding wild-type allele (WT) and the cre transgene (cre). Recombination (rec) has occurred not only in the uterus of knockout and heterozygous mice as expected, but also in the uterus of control mice and in tails of control and knockout mice indicating smooth muscle but also germline activity of the cre-recombinase. Primers to obtain WT, lox, and rec signals are given in Figure 15. B) Real-Time PCR analysis revealed the expression of titin's exons encoding parts of the N-terminus (*ZEx3*), N2A region (*N2A*) and C-terminus (*MEx6*) in control (n=3), heterozygous (n=3), and knockout (n=3) mice as well as the lack of mRNA encoding titin's kinase region (*MEx1-2*) in knockout animals (mean with SEM; Two-way ANOVA  $P < 0.001$  \*\*\*). The mRNA levels were normalized to 18S RNA and expression is displayed as fold change relative to the control.

To confirm the genotype of control, heterozygous, and knockout mice of the SMcTiMEx1-2 strain and of SMMHCcre animals containing the transgene (Cre+), tail and uterine tissues were first analyzed for the presence of the floxed titin allele as well as the cre transgene. As expected for both tissues, control and knockout mice carried homozygous the floxed allele (lox), heterozygous mice had a floxed as well as a wild-type allele (WT), and Cre+ control mice had only the titin wild-type allele. The cre transgene (cre) was present in the Cre+ control, heterozygous, and knockout mice. DNA of control mice did not lead to a signal in the cre-PCR. The PCR detecting the recombination of the floxed titin allele (rec) revealed that recombination occurred in uteri of knockout, heterozygous, and unpredicted also in control mice, but not in Cre+ control animals. Additionally, control and homozygous mice were recombined in the tail. Since recombination was observable in uteri of control animals and also in tails of control and knockout mice, we concluded that beside the smooth muscle recombination, which is shown by the recombination in heterozygous animals and in Figure 16, also unspecific recombination has happened independent of the presence of the cre-recombinase. This finding was confirmed by de Lange et al. (de Lange et al., 2008), who described the germline activity of the SMMHC

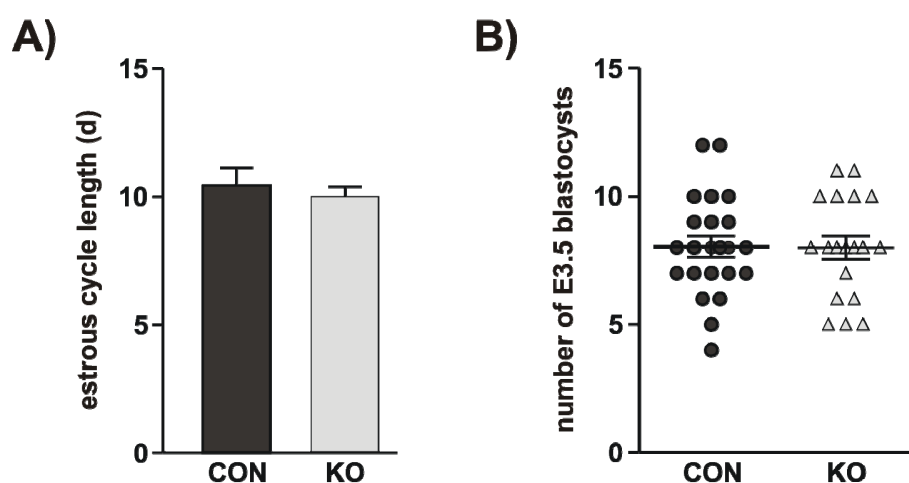
promoter. They showed that the activity of the cre-recombinase in male germ cells is irrespective of the cre-genotype and ends prior to fertilization.

The amount of titin mRNA after deletion of titin's M-band exons 1 and 2 in non-pregnant uterus was quantified by Real-Time PCR (Figure 17B). It revealed the expression of titin regions including the N2A region (*N2A*) as well as the N- and C-terminus represented by the Z-disc exon 3 (*ZE<sub>x</sub>3*) and the M-band exon 6 (*MEx<sub>6</sub>*) in uterus of control, heterozygous, and knockout mice of the SMcTiMEx1-2 strain. In opposition to control and heterozygous mice, the mRNA of titin's M-band exons 1 and 2 (*MEx1-2*) could not be detected anymore in knockout animals. Nevertheless, the expression of titin's C-terminus was not affected by the deletion of the M-band exons 1 and 2 coding for the kinase region in these females.

## 5.2.2 Titin's kinase region is essential for embryo implantation

### 5.2.2.1 Normal preimplantational embryo development in titin's kinase region deficient mice

We were able to efficiently delete titin's M-band exons 1 and 2 encoding the kinase region in knockout mice. Knockout animals did not have an obvious phenotype so that we generated a suitable mouse model to address a smooth muscle function of titin's kinase region during pregnancy. To distinguish effects on non-pregnant uterus and preimplantational embryonic development from effects during embryo implantation, we investigated the estrous cycle length of non pregnant uteri and the number of E3.5 blastocysts (Figure 18).



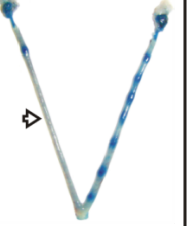









**Figure 18: Normal estrous cycle length and number of blastocysts in knockout females.** A) The days (d) of estrous cycle length did not differ between control (CON; n=7) and knockout animals (KO; n=7; mean with SEM; T-test  $P>0.05$ ). B) The number of blastocysts at E3.5 recovered from control (n=23) and knockout animals (n=19) was the same in both groups (mean with SEM; T-test  $P>0.05$ ).

The estrous cycle did not vary between knockout and control mice (~10.0 d and ~10.4 d, respectively; Figure 18A). Furthermore, metestrus, diestrus, proestrus, and estrus were clearly distinguishable in control and knockout females including the typical presence of leucocytes and epithelial cells. Hence we concluded that the deletion of titin's kinase region did not affect the recurring changes of the non pregnant uterus in response to ovarian hormones so that we were able to set up timed matings to obtain pregnant females. The amount of blastocysts at E3.5 was the same for control and knockout mice (~8; Figure 18B). There was also no difference in morphology of blastocysts recovered from control and knockout uteri. These data demonstrated normal ovulation, fertilization, transport of the developing embryo through the oviduct, and blastocyst development.

#### 5.2.2.2 Impaired implantation affects embryo positioning, number of implantation sites, and uterine maturation

Embryo implantation studies were done at E4.5 and E5.5 to investigate the implantation time and positioning of the embryos within the uterus. Figure 19 shows that the loss of titin's kinase region led to clear phenotypic changes as visualized by Evans Blue staining.

	CON	KO			
	normal	IS < 5	mislocalized	crowding	normal
<b>E4.5</b>					
	89.5% (17)	22.7% (5)	22.7% (5)	13.6% (3)	41% (9)
<b>E5.5</b>					
	91% (21)	22.7% (5)	27.3% (6)	13.6% (3)	36.4% (8)

**Figure 19: Impaired embryo implantation in knockout females.** Evans Blue staining at E4.5 and E5.5 shows on-time implantation that is impaired in knockout (KO) uteri resulting in a reduced number of implantation sites (IS < 5, blue), mislocalization (white arrows indicate lack of implantation sites), and crowding (black arrows) compared to the equally distributed implantation sites in control (CON) mice. The percent distribution as well as the total number of investigated animals is indicated. Bar: 1 cm.

Embryo implanted on-time in knockout females because implantation sites (IS) were already detectable at E4.5 as in control mice. The implantation sites were equally distributed on both uterine horns and evenly spaced in ~90% of the control uteri at E4.5 and E5.5. In contrast, only ~39% of the knockout mice had a normal implantation pattern at either time point. We classified the uteri with impaired implantation into three groups with consistent distribution at E4.5 and E5.5. Knockout uteri showed in 22.7% less than five implantation sites and in 13.6% crowding of two or more implantation sites, whereas this clustering did not occur in a special segment of the uterus. The positioning of the implantation sites were considered to be mislocalized, if more than triple implantation sites were found in one uterine horn compared to the other. This was the case in ~24% of knockout animals. Rarely, knockout uteri exhibited multiple defects.

We investigated the number of implantation sites at E4.5 and E5.5 of control and titin kinase deficient knockout mice in more detail (Figure 20A).

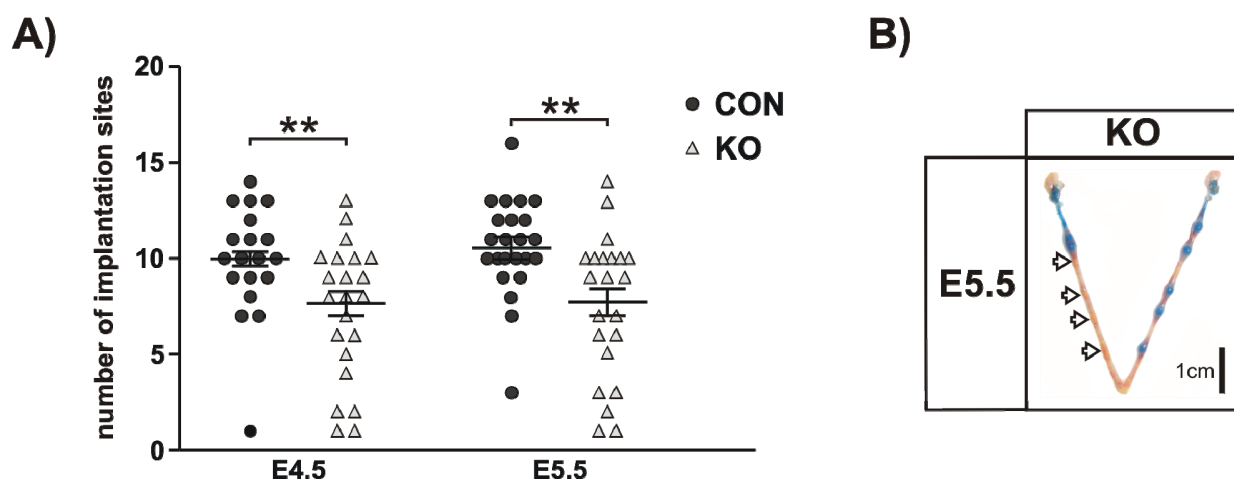


**Figure 20: Reduced number of implantation sites in knockout uteri implies a defect during the penetration phase.** A) The number of implantation sites at E4.5 and E5.5 varied more in knockout mice (KO; E4.5 n=22; E5.5 n=22) compared to control animals (CON; E4.5 n=19; E5.5 n=23) and was additionally significantly reduced by ~26% (mean with SEM; Two-way ANOVA  $P < 0.01$  \*\*). B) In one knockout uterus it was possible to observe embryos that have attached but did not develop further as shown by lack in Evans Blue staining at E5.5 (white arrows). Bar: 1 cm.

At E4.5 and E5.5, the number of implantation sites varied more in knockout animals compared to control mice and was additionally significantly reduced by ~26%. Since comparable numbers of blastocysts were available for implantation in control and knockout uteri and the diminished amount of implantation sites in knockout uteri was identical at E4.5 and E5.5, we concluded that the loss of titin's kinase region led to defects during the penetration phase of embryo implantation, whereas apposition and attachment were not affected. This finding was confirmed by one knockout uterus, in which four implantation sites have not further developed (Figure

20B). It was also not possible to get blastocysts from E4.5 uteri that showed a reduced number of implantation sites indicating proper embryo attachment.

The change of the uterine wet weight in response to embryo implantation was determined as an index for vascularization and decidualization, which occur during the penetration phase. The uterus weight of knockout and control animals at E3.5, E4.5, and E5.5 was measured and normalized to the body weight. E3.5 was confirmed by the presence of blastocysts and only uteri with ten implantation sites were taken into account for E4.5 and E5.5 (Figure 21).

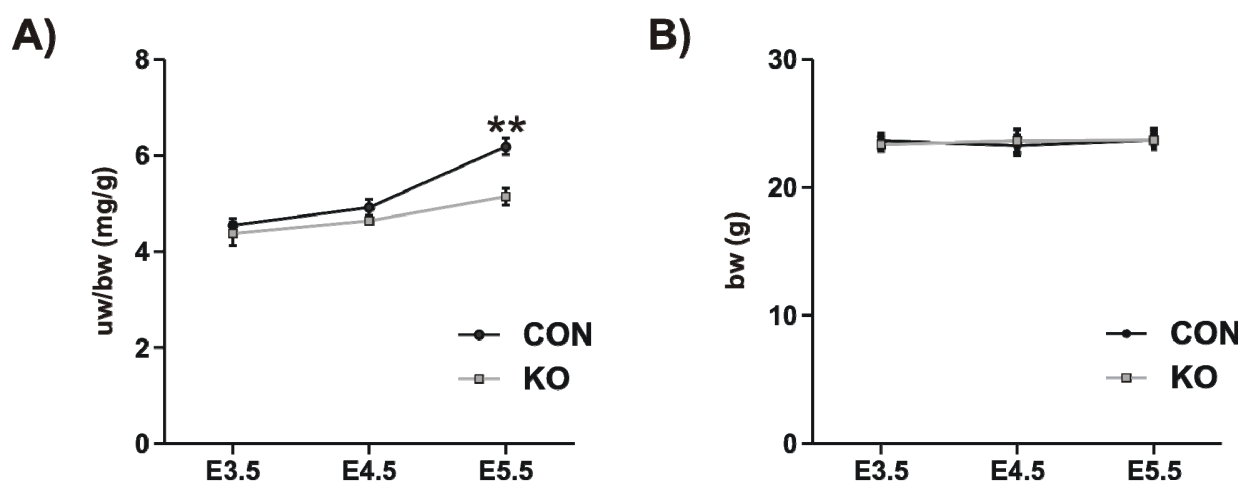


**Figure 21: Delayed development of knockout uteri during the penetration phase.** A) Between E3.5 to E5.5 the uterus weight to body weight (uw/bw) ratio of knockout (KO) and control (CON) animals increased continuously. There was no difference between knockout and control animals at E3.5 (KO n=10; CON n=11) and E4.5 (KO n=4; CON n=4), but knockout uteri showed a decreased uterus weight to body weight ratio at E5.5 (KO n=6; CON n=6; mean with SEM; Two-way ANOVA  $P < 0.01$  \*\*). E3.5 was determined by the presence of blastocysts and for E4.5 and 5.5 only uteri with 10 implantation sites were used for evaluation. B) The delayed development of the knockout uteri was independent of the body weight (bw), which did not differ between control and knockout mice at E3.5, E4.5, and E5.5 (mean with SEM; Two-way ANOVA  $P > 0.05$ ).

The uterus weight to body weight (uw/bw) ratio of knockout and control animals increased steadily from E3.5 to E5.5 (Figure 21A). In contrast to E3.5 and E4.5, knockout uteri had a decreased uterus weight to body weight ratio at E5.5 in comparison to control females. This reduction in the uterus weight to body weight ratio was independent of the body weight that did not vary between the two groups and the investigated time points (Figure 21B). Since the increase of the uterus weight in the milligram range cannot be due to the developing embryo during early pregnancy, we could show that the absence of the titin kinase region in smooth muscle led to delayed uterine development in the penetration phase of embryo implantation. Additionally, the heart weight to body weight ratio was determined using the same set of animals (supplement Figure 31). There was no difference between control and knockout animals



indicating that the deletion of titin's kinase region in vascular smooth muscle cells did not cause an obvious phenotype.

To exclude, that the presence of the cre-recombinase in smooth muscle of knockout animals resulted in the implantation defects, embryo implantation studies were also conducted with heterozygous and Cre<sup>+</sup> control animals that contained the cre-recombinase (Figure 22). E5.5 was investigated because at this time point knockout females had both impaired implantation and delayed uterine development. Only uteri with ten implantation sites were used for evaluation.

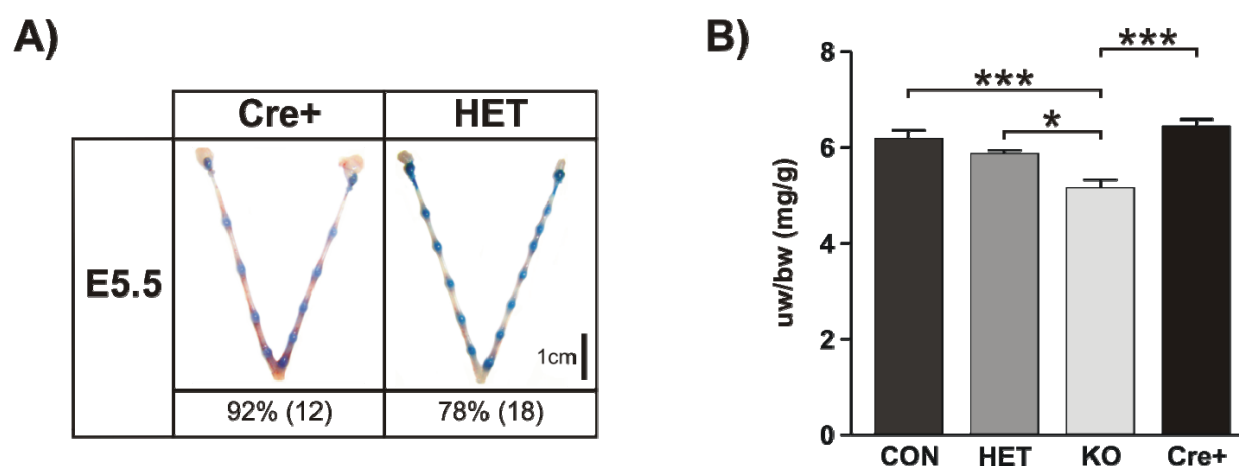


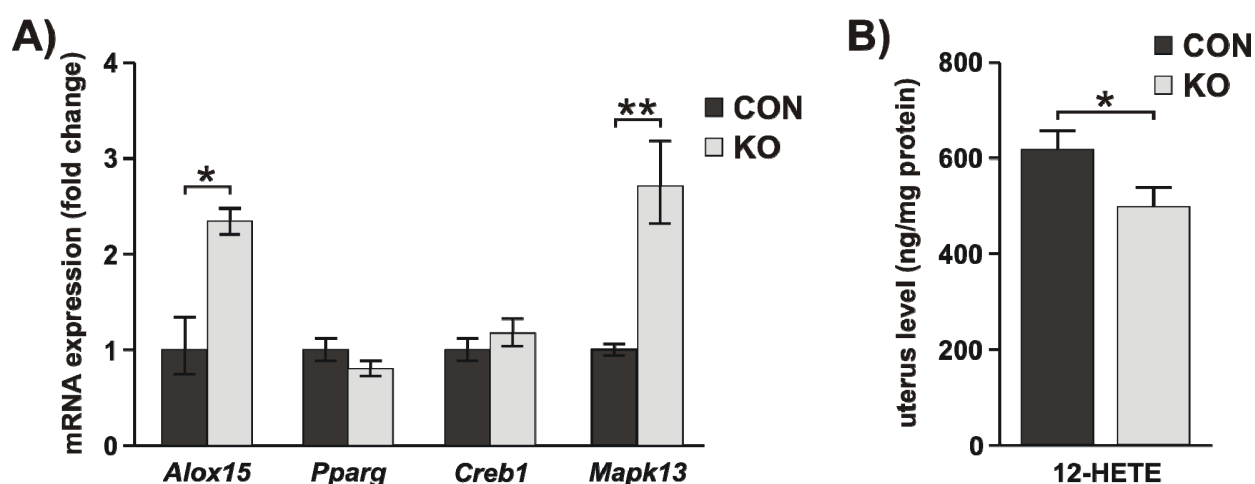
**Figure 22: The phenotype observed in the knockout females was due to the deletion of titin's kinase region.** A) Although containing the cre-recombinase, Cre<sup>+</sup> control (Cre<sup>+</sup>) and heterozygous (HET) mice had normal embryo spacing and distribution as well as more than four implantation sites. The percent distribution and the total number of investigated animals is given. Bar: 1 cm. B) At E5.5, the uterus weight to body weight (uw/bw) ratio of Cre<sup>+</sup> control and heterozygous animals was similar to the control animals (CON). The knockout (KO) uterus weight to body weight ratio was reduced compared to the other three groups (CON n=6; HET n=5; KO n=6; Cre<sup>+</sup> n=3; mean with SEM; one-way ANOVA P<0.05 \* and P<0.001 \*\*\*). Only uteri with 10 implantation sites were taken into account.

As shown by Evans Blue staining in Figure 22A, 92% of the Cre<sup>+</sup> control mice and 78% of the heterozygous mice had a normal implantation including even embryo spacing and a normal number of implantation sites as the control mice (Figure 19). The uterus weight to body weight ratio of Cre<sup>+</sup> control mice and heterozygous mice was similar to the control animals, which were cre-recombinase negative. In contrast, the uterus weight to body weight ratio at E5.5 of knockout animals was reduced compared to littermate control animals as well as to Cre<sup>+</sup> control and littermate heterozygous mice (Figure 22B). This effect was independent of the body weight (supplement Figure 31B). Hence we concluded that the phenotype observed in knockout females was not due to the cre-recombinase, but caused by the deletion of titin's kinase region.



### 5.2.3 Loss of titin's kinase region influences arachidonic acid metabolism

It has been shown that mice with null mutation for *Alox15* that encodes the leukocyte 12/15-lipoxygenase (L-12/15-LOX) have a reduced number of embryo implantation sites (Li et al., 2004) similar to the phenotype we observed in the knockout animals lacking titin's kinase region (Figure 20). Hence we investigated the mRNA level (Figure 23A) of *Alox15* as well as of the genes *Pparg*, *Creb1*, and *Mapk13* encoding the peroxisome proliferator-activated receptor  $\gamma$  (PPAR $\gamma$ ), the cAMP responsive element binding protein 1 (CREB1), and the mitogen-activated protein kinase 13 (MAPK13), which have been implicated to be possible downstream targets of metabolites derived from the L-12/15-LOX (Reddy et al., 2002; Li et al., 2004). Uterine tissue of E3.5 pregnant mice was used because previous work has demonstrated that *Alox15* has the highest expression level at E3.5 (Li et al., 2004).



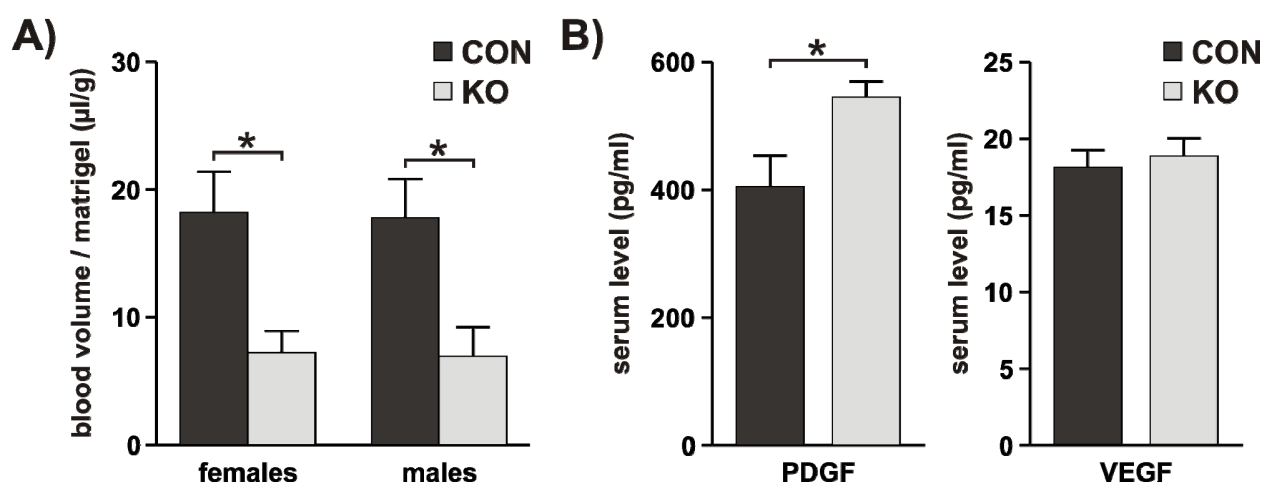
**Figure 23: Deletion of titin's kinase region affected arachidonic metabolism.** A) Real-Time PCR analysis revealed the upregulation of *Alox15* mRNA as well *Mapk13* mRNA in knockout (KO; n=3) compared to control (CON; n=3) animals using E3.5 uterine tissue. The genes *Pparg* and *Creb1* encoding two other possible downstream targets of the L-12/15-LOX, the PPAR $\gamma$  and the CREB1, were unchanged on mRNA level. The mRNA levels were normalized to 18S RNA and expression is displayed as fold change relative to the control (mean with SEM; T-test comparing CON and KO of one primer/probe set  $P < 0.05$  \* and  $P < 0.01$  \*\*). B) Compared to control animals (n=12), the uterine levels of 12-HETE, which is produced from arachidonic acid by the L-12/15-LOX, were reduced by ~20% in E3.5 pregnant knockout females (n=13). The metabolite concentration is displayed relative to the total protein amount in the sample (mean with SEM; T-test  $P < 0.05$  \*).

Figure 23A shows mRNA upregulation of *Alox15* and *Mapk13* in knockout animals compared to control animals. There was no significant difference in the uterine mRNA level of *Pparg* and *Creb1* between both groups. Since the L-12/15-LOX catalyzes among others the formation of 12-HETE from arachidonic acid that is important for embryo implantation (Li et al., 2004),

uterine 12-HETE levels of E3.5 pregnant mice were measured (Figure 23B). The uterine 12-HETE levels in knockout animals were ~20% less in comparison to control animals.

#### 5.2.4 Aberrant angiogenesis in knockout animals lacking titin's kinase region

The adaption of the uterus to enable implantation of the embryo requires changes in vascular permeability and angiogenesis. Since the SMcTiMEx1-2 knockout females had a reduced uterine wet weight in response to embryo implantation (Figure 21), which is a measurement for vascularization and decidualization, we investigated angiogenesis *in vivo* in female and male mice (Figure 24A). The angiogenesis was induced by VEGF because this angiogenic growth factor has been shown to be a key regulator for angiogenesis (Carmeliet et al., 1996; Fong et al., 1995) and also to be necessary for implantation to occur (Rockwell et al., 2002).



**Figure 24: Altered angiogenesis and PDGF-B serum levels in knockout mice.** A) VEGF-induced angiogenesis *in vivo* was ~60% reduced in knockout (KO) females (n=10) and ~54% in knockout males (n=8) in comparison to the corresponding control group (CON females n=10; CON males n=10). The vascularization was measured by assessing the hemoglobin content of matrigel plugs, which is expressed as blood volume content within the matrigel plug (mean with SEM; Two-way ANOVA  $P < 0.05$  \*). B) Multiplex bead immunoassay to determine cytokines in pregnant E3.5 mice revealed a ~34.5% increase in the PDGF-B serum levels of knockout animals (n=13) in comparison to control animals (n=14; mean with SEM; T-test  $P < 0.05$  \*). The same amount of VEGF was present in the serum of knockout (n=16) and control (n=16) animals (mean with SEM; T-test  $P > 0.05$ ). The metabolite concentration is illustrated per serum volume.

*In vivo* blood vessel formation, which was measured as blood volume content within matrigel implants, was reduced ~60% in knockout females and ~54% in knockout males compared to the control mice (Figure 24A). Hence we concluded that the deletion of titin's kinase region in smooth muscle cells resulted in an angiogenesis defect, which was independent of the gender. To

correlate the defects in angiogenesis and embryo implantation with changes in cytokine levels, the content of FGF basic, G-CSF, IL-1 $\beta$ , IL-6, IL-15, IP-10, LIF, MCP-1, PDGF-B, TNF- $\alpha$ , and VEGF was determined in serum and uterine tissue of E3.5 pregnant mice. We found a ~34.5% increase of the growth factor PDGF-B in sera obtained from knockout mice compared to the control group (Figure 24B). Serum VEGF levels were unchanged indicating that impaired angiogenesis in knockout animals was not due to a defect in responding to VEGF. Also the other cytokines did not differ in the serum (supplement Figure 32) as well as in the uterine levels (supplement Figure 33). It was not possible to detect FGF basic, LIF, IL-15, IP-10, and MCP-1 in the serum and FGF basic, G-CSF, IL-15, PDGF-B, and VEGF in the uterine tissue.

Since PDGF-B is responsible for the migration of pericytes and vascular smooth muscle cells to the site of angiogenesis (Lindahl et al., 1997; Hellström et al., 1999), we tested the ability of smooth muscle cells that were isolated from the aorta of knockout and control animals to migrate in response to  $10^{-10}$  M PDGF-B (Figure 25A). The migration rate of smooth muscle cells is indicated relative to the corresponding control without chemoattractant, which was set to be 100%.

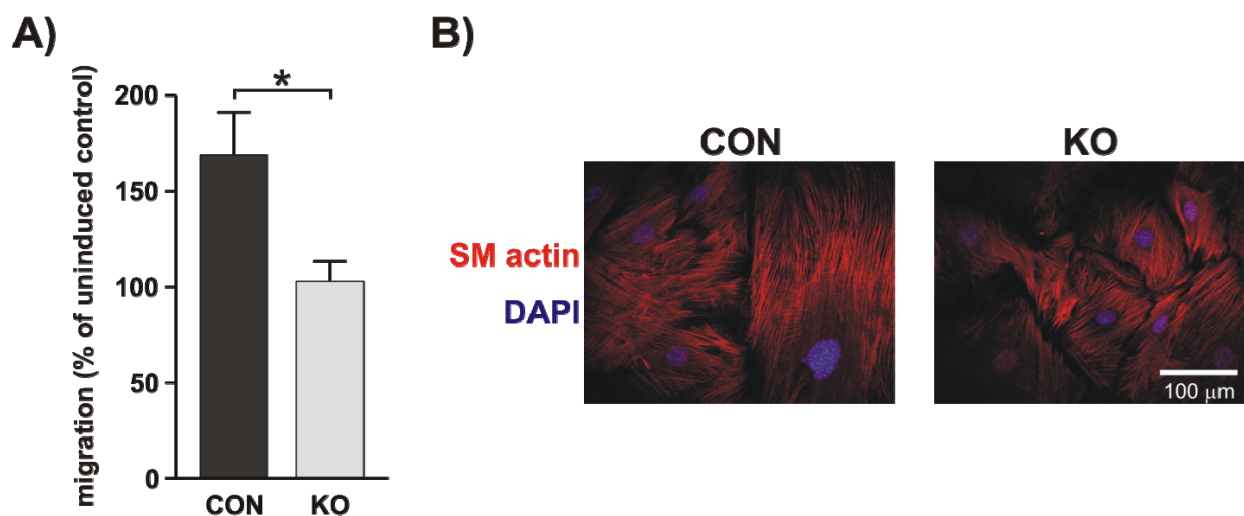


**Figure 25: Knockout smooth muscle cells did not migrate in response to PDGF-B.** A) Migration study with smooth muscle cells isolated from the aorta of knockout (KO; n=6) and control (CON; n=6) animals using  $10^{-10}$  M PDGF-B as chemoattractant revealed that knockout smooth muscle cells failed to migrate. In contrast, control smooth muscle cells showed a ~69% increase in migration in response to PDGF-B. The migration rate is given relative to the migration of the corresponding smooth muscle cells without chemoattractant, which was set to 100% (mean with SEM; T-test  $P < 0.05$  \*). B) Immunostaining using an antibody against smooth muscle actin (red) of cultures used for the migration studies confirmed the presence of >90% knockout (n=6) and control (n=6) smooth muscle cells. Nuclei of the cells were co-stained with DAPI (blue) to evaluate the amount of smooth muscle actin positive cells. Bar: 100  $\mu$ m.

Knockout smooth muscle cells did not migrate in response to PDGF-B because they had the same migration rate as knockout smooth muscle cells without chemoattractant (Figure 25A). On

the contrary, smooth muscle cells obtained from control animals migrate by PDGF-B stimulation ~69% more compared to their basal migration rate. The presence of >90% smooth muscle cells in cultures used for the migration study was confirmed by detecting the cell type restricted intermediate filament smooth muscle actin (Figure 25B). Since knockout smooth muscle cells did not migrate in comparison to control smooth muscle cells, we concluded that the loss of titin's kinase region in smooth muscle cells affects cell migration. We assume that this migration defect led to impaired *in vivo* angiogenesis in knockout mice (Figure 24A).

## 5.2.5 Alteration of tissue remodeling in titin's kinase region deficient animals

### 5.2.5.1 Expression of *Murf1* and *Fhl2* depends on titin's kinase region

The homozygous deletion of titin's M-band exons 1 and 2 has caused the loss of binding sites for MuRF1, MuRF2, T-cap, NBR1, p62, calmodulin (CALM1), FHL2, and myomesin (Myom1) in knockout animals (Figure 29). To elucidate, which genes encoding these M-band binding proteins are expressed in smooth muscle and contribute to the phenotype, expression analysis was performed using uterine tissue of E3.5 pregnant mice (Figure 26).

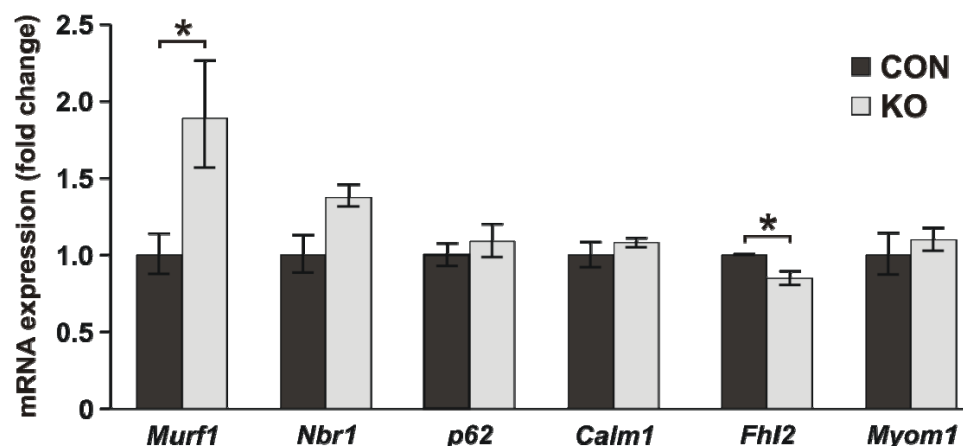


**Figure 26: Altered expression of *Murf1* and *Fhl2* in knockout uteri.** Real-Time PCR was performed to analyze the mRNA level of genes encoding proteins that bind to titin's kinase region, which is deleted in the knockout animals. *Murf1* expression was upregulated in knockout animals (KO; n=3) compared to control mice (CON; n=3) using uterine tissue from E3.5 pregnant females. Moreover, the transcription level of *Fhl2* was reduced in knockout uteri. The expression of *Nbr1*, *p62*, *Calm1*, and *Myom1* was similar in both groups. The mRNA levels were normalized to 18S RNA and expression is displayed as fold change relative to the control (mean with SEM; T-test comparing CON and KO of one primer/probe set P<0.05 \*).

The expression of *Murf1* was upregulated in knockout animals in comparison to control mice (Figure 26). Furthermore, the transcript level of *Fhl2* was little but significant diminished in the

uterine tissue of knockout mice. The expression of *Nbr1*, *p62*, *Calm1*, and *Myom1* was unaffected in knockout and control females. The mRNA of the titin M-band binding proteins T-cap and MuRF2, which forms heterodimers with MuRF1, could not be detected in uterine tissue. Since titin's kinase region has been implicated as a regulator of contractile function by effecting calcium handling (Peng et al., 2007), we also investigated the expression of the genes encoding the calcium-related proteins PKC $\delta$ , PKC $\epsilon$ , S100A1, L-type calcium channel (CACNA1C), calcium/calmodulin-dependent protein kinase II alpha (CAMK2A), and calbindin 1 (CALB1). The expression level of these genes was unchanged in E3.5 pregnant uterine tissue (supplement Figure 34).

#### 5.2.5.2 The transcription level of *Cox2* and *Lpar3* is not affected

Reproductive failure including reduced litter size and implantation defects is frequently associated with changes in expression of the genes *Cox2* and *Lpar3* encoding COX2 and the lysophosphatic acid receptor LPA3 (Lim et al., 1997; Matsumoto et al., 2002; Ye et al., 2005). It has also been shown that LPA3-mediated signaling regulates embryo spacing and implantation timing (Hama et al., 2007; Ye et al., 2005). To investigate if the transcript level of *Cox2* and *Lpar3* was affected upon the loss of titin kinase region, uteri of E3.5 pregnant control and knockout animals were analyzed by Real-Time PCR (Figure 27).

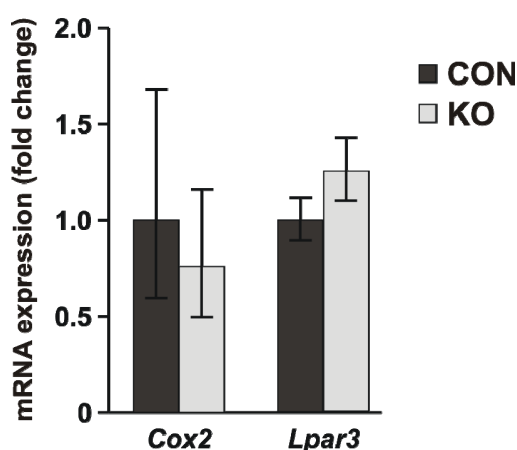


**Figure 27: Loss of titin's kinase region did not alter the expression of *Cox2* and *Lpar3*.** The transcript level of the genes *Cox2* and *Lpar3* encoding COX2 and LPA3, which are both known as regulators of embryo implantation, were unchanged in knockout (KO; n=3) compared to control (CON; n=3) animals investigating E3.5 pregnant uteri. The mRNA levels were normalized to 18S RNA and expression is displayed as fold change relative to the control (mean with SEM; T-test comparing CON and KO of one primer/probe set  $P>0.05$ ).

As shown in Figure 27, the expression of *Cox2* as well as *Lpar3* was not significantly changed in knockout animals compared to control mice.

### **5.2.5.3 Alterations of structural and ubiquitin-proteasome related proteins**

Proteins related to the progression of the phenotype caused by titin's kinase region deficiency were investigated using 2D-gel electrophoresis. Uterine tissue of E3.5 pregnant knockout and control animals was analyzed (supplement Figure 35). In total we have found 106 proteins that were altered comparing knockout and control animals. 32 proteins were downregulated and 74 proteins were upregulated in the knockout uteri, of which 20 could be identified so far (Figure 28, supplement Table 11). ANXA2, CKB, HSPB1, PDIA4, PSMC2, TAGLN were reduced in the knockout uteri and ARPC2, CAPG, CAR2, COL6A2, DNAJA1, ETFDH, FGA, HNRNPAB, NDUFS3, PCX, SFRS3, TPI1, and VIM accumulated in the knockout uteri (Figure 28). Depending on their function, these proteins belong to metabolism (CKB, ETFDH, NDUFS3, PCX, TPI1) or the heat shock and proteasomal stress response (HSPB1, PDIA4, PSMC2, DNAJA1), are related to the cytoskeleton (TAGLN, ARPC2, CAPG, VIM), or have other functions (ANXA2, CAR2, COL6A2, FGA, HNRNPAB, SFRS3). Hence we concluded that loss of the titin kinase region affected uterine tissue remodeling since structural proteins as well as proteins of the ubiquitin-proteasome pathway were changed.

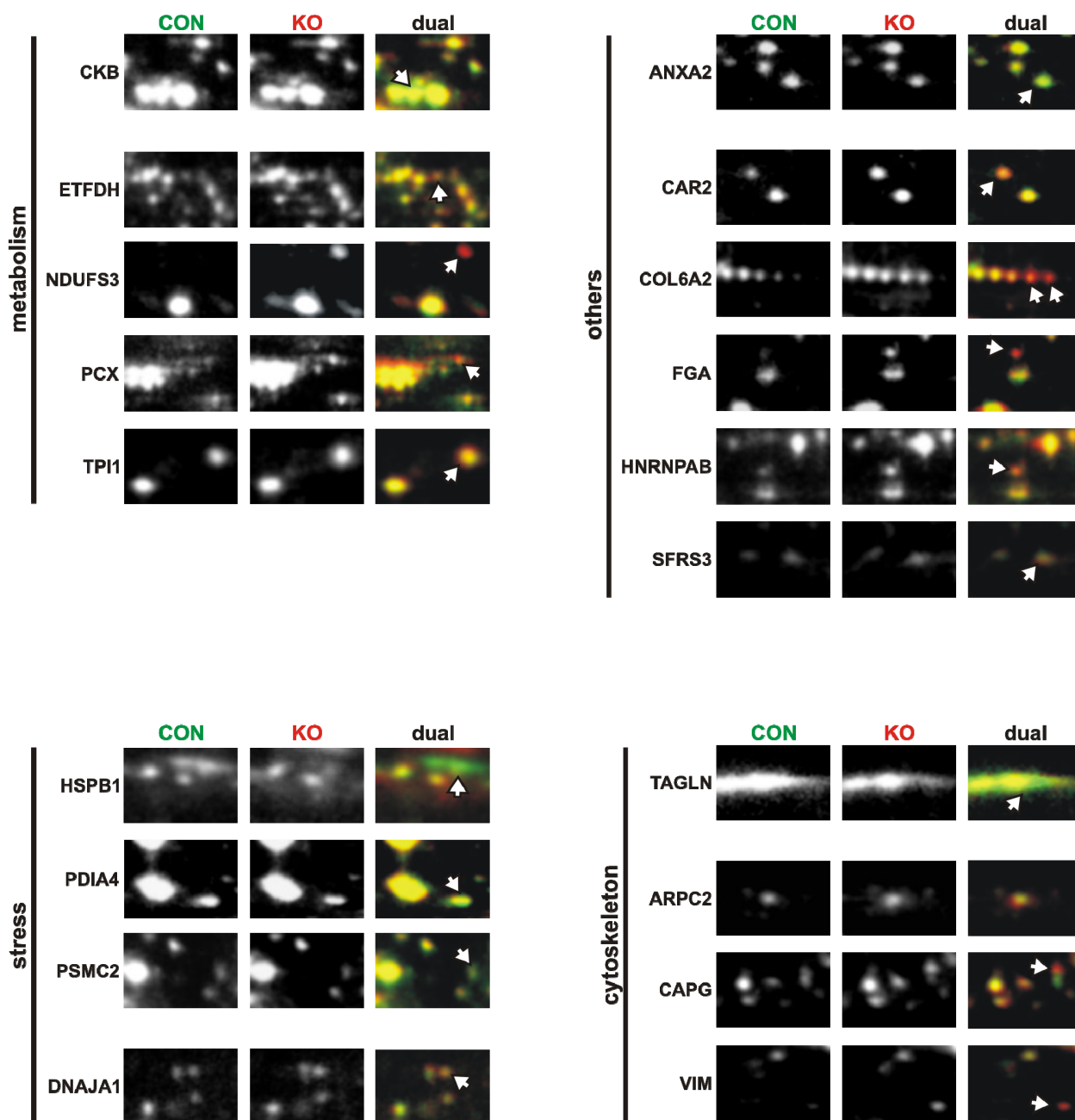


**Figure 28: Impaired heat shock response and altered cytoskeleton-related proteins in knockout uteri.** 2D-gel electrophoresis was performed to compare the proteins of E3.5 pregnant uteri of control (CON; green; n=6) and knockout (KO; red; n=6) mice. The Delta2D software colorized the control protein spots green and the knockout protein spots red leading in the dual view to yellow spots, if the same amount of protein is present in both groups (T-test  $P < 0.1$  \*; white arrows point the changed protein spots). Downregulation in knockout uteri is indicated by the green spots in the dual view for the proteins annexin A2 (ANXA2), brain creatine kinase (CKB), heat shock protein 1 (HSPB), protein disulfide-isomerase A4 (PDIA4), proteasome 26S subunit ATPase 2 (PSMC2), and transgelin (TAGLN). Accumulation of proteins in knockout uteri is indicated by red spots in the dual view for the proteins actin related protein 2/3 complex (ARPC2), capping protein (CAPG), carbonic anhydrase 2 (CAR2), collagen type VI alpha 2 (COL6A2), DnaJ (Hsp40) homolog (DNAJA1), electron transferring flavoprotein dehydrogenase (ETFDH), fibrinogen (FGA), heterogeneous nuclear ribonucleoprotein A/B (HNRNPAB), NADH dehydrogenase (ubiquinone) Fe-S protein 3 (NDUFS3), pyruvate carboxylase (PCX), splicing factor arginine/serine-rich 3 (SFRS3), triosephosphate isomerase 1 (TPI1), and vimentin (VIM).

## 6 Discussion

Aim of this study was the functional and morphological characterization of titin in smooth muscle. So far, only expression profiling, localization, and *in vitro* interaction studies for smooth muscle titin and the titin-like protein smitin have been performed, but a role has not been assigned (Kim and Keller, 2002; Chi et al., 2005, 2008; Labeit et al., 2006). Therefore, a smooth muscle specific knockout of titin's M-band exons 1 and 2 was used in our research to address a function for titin in uterine smooth muscle. Furthermore, the new titin-DsRed knockin mouse model TiEx28DsRed was established to facilitate the detection of smooth muscle titin.

In the TiEx28DsRed mouse strain, the coding sequence of the red fluorescence protein DsRed was inserted into exon 28 of the titin gene (Figure 7). The advantage of the presence of a fluorescence protein within titin is live cell imaging and the availability of commercial antibodies against DsRed. In contrast, there are only few titin antibodies purchasable. Hence the DsRed will help to detect smooth muscle titin, especially because the transcript level of smooth muscle titin is ~100 fold less than in skeletal muscle (Labeit et al., 2006) and therefore its verification on protein level limited. Furthermore, only the domain composition of one smooth muscle isoform is proposed based on expression analysis of human aorta, bladder, carotid, and stomach (Labeit et al., 2006). Since titin in striated muscle is alternatively spliced during embryonic development as well as in different tissues (Labeit and Kolmerer, 1995; Cazorla et al., 2000; Freiburg et al., 2000; Bang et al., 2001a; Sorimachi et al., 1997), it is also likely that different smooth muscle titin isoforms exist to determine muscle elasticity. Hence it is not known, if the antibodies used in the previous smooth muscle titin studies will also react against other tissue, such as uterus. The only study that has been done in mammals on protein level detected smooth muscle titin in porcine aorta and stomach by Western blotting as well as in cultured human aortic smooth muscle cells and in the tunica media of bovine aorta by immunofluorescence (Labeit et al., 2006). Smitin, the titin-like protein found in chicken gizzard muscle has been localized in the smooth muscle contractile apparatus as well as detected by Western blotting (Kim and Keller, 2002). So far, smooth muscle titin has not been detected on protein level in murine tissue or cells, which is required to gain more confidence to study smooth muscle titin by a loss of function approach with available titin knockout mouse models. A publication of Chi and colleagues have demonstrated by RT-PCR the expression of titin's exon 28 in human carotid artery, bladder, and uterus (Chi et al., 2008). Since our titin-DsRed knockin mice carry the coding sequence of the DsRed within exon 28, the TiEx28DsRed mouse



strain will help to conclusively show the existence of smooth muscle titin and its localization within the contractile unit to incorporate titin in the model of smooth muscle structure.

After successful cloning of the targeting vector DsRedKI (Figure 8), the efficiency of its homologous recombination into the titin locus of the ES cells was 1:192 (Figure 9). The efficiency depends on the length of homologous sequence and the amount of repetitive sequence that is present within the long arm of the targeting vector (Hasty et al., 1991). Furthermore, isogenicity of the targeting vector to the ES cell line used alters gene targeting frequency (Deng and Capecchi, 1992; van Deursen and Wieringa, 1992). As homologous recombination occurs during the S-phase of the cell cycle, also cell cycle rates of the ES cell lines are important (Wong and Capecchi, 1987; Udy et al., 1997). Accordingly, Udy and colleagues have found efficiencies from 1:50 to 1:1033 with the same targeting construct depending on the ES cell lines used. The achieved homologous recombination frequency of the DsRedKI into the titin gene was within the expected range at the upper level of efficiency. Nevertheless, the ES cell clone E3 did not incorporate the full targeting vector, as it was not possible to detect the DsRed in ES cells differentiated into cardiomyocytes (Figure 10). Nevertheless, the neomycin resistance cassette was incorporated into the titin locus of the ES cell clone E3 because this clone survived the selection with the antibiotic G418 and was positive in the ES cell genotyping PCR (Figure 9). This PCR did not detect the lack of the DsRed coding sequence since the forward primer binds within the neomycin resistance cassette and the reverse primer outside of the targeting in front of its short arm within the titin gene (Figure 7). For the ES cell clone F5, the integration of the targeting vector DsRedKI into the titin locus was verified by PCR (Figure 9) as well as the presence of the DsRed within titin and its proper localization within the sarcomere on protein level (Figure 10). This clone was used to generate chimeras, in which ES cells contributed to the germ line cells so that the DsRed-targeted titin gene was passed to the next generation. The neomycin resistance cassette was removed with the help of the FLP-recombinase in animals carrying heterozygous the targeted allele leaving only a FRT-site in the intron sequence between exon 28 and 29 (Figure 7). These mice were used to generate the mouse colony of the TiEx28DsRed strain (Figure 11) to exclude that knockin animals get a distinct phenotype caused by the neomycin resistance cassette as reported previously (Kaul et al., 2000).

In heart and skeletal muscle titin is alternatively spliced in particular the PEVK and N2B region as well as in the Ig domain regions of the I-band region (Labeit and Kolmerer, 1995; Cazorla et al., 2000; Freiburg et al., 2000; Bang et al., 2001a). Furthermore, the short novex 3 isoform does not contain titin's A-band and M-band region as well as large parts of the I-Band region because it has an alternative titin C-terminus (Bang et al., 2001a). Therefore the DsRed should be

inserted close to titin's N-terminus to be present in all titin splice isoforms (Figure 4). Splicing also varies the number of Z-repeats at titin's central Z-disc (Gautel et al., 1996; Sorimachi et al., 1997). In contrast to rabbit uterus, in which the entire Z-repeat region is missing although titin could be detected (Sorimachi et al., 1997), it has been shown that part of the Z-repeat region is present in human smooth muscle including uterus (Chi et al., 2008). In addition, the insertion of DsReds within titin's Z-disc region could interfere titin signaling and the integration of titin's N-terminus into the Z-disc of the sarcomere by disturbing binding sites for sANK1 (Kontrogianni-Konstantopoulos and Bloch, 2003), T-cap (Gregorio et al., 1998; Mues et al., 1998),  $\alpha$ -actinin (Ohtsuka et al., 1997a, b; Gregorio et al., 1998), or obscurin (Bang et al., 2001a; Young et al., 2001). The DsRed within titin's Z-disc region could also cause a thicker Z-disc because a longer titin molecule would displace the positions of binding sites for Z-disc proteins, such as  $\alpha$ -actinin that links titin to the thin filament system (Ohtsuka et al., 1997a, b; Gregorio et al., 1998). Changing the thickness of the Z-disc could influence the mechanical properties of the sarcomere because the width of the Z-band is considered to be a fundamental property of the muscle fiber type (Rowe, 1973; Yamaguchi et al., 1985) and correlates with the number of titin Z-repeats (Sorimachi et al., 1997; Peckham et al., 1997). Furthermore, a thicker Z-disc could change the stability of the sarcomere as well as sterically disturb possible interactions of titin binding partners on opposite titin molecules that overlap in the Z-disc (Knupp et al., 2002). Hence titin's exon 28 was chosen for insertion of the DsRed coding sequence because it is located at titin's Z-disc to I-band junction, in which no protein binding sites are known. It encodes unique sequences and Ig domains (Bang et al., 2001a). To not disrupt titin's domain structure, the DsRed coding sequence was inserted in front of the Ig domain I1 of titin's I-band segment preserving the reading frame (Figure 7).

Heterozygous as well as homozygous DsRed knockin mice had the same lifespan as wild-type littermates as well as normal fertility and offspring at the expected Mendelian ratios. The viability of knockin animals demonstrated that the DsRed did not affect the integration of the titin-DsRed into the Z-disc of the sarcomere. Otherwise, homozygous knockin mice would be embryonic lethal comparable to a titin M-band deficient mouse model, in which the lack of titin's integration into the M-band led to sarcomere disassembly and death at E11 (Weinert et al., 2006). Proper sarcomere assembly was also confirmed by immunofluorescence studies of quadriceps as example of skeletal muscle and heart, which show an alternating striated pattern by DsRed emitted fluorescence and M8/M9 antibody staining (Figure 14). The integration of the DsRed into titin did not affect its fluorescence properties as it was possible to monitor the fluorescence emitted by the DsRed in heterozygous and homozygous knockin mice. In

cardiomyocytes that we obtained by differentiating ES cells, the DsRed was only detected with the help of an antibody (Figure 10) because the newly formed cardiomyocytes were not highly packed with myofibrils so that the fluorescence was under the detection limit.

The body weight and heart weight to body weight ratio of TiEx28DsRed animals was determined to investigate if expression of the titin-DsRed causes atrophy or hypertrophy of the heart as it has been shown by several groups that mutations within the titin gene cause cardiomyopathy (Radke et al., 2007; Granzier et al., 2009; Itoh-Satoh et al., 2002; Peng et al., 2006). The body weight as well as heart weight to body weight ratio of heterozygous and homozygous knockin mice was unchanged compared to the wild-type animals (Figure 12) indicating that the DsRed within titin did not affect its signaling function leading to atrophy or hypertrophy.

The titin-DsRed mouse model was further analyzed using heart, quadriceps, and soleus muscle. Coomassie staining of wild-type, heterozygous, and homozygous TiEx28DsRed samples (Figure 13A) verified the presence of the N2BA and the shorter N2B isoform in heart, whereas the N2B isoform was predominantly present consistent with previous studies (Neagoe et al., 2002). Furthermore, the two N2A isoforms of quadriceps and the longest N2A isoform of soleus were detected in the adult mice independent of the genotype. This indicates normal postnatal titin splicing of skeletal muscle because after birth all muscle types initially express a single titin isoform that gradually decreases in size, whereas a second titin isoform appears in quadriceps of adult mice (Ottenheijm et al., 2009b). Using an antibody against DsRed, the presence of the fluorescence protein was confirmed in heterozygous and homozygous mice. The intact full length titin T1 but not in its break down product T2 was detected (Figure 13B). T2 constitutes titin's A-band and C-terminal region because it is formed by cleavage of T1 titin within the I-band (Matsuura et al., 1991; Ohtsuka et al., 1992) so that the DsRed at titin's N-terminal part was cut off. In contrast, the M8/M9 antibody that is specific for titin's C-terminal Ig domains M8 and M9 reacted with T1 and T2 of heart, quadriceps, and soleus samples from wild-type, heterozygous, and homozygous TiEx28DsRed mice (Figure 13B). Hence the DsRed did not affect the expression and translation of titin.

Our titin-DsRed mouse model, which incorporates the coding sequence of the DsRed within exon 28, was characterized in striated muscle, in which titin has been well studied. Mice that carried heterozygous or homozygous the titin-DsRed did not have an obvious phenotype with regard to fertility, heart weight to body weight ratio, and appropriate sarcomere assembly. DsRed incorporated close to titin's N-terminus at the Z/I-junction of the sarcomere was able to emit fluorescence, but it was also possible to detect this protein with an antibody. Since it has been

shown that exon 28 is expressed in human carotid artery, bladder, and uterus (Chi et al., 2008), we established a suitable tool to visualize titin in embryonic and adult smooth muscle. In particular we are interested in the localization of titin in the uterus to complement our analysis of titin's kinase region during early pregnancy.

Titin's kinase region, which is encoded by titin's M-band exons 1 and 2, has essential functions in mature and in embryonic striated muscle as revealed by previous studies. Deletion of titin's kinase region during late embryonic development resulted in altered contractility of skeletal muscle, disassembly of the sarcomere, and early death indicating a critical role for maintaining the muscle structure (Gotthardt et al., 2003; Peng et al., 2006; Ottenheijm et al., 2009a). Furthermore, results obtained by the loss of titin's kinase region in adult mouse hearts suggest that titin's kinase region regulates contractile functions via calcium handling (Peng et al., 2007). In the conventional knockout model of titin's M-band exons 1 and 2, embryos died due to mechanical instability of sarcomeres although the initial assembly of sarcomeres was unaffected (Weinert et al., 2006). Since important functions for titin's kinase region have been addressed for striated muscle, we speculated that titin's kinase region is also required in adult smooth muscle. Moreover, titin's kinase is highly conserved in vertebrate and invertebrates suggesting an essential function in muscle tissue (Gautel et al., 1995). The importance of titin's kinase in maintaining the turnover of muscle proteins has been demonstrated by a point mutation in the human kinase domain that causes myopathy (Lange et al., 2005). We hypothesized that the titin kinase of smooth muscle performs the functions that have been proposed for striated muscle, namely signal transduction and stretch sensor to regulate protein expression in a strain-dependent manner via substrates (Tskhovrebova and Trinick, 2003; Granzier and Labeit, 2004; Lange et al., 2005). Here, we show the presence of a titin transcript that includes Z-disc, N2A, and M-band exons in uterine tissue (Figure 17). Other studies have confirmed the expression of a titin transcript encoding the N-terminus in uterus by RT-PCR (Sorimachi et al., 1997; Labeit et al., 2006; Chi et al., 2008). The transcription level of the M-band exons 1, 2, and 6 was similar to the expression of the Z-disc exon 3 and the N2A exon and there was no transcript of titin's M-band exons 1 and 2 in our knockout mice. This led us to the conclusion that titin's kinase region is expressed in uterine tissue although results obtained by Labeit and coworkers suggest that smooth muscle titin consists of Z-disc, I-band, and A-band parts with an alternative C-terminus devoid of an M-band segment (Labeit et al., 2006). In this study human aorta, bladder, carotid, and stomach have been investigated, but not uterus. Compared to striated muscle, the expression level of smooth muscle titin is ~100 fold less (Labeit et al., 2006), which we also observed at the

high cycle threshold value during our Real-Time PCR analysis. It is predicted that the extensible I-band regions are short in smooth muscle titin (Labeit et al., 2006) so that stretch will result in relatively high forces, which would compensate for smooth muscle titin's low abundance.

To study the function of smooth muscle titin (Figure 15), we used a cre-recombinase under the control of the smooth muscle myosin heavy chain promoter after demonstrating that it led to recombination in uterine smooth muscle cells (Figure 16). We were able to efficiently delete titin's M-band exons 1 and 2 in uterus of knockout females in comparison to control mice (Figure 17). Our knockout and control mice carried one universally recombined titin allele due to germline activity of the cre-recombinase (Figure 17A). This is consistent with recently published work, which shows that the cre-recombinase activity in male germ cells is independent of the cre-genotype and ends prior to fertilization (de Lange et al., 2008). Hence recombination occurred in all haploid male germ cells, in which the floxed allele was present, but did not affect the female allele. As a result, the control and knockout animals of the SMcTiME<sub>x1-2</sub> strain carried universally one deleted titin allele, whereas the smooth muscle activity of the cre-recombinase caused also recombination of the second titin allele in the knockout animals resulting in the complete loss of titin's M-band exons 1 and 2. Heterozygous mice contained one deleted allele in smooth muscle caused by the smooth muscle cre-activity. Although heterozygously recombined (Figure 17B), the control and heterozygous mice still expressed titin's M-band exons 1 and 2 and did not display impaired implantation (Figure 19, Figure 20, Figure 21, Figure 22). We also controlled that the cre-recombinase did not cause the phenotype (Figure 22) as it has been reported for mammalian cells (Loonstra et al., 2001).

The smooth muscle specific loss of titin's kinase region did not lead to an obvious phenotype since the mice were viable and also had the same body weight as well as heart weight to body weight ratio as their litter mate controls (Figure 21B, supplement Figure 31). An altered heart weight to body weight ratio could indicate vascular defects that change the load on the heart by altering the blood flow or that lead to dysfunction of the coronary vasculature (Bellomo et al., 2000). The expression of the SMMHC cre-recombinase transgene starts in late embryonic development at E12.5 (Xin et al., 2002). In addition, titin has a long half life of ~3 days (Isaacs et al., 1989) so that the complete replacement of the wild-type with the mutant titin takes time. Mice, in which the striated muscle specific deletion of titin's kinase region started in late embryonic development, did also not show an obvious phenotype until three weeks of age (Gotthardt et al., 2003). At this time only 30-40% of total titin lacks the kinase region (Ottenheijm et al., 2009a). Hence, a strong smooth muscle phenotype was not expected. Moreover angiogenesis only contributes to organ growth after birth but most blood vessels

remain quiescent during adulthood (Carmeliet, 2005). Then angiogenesis occurs only in the female reproductive system and in response to pathological stimuli such as inflammation and wound healing.

More understanding of preimplantation and implantation biology will help to improve fetal health and female fertility. The SMcTiMEx1-2 strain was a suitable mouse model to challenge the uterine tissue by pregnancy that involves smooth muscle contraction, angiogenesis, and tissue remodeling. Our studies demonstrate a critical role in embryo implantation for titin's kinase domain and its surrounding regions, which both contain binding sites for multiple proteins. The deletion of titin's M-band exons 1 and 2 resulted in altered embryo spacing (Figure 19). Thereby the embryo implantation sites were mostly localized in only one uterine horn (~24%) or crowded (13.6%). Furthermore, we observed 4 or fewer implantation sites in 22.7% of knockout females. Additionally, the amount of implantation sites was significantly reduced (Figure 20A). The aberrant implantation was confirmed for both E4.5 and E5.5, which also verified on-time implantation in knockout females before E4.5. These data indicate that the loss of titin's kinase region could involve direct effects on the female reproductive system. To explore this possibility, we investigated estrous cycle length, embryo transport through the oviduct, and blastocyst development as major events in female reproduction (Figure 18). There was no difference resulting in the same amount of E3.5 blastocysts available for implantation in control and knockout animals. Furthermore, knockout uteri did not display hypoplasia as the uterus weight to body weight ratio was comparable to the control group at E3.5 and E4.5 (Figure 21). Therefore the reduced number of implantation sites in knockout females was caused by an impaired implantation. The amount of E3.5 blastocysts (Figure 18B) were determined by flushing the uterine horns and counting. The average number of implantation sites (Figure 20A) were determined by Evans Blue staining so that the number of both experiments differ.

The implantation phenotype upon loss of titin's kinase region resembles the targeted deletion of the genes encoding the LPA receptor LPA3 as well as the cytosolic phospholipase A<sub>2α</sub> (cPLA2) (Ye et al., 2005; Song et al., 2002). A similar phenotype has also been reported for mice and rats that were treated with indomethacin, which is an inhibitor of cyclooxygenases (Kennedy, 1977; Kinoshita et al., 1985). These mouse models had a reduced litter size and altered embryo spacing, but in contrast to our titin's kinase region deficient mouse model also delayed implantation. Additionally, cPLA2 knockout mice exhibited impaired preimplantational embryonic development (Table 10). COX2 deficient mice have implantation defects as well, but more severe other reproductive failures in ovulation, fertilization and decidualization (Lim et al., 1997). In these previously described mouse models the prostaglandin biosynthesis was impaired,

since cPLA2 is an important enzyme for the arachidonic acid production that is converted by COX2 to the prostaglandin H2. Also the loss of LPA3 could be correlated to the cPLA2–arachidonic acid–COX2–prostaglandin signaling pathway because reduced *Cox2* expression and prostaglandin levels in E3.5 pregnant uteri of this mouse model has been shown (Ye et al., 2005). The deletion of titin’s kinase region did not alter the expression of *Cox2* and *Lpar3* in E3.5 pregnant uteri compared to control females (Figure 27). Consistent with our findings, it has not been possible to correct uneven embryo spacing and the decrease of embryo implantation sites in cPLA2, COX2, and LPA3 deficient mice by rescuing the prostaglandin reduction with prostaglandin E2 and carbaprostacyclin administration (Song et al., 2002; Lim et al., 1999; Ye et al., 2005). This rescue only restored on-time implantation indicating that prostaglandin biosynthesis is crucial to determine the window of implantation and independent effects of arachidonic acid are involved in embryo spacing and the implantation reaction, which is impaired by the loss of titin’s kinase region.

**Table 10: Knockout mouse models with an implantation phenotype.**

Knockout model	Reduced number of implantation sites	Mislocalization and crowding	Delayed implantation	Preimplantational effects
titin’s kinase region	yes	yes	no	no
LPA3	yes	yes	yes	no
cPLA2	yes	yes	yes	yes (mild)
COX2	yes (severe)	not detectable	yes	yes (severe)
L-12/15-LOX	yes	unknown	no	unknown

Another pathway that regulates implantation through arachidonic acid metabolism is described in mice carrying a null mutation for gene encoding the L-12/15-LOX that catalysis the formation of hydroxyeicosatetraenoic acids from arachidonic acid (Li et al., 2004). It has been shown that the expression of *Alox15* in uterus is induced by progesterone with a maximum before implantation, which results in an increased uterine level of 12-HETE (Li et al., 2004). Therefore Real-Time PCR, metabolite measurement, and proteomics were conducted with tissue from E3.5 pregnant mice. This time point also minimized changes due to secondary effects. Li and coworkers have shown that deletion of the L-12/15-LOX caused a reduced number of implantation sites at on-time implantation (Li et al., 2004). For this mouse model nothing is reported about the localization of the implantation sites within both uterine horns (Table 10).

Nevertheless, this implantation phenotype is markedly similar to the females lacking titin's kinase region (Figure 20). Consistently, both knockout models had reduced uterine levels of 12-HETE before implantation (Figure 23B; Li et al., 2004). It has been shown that additional inhibition of the epidermal 12/15-lipoxygenase (E-12/15-LOX) activity reduced the uterine 12-HETE level and blocked embryo implantation nearly completely in L-12/15-LOX knockout mice (Li et al., 2004). Hence the partial but not total loss of implantation sites can be explained by the compensatory effect of the E-12/15-LOX that caused residual 12-HETE production in uterine tissue. Li and colleagues also have uncovered that the reduction of embryo implantation caused by an E- and L-12/15-LOX inhibitor could be reversed by a PPAR $\gamma$  agonist. These results suggest that PPAR $\gamma$  is a downstream target of 12-HETE and important during early pregnancy. We found in our knockout model of titin's kinase region no upregulation of *Pparg* expression (Figure 23A). Nevertheless, there might be a change on protein level or activation of the PPAR $\gamma$ . Hence, we will try to rescue the reduced number of implantation sites using a PPAR $\gamma$  selective agonist to ascertain if titin's kinase region is related to this signaling pathway.

Although L-12/15-LOX and its metabolite 12-HETE have been identified as important regulator of implantation, the precise biological events that caused the reduced number of embryo implantation sites remain elusive. It needs to be considered that the L-12/15-LOX has a wide distribution. It is not only expressed in the surface and glandular epithelial cells of the uterus, but also in vascular smooth muscle cells (Li et al., 2004; Natarajan et al., 1993). 12-HETE has been implicated in inflammation-related and other physiological pathways such as angiogenesis that is completed by the recruitment of vascular smooth muscle cells (Connolly and Rose, 1998; Nie et al., 2006). Angiogenesis is an essential physiological component of pregnancy because a richly vascularized uterine tissue is needed for implantation and development of the placental vasculature to facilitate the transport of nutrients and oxygen to the embryo. It occurs together with increased vascular permeability at the site of blastocyst apposition and is extended during the penetration phase (Plaks et al., 2006; Schlafke and Enders, 1975). The reduced number of implantation sites in mice lacking titin's kinase region is related to this phase because we could not flush blastocysts from E4.5 knockout uteri indicating that apposition and attachment of blastocyst occurred normally. Furthermore, we detected in one knockout uterus implantation sites that have not further developed (Figure 20B) and the number of implantation sites in knockout females was already reduced at E4.5 (Figure 20A). The knockout uteri also had a delayed development during early pregnancy at E5.5 as measured by the uterus weight to body weight ratio (Figure 21). This indicates that the deletion of titin's kinase regions affected uterine vascularization or decidualization. Consistent with these findings, the *in vivo* angiogenesis



studies revealed decreased angiogenesis in response to VEGF in knockout mice (Figure 24A). Thus, the reduced number of implantation sites appears to be at least in part due to impaired angiogenesis, which is likely independent of VEGF as our knockout and control animals had the same VEGF serum levels (Figure 24B). This is in agreement with results obtained by Matsumoto and coworkers, who showed that VEGF directs uterine vascular permeability and angiogenesis during the preimplantation and attachment phase driven by prostaglandins (Matsumoto et al., 2002). Accordingly mice that carry a null mutation for the gene encoding COX2 already exhibited implantation defects during the initial attachment phase (Lim et al., 1997).

Our investigation revealed PDGF-B as growth factor that might be involved in vascular growth and remodeling during early stages of pregnancy dependent on titin's kinase region since the PDGF-B serum levels were increased in pregnant knockout mice (Figure 24B). TNF- $\alpha$ , another angiogenic agent that is regulated at the time of implantation (De et al., 1993), was unchanged indicating a specific role for PDGF-B. It is known that PDGF-B activates intracellular phospholipases producing arachidonic acid, which is metabolized by lipoxygenases, cyclooxygenases, and cytochrome P-450 oxygenases (Smith, 1989). It has been demonstrated that PDGF-B induces L-12/15-LOX activity and *Alox15* expression in vascular smooth muscle cells (Natarajan et al., 1996). In addition, the L-12/15-LOX product 12-HETE causes extracellular matrix production as well as vascular smooth muscle cell migration (Nakao et al., 1982; Natarajan et al., 1994). Hence we tested if smooth muscle cell migration was altered. We discovered that smooth muscle cells lacking titin's kinase region did not migrate in response to PDGF-B (Figure 25). These data together with the decreased uterine levels of 12-HETE indicate that titin's kinase region affected PDGF-B and its mediator 12-HETE and thereby cell migration. This is consistent with previous findings that PDGF-induced chemotactic effects were significantly blocked by lipoxygenase inhibitors (Natarajan et al., 1996; Gu et al., 2001; Patricia et al., 2001). PDGF-induced migration was also reduced in vascular smooth muscle cells obtained from the L-12/15-LOX knockout model (Reddy et al., 2003). Since angiogenesis requires vascular smooth muscle cells, which are recruited to the site of vessel formation by PDGF-B (Lindahl et al., 1997; Hellström et al., 1999), it is tempting to speculate that the reduced number of implantation sites in titin's kinase region and L-12/15-LOX knockout mice was caused by impaired vessel formation or remodeling. The newly formed blood vessels were not stabilized properly by the recruitment of smooth muscle cells. Therefore, embryos implantation was hampered but could be partially rescued by the activity of the E-12/15-LOX activity. The PDGF-B levels were increased to compensate the smooth muscle migration failure.

Prospective experiments will be done to confirm the link of 12-HETE to titin's kinase region. We will try to rescue the migration phenotype of knockout smooth muscle cells by overexpressing L-12/15-LOX or by 12-HETE supplement. Moreover we will use other chemoattractants than PDGF-B to investigate, if the migration defect is specific to 12-HETE–PDGF-B signaling. It might be a general defect since stretch sensor is one proposed function of titin's kinase (Tskhovrebova and Trinick, 2003; Granzier and Labeit, 2004; Lange et al., 2005). The titin molecule is a possible candidate to sense stretch and to convert it into a biochemical signal because it contains besides the kinase domain also elastic spring elements as well as multiple protein binding and phosphorylation sites.

Expression analysis of genes encoding M-band interaction partners (Figure 29), whose binding sites have been deleted in titin's kinase region deficient animals, revealed no alteration of *Nbr1* and *p62* that are expressed in smooth muscle and encode postulated kinase substrates (Figure 26).

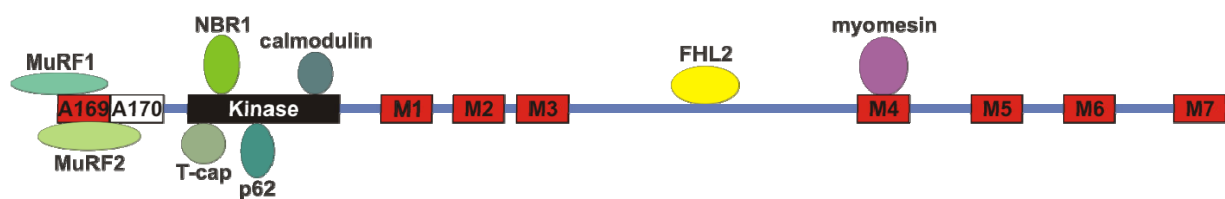


**Figure 29: Binding partners of titin's kinase region.** The binding proteins of titin's kinase region are shown (structural proteins: purple; adapter proteins: yellow; signaling proteins green). The protein domains, which are encoded by titin's M-band exons 1 and 2 that are deleted in our knockout model, are also depicted (Ig domains (red), FN3 domain (white), unique sequences (blue), kinase domain (black)). The domains of titin's kinase region of the A-band (A169, A170) and of the M-band (M1-M7) are specified. Modified from Gotthardt et al., 2003.

A small reduction of *Fhl2* transcripts was observed (Figure 26). The knockout models of titin's PEVK and N2B segment also had only a little or no change, respectively, in the *Fhl2* expression in heart, but a strong effect on protein level (Granzier et al., 2009; Radke et al., 2007). Hence, future studies will show, if there is a change in protein amount of uterine tissue obtained from titin's kinase region deficient mice. FHL2 will be investigated because it participates in wound healing by contributing to gene expression, cytoarchitecture, cell adhesion, signal transduction, and migration. Wound healing and pregnancy are related because they share the need for angiogenesis and remodeling of the extracellular matrix. Therefore, we will conduct wound healing studies in the future. Of note, it has been shown that impaired wound healing in FHL2 knockout mice is due to disturbed collagen metabolism (Kirfel et al., 2008). Titin's kinase region deficient knockout uteri pregnant at E3.5 had an increased amount of collagen type VI alpha 2

(COL6A2; Figure 28), which is involved in the decidualization of embryo implantation (Mulholland et al., 1992). Hence, we will test the decidual reaction of our knockout females *in vivo* by artificial induction of decidualization. Moreover it has been shown that FHL2 translocates to the nucleus triggered by LPA and S1P (Müller et al., 2002). LPA and S1P are both important for successful implantation (Ye et al., 2005; Mizugishi et al., 2007). In addition, sphingolipid metabolism regulates uterine decidualization and blood vessel stability and S1P is required for PDGF-B guided migration of vascular smooth muscle cells during angiogenesis (Liu et al., 2000; Allende and Proia, 2002; Spiegel and Milstien, 2003).

*Murf1* had an increased transcription level in pregnant uteri that were deficient in titin's kinase region (Figure 26). Further studies will provide insight if the M-band binding protein MuRF1 is also upregulated on protein level. Despite the deletion of the MuRF1 binding site, a higher MuRF1 protein amount has been detected in adult heart lacking titin's kinase region (Peng et al., 2007). The increased level of the ubiquitin ligase MuRF1 might result in increased ubiquitination and thereby in alteration of heat shock response and protein degradation. Previous studies suggest that the ubiquitin-proteasome pathway effects embryo implantation probably by being involved in degradation and remodeling of the uterine tissue during decidualization (Wang et al., 2004). Indeed, we observed upregulation of the DnaJ (Hsp40) homolog (DNAJA1) and downregulation of the heat shock protein 1 (HSPB1), the protein disulfide-isomerase A4 (PDIA4), and the proteasome 26S subunit ATPase 2 (PSMC2; Figure 28) on protein level. Components of the ubiquitin-proteasome pathway were also altered in striated muscle specific titin's kinase region knockout mice (Peng et al., 2006). The reduced amount of uterine 12-HETE in our knockout mice that is contrary to the upregulated transcriptional level of *Alox15* (Figure 23) might be caused by variation of the ubiquitin-dependent protein degradation via proteasomes leading to a reduction in L-12/15-LOX protein amount. There could also be a link between MuRF1 and FHL2 because it has been shown that the FHL2 protein level is increased in mice deficient for both MuRF1 and MuRF2 (Witt et al., 2008).

Beside the effect on heat shock response and protein degradation, the proteins that were changed in E3.5 pregnant knockout uteri mainly belong to metabolism and the cytoskeleton (Figure 28). This is consisting with findings from quadriceps of the striated muscle specific titin's kinase knockout (Raddatz et al., 2008). Differential regulation of proteins of the cytoskeleton such as transgelin (TAGLN), actin related protein 2/3 complex (ARPC2), capping protein (CAPG), and vimentin (VIM) support the hypothesis that deletion of titin's kinase region caused altered tissue remodeling in early pregnancy as already indicated by an impaired ubiquitin-proteasome pathway. Fibrinogen (FGA) and the splicing factor arginine/serine-rich 3 (SFRS3), which were

accumulated in pregnant knockout uteri (Figure 28), have been related to implantation in previous studies. It has been demonstrated that fibrinogen is crucial for maintenance of pregnancy by supporting development of fetal-maternal vascular communication and by stabilizing embryo implantation (Iwaki et al., 2002). The splicing factor arginine/serine-rich 3 was identified as marker for uterine receptivity (Reese et al., 2001). The findings confirm the implantation defect in titin's kinase knockout mice.

To gain more insight into the signaling pathways that are affected in our knockout mice, we investigated cytokines in uterus and serum of pregnant mice. We focused on cytokines that have been related to implantation in mice but also to recurrent miscarriage of women and a cytokine profile that is predictive for *in vitro* fertilization (Jasper et al., 2007; Boomsma et al., 2009). The tested cytokines were not altered (supplement Figure 32, Figure 33). Most remarkable, LIF that is a key regulator for implantation (Stewart et al., 1992) was unchanged indicating that implantation normally initiated in titin's kinase knockout animals. This is similar to the LPA3 knockout mouse model that also exhibited impaired implantation (Ye et al., 2005).

Relevant to our work were also previous experiments that have been done with smooth muscle cells obtained from L-12/15-LOX knockout mice. It has been shown that they had reduced activation of the mitogen-activated protein kinase 14 (MAPK14) and the CREB1, which both mediate cellular effects induced by 12-HETE (Reddy et al., 2002). MAPK14 knockout females have defects in placental angiogenesis leading to embryonic death (Mudgett et al., 2000; Adams et al., 2000). In contrast to the transcript level of *Creb1* that was unchanged, we found in uteri from our knockout animals increased expression of *Mapk13* (Figure 23A). *Mapk13* encodes the MAPK13, which is homologous to MAPK14 but has different substrate specificity (Hu et al., 1999). Future studies will expose if the activation of the kinases MAPK13 and MAPK14 occurs differently upon loss of titin's kinase region in pregnant uterus thereby modulating signaling pathways that might be responsible for altered growth factor response via the mediator 12-HETE.

So far, we investigated the pathway leading to a reduced number of implantation sites. The molecular mechanisms underlying crowding and mislocalization of embryo implantation sites, which are most likely related to smooth muscle contraction, are unknown. It has been shown that titin's kinase region acts as a regulator of contractile function by calcium handling (Peng et al., 2007). The expression of selected genes encoding calcium related proteins (supplement Figure 34) did not differ in titin's kinase region deficient pregnant knockout uteri. Also the transcript level of *Lpar3* encoding LPA3, which has been shown to mediate embryo spacing as well as implantation via different signaling pathways (Hama et al., 2007), was unchanged (Figure 27). It

might be that LPA3 is altered on protein level or that titin's kinase region is downstream of LPA3 signaling. Hence, additional studies are required to understand smooth muscle titin's mechanical and signaling function. Protein kinase G (PKG) will be investigated because titin and the actin related protein 2/3 complex (ARPC2), which is upregulated on protein level in pregnant knockout uteri (Figure 28), were identified to be *in vitro* PKG substrates in pregnant rat uteri (Huang et al., 2007). Using our proteomics approach, we will also generate a protein reference map for pregnant mouse uterus after analyzing more protein spots. Identification of proteins based on their migration in 2D-gels will provide a molecular basis for functional and pathophysiological studies that will help to elucidate pregnancy in more details.

To investigate titin's kinase region deficient mice in pregnancy, timed matings were set up so that the genotypes of the embryos, which developed in control and knockout females, were similar. Hence, knockout males were bred with control females and control males were bred with knockout females. However, activity of the cre-recombinase before and after fertilization in knockout females caused recombination of both titin alleles independent of the genotype of the embryo in 100% (de Lange et al., 2008). In control females, the cre-recombinase activity in the male germ cells ended prior to fertilization. This led to ~50% of embryos with universal deletion of both titin alleles taken into account that control and knockout animals carried one universally recombined allele. Since 100% of the embryos that developed in knockout females and only ~50% of the embryos that developed in control females were deficient in titin's kinase region, blastocyst transfer experiments will be done to distinguish maternal from embryonic effects. The lack of titin's kinase region in the embryo itself might contribute to the phenotype because results obtained from Du and colleagues indicate that the trophectoderm of the blastocyst, which mediates the implantation of the embryo into the endometrium, expresses titin (Du et al., 2007). Hence, titin has been implicated in being involved in promoting human trophoblast growth and invasiveness (Du et al., 2007; Xie et al., 2010). Additionally, Xie and coworker could correlate enhanced invasiveness of trophoblasts with titin expression and speculate that a lack in invasiveness is related to miscarriage in human (Xie et al., 2010). Other results show altered expression of titin in chorionic villous samples of embryos (Farina et al., 2009). These samples were obtained from women, who have developed later in pregnancy preeclampsia (pregnancy-induced hypertension), highlighting the importance of titin at the embryo-maternal interface. These results suggest that the trophoblast of the blastocyst, which is deficient in titin's kinase region, could contribute to the reduction of embryo implantation sites.

Our data provide the first genetic evidence for a role of smooth muscle titin because embryo implantation studies indentified changes in titin kinase deficient females in comparison to control mice. The aberrant implantation demonstrated at E4.5 and E5.5 resulted in mislocalization and crowding as well as a reduced number of embryo implantation sites. We related the decreased number of implantation sites to the penetration phase because the estrous cycle length, embryo transport through the oviduct, blastocyst development, and blastocyst attachment occurred normally. Loss of titin's kinase region caused altered expression of the genes encoding the M-band binding proteins MuRF1 and FHL2 as well as the L-12/15-LOX. Consistently, we found an influence on arachidonic acid metabolism with a decreased level of its metabolite 12-HETE in pregnant uterus. Angiogenesis was reduced in knockout mice, whereas we identified PDGF-B as potential angiogenic factor that is altered by the loss of titin's kinase region. Knockout smooth muscle cells did not migrate in response to PDGF-B. Therefore we speculate that the impaired angiogenesis was due to a failure in stabilizing nascent vessels because the recruitment of smooth muscle cells to the site of vessel formation was hampered. Since angiogenesis is required for embryo implantation, aberrations in these processes might contribute to pregnancy loss. Hence it is tempting to speculate that the angiogenesis defect in our knockout mice is the reason for the reduced number of implantation sites because some embryos were not able to implant properly. This is the first link of the titin's kinase region to PDGF-B and its mediator 12-HETE. Thereby, titin was identified as a new molecular regulator of angiogenesis during early pregnancy, which influences female fertility. So far, impaired vascular development that may lead to implantation failure and early miscarriage in humans has not been well studied, although disruption of angiogenesis at the site of implantation is associated with poor reproduction in humans (Meegdes et al., 1988; Vuorela et al., 2000). Moreover, it is also possible that complications in later pregnancy, which affect fetal health (intrauterine growth restriction) and maternal health (preeclampsia), are associated with molecular and cellular implantation defects (Reynolds et al., 2006). Hence, a better understanding of implantation biology will improve female fertility and fetal health because it will allow novel therapeutic advances. Tissue availability restricts studies in human, but mouse models are a suitable tool of embryo implantation because similarities between species exist. Using the knockout model of titin's kinase region, we discovered a potential molecular mechanism of angiogenesis during early pregnancy *in vivo*, which needs to be carefully interpreted in addressing human fertility and clinical relevance.

## 7 Outlook

The DsRed knockin mouse model that we generated will not only help to visualize smooth muscle titin, but also to study titin in striated muscle. Our objective is to uncover the molecular mechanisms underlying sarcomere assembly, disassembly, and turnover in myofibrillogenesis and adulthood, which is important in the physiological adaptation of muscle growth and in disease. Because of titin's large size, it is not possible to express titin tagged with a fluorescence protein in cell culture as it has already been done for several sarcomeric proteins (Wang et al., 2005). Hence our mouse model provides a novel approach to visualize titin's sequential integration into and disintegration from the sarcomere at different stages of development *in vivo* using live cell imaging. The analysis of protein turnover as well as mobility of titin along the sarcomere *in vivo* will be done utilizing photobleaching.

The smooth muscle specific knockout of titin's kinase region displayed an implantation phenotype. There is still a need to unravel the pathways responsible for smooth muscle contraction that led to crowding and mislocalization of embryo implantation sites. Fetal and maternal health, e.g. by reducing ectopic pregnancies, placenta previa, as well as pre-term labor, will benefit from an increased knowledge of uterine contraction at cellular and molecular level. So far, we analyzed the molecular mechanism underlying the reduced number of implantation sites indicating that titin's kinase region is involved in angiogenesis via PDGF-B. Angiogenesis in adults is crucial for embryo implantation and wound healing, but an imbalance in angiogenesis also contributes to malignant, inflammatory, ischemic, infectious, and immune diseases. Hence, the increased understanding of angiogenesis will help to improve fetal health and female fertility as well as therapeutic strategies, such as revascularization of ischemic tissues or inhibition of angiogenesis in cancer and skin disorders. The relevance of PDGF-B signaling as a therapeutic target has been demonstrated because inhibition of the PDGF-B and VEGF pathway in a transgenic mouse model of pancreatic islet tumors resulted in antiangiogenic and antitumor effects (Bergers et al., 2003). Furthermore, it has been shown that the inhibition of PDGF-B signaling reduced interstitial tumor pressure thereby enhancing the effect of chemotherapy (Pietras et al., 2001, 2002). We will investigate the role of titin in angiogenesis in more detail focusing on smooth muscle migration in response to PDGF-B, which might be important for angiogenesis in health and disease.

## 8 Bibliography

Abulafia O, Sherer DM. 1999. Angiogenesis of the endometrium. *Obstet Gynecol* 94:148-153.

Adams RH, Porras A, Alonso G, Jones M, Vintersten K, Panelli S, Valladares A, Perez L, Klein R, Nebreda AR. 2000. Essential role of p38alpha MAP kinase in placental but not embryonic cardiovascular development. *Mol. Cell* 6:109-116.

Alberts B, Johnson A, Lewis J, Raff M, Roberts K, Walter P. 2002. Part IV Chapter 16 (The Cytoskeleton). In: *Molecular Biology of the Cell, Fourth Edition*. 4th ed. Garland Science.

Allen E. 1922. The oestrous cycle of the mouse. *Am J Anat* 30:297-371.

Allende ML, Proia RL. 2002. Sphingosine-1-phosphate receptors and the development of the vascular system. *Biochim. Biophys. Acta* 1582:222-227.

Armulik A, Abramsson A, Betsholtz C. 2005. Endothelial/pericyte interactions. *Circ. Res* 97:512-523.

Arya R, Kedar V, Hwang JR, McDonough H, Li H, Taylor J, Patterson C. 2004. Muscle ring finger protein-1 inhibits PKC{epsilon} activation and prevents cardiomyocyte hypertrophy. *J. Cell Biol* 167:1147-1159.

Austin C, Battey J, Bradley A, Bucan M, Capecchi M, Collins F, Dove W, Duyk G, Dymecki S, Eppig J, et al. 2004. The knockout mouse project. *Nat Genet* 36:921-924.

Bagby R. 1986. Toward a comprehensive three-dimensional model of the contractile system of vertebrate smooth muscle cells. *Int. Rev. Cytol* 105:67-128.

Bähler M, Wallimann T, Eppenberger HM. 1985. Myofibrillar M-band proteins represent constituents of native thick filaments, frayed filaments and bare zone assemblages. *J. Muscle Res. Cell. Motil* 6:783-800.

Bandyopadhyay A, Zhu Y, Malik SN, Kreisberg J, Brattain MG, Sprague EA, Luo J, López-Casillas F, Sun L. 2002. Extracellular domain of TGFbeta type III receptor inhibits angiogenesis and tumor growth in human cancer cells. *Oncogene* 21:3541-3551.

Bang M, Centner T, Fornoff F, Geach A, Gotthardt M, McNabb M, Witt C, Labeit D, Gregorio C, Granzier H, et al. 2001a. The complete gene sequence of titin, expression of an unusual approximately 700-kDa titin isoform, and its interaction with obscurin identify a novel Z-line to I-band linking system. *Circ Res* 89:1065-1072.



- Bang M, Mudry R, McElhinny A, Trombitas K, Geach A, Yamasaki R, Sorimachi H, Granzier H, Gregorio C, Labeit S. 2001b. Myopalladin, a novel 145-kilodalton sarcomeric protein with multiple roles in z-disc and i-band protein assemblies. *J Cell Biol* 153:413-428.
- Baumeister A, Arber S, Caroni P. 1997. Accumulation of muscle ankyrin repeat protein transcript reveals local activation of primary myotube endcompartments during muscle morphogenesis. *J. Cell Biol* 139:1231-1242.
- Bellomo D, Headrick JP, Silins GU, Paterson CA, Thomas PS, Gartside M, Mould A, Cahill MM, Tonks ID, Grimmond SM, et al. 2000. Mice Lacking the Vascular Endothelial Growth Factor-B Gene (Vegfb) Have Smaller Hearts, Dysfunctional Coronary Vasculature, and Impaired Recovery From Cardiac Ischemia. *Circ Res* 86:e29-35.
- Bergers G, Song S. 2005. The role of pericytes in blood-vessel formation and maintenance. *Neuro-oncology* 7:452-464.
- Bergers G, Song S, Meyer-Morse N, Bergsland E, Hanahan D. 2003. Benefits of targeting both pericytes and endothelial cells in the tumor vasculature with kinase inhibitors. *J. Clin. Invest* 111:1287-1295.
- Bethesda Research Laboratories. 1986. BRL pUC host: *E. coli* DH5 $\alpha$  competent cells. *Focus* 8:1-2.
- Bodine S, Latres E, Baumhueter S, Lai V, Nunez L, Clarke B, Poueymirou W, Panaro F, Na E, Dharmarajan K, et al. 2001. Identification of ubiquitin ligases required for skeletal muscle atrophy. *Science* 294:1704-1708.
- Boomsma CM, Kavelaars A, Eijkemans MJC, Lentjes EG, Fauser BCJM, Heijnen CJ, Macklon NS. 2009. Endometrial secretion analysis identifies a cytokine profile predictive of pregnancy in IVF. *Hum. Reprod* 24:1427-1435.
- Bradford MM. 1976. A rapid and sensitive method for the quantitation of microgram quantities of protein utilizing the principle of protein-dye binding. *Anal. Biochem* 72:248-254.
- Bradley A, Evans M, Kaufman MH, Robertson E. 1984. Formation of germ-line chimaeras from embryo-derived teratocarcinoma cell lines. *Nature* 309:255-256.
- Bullard B, Ferguson C, Minajeva A, Leake M, Gautel M, Labeit D, Ding L, Labeit S, Horwitz J, Leonard K, et al. 2004. Association of the chaperone  $\alpha$ B-crystallin with titin in heart muscle. *J Biol Chem* 279:7917-7924.
- Carmeliet P, Ferreira V, Breier G, Pollefeyt S, Kieckens L, Gertsenstein M, Fahrig M, Vandenhoek A, Harpal K, Eberhardt C, et al. 1996. Abnormal blood vessel development and lethality in embryos lacking a single VEGF allele. *Nature* 380:435-439.
- Carmeliet P. 2005. Angiogenesis in life, disease and medicine. *Nature* 438:932-6.

Carson DD, Bagchi I, Dey SK, Enders AC, Fazleabas AT, Lessey BA, Yoshinaga K. 2000. Embryo implantation. *Dev. Biol* 223:217-237.

Cazorla O, Freiburg A, Helmes M, Centner T, McNabb M, Wu Y, Trombitas K, Labeit S, Granzier H. 2000. Differential expression of cardiac titin isoforms and modulation of cellular stiffness. *Circ Res* 86:59-67.

Centner T, Yano J, Kimura E, McElhinny A, Pelin K, Witt C, Bang M, Trombitas K, Granzier H, Gregorio C, et al. 2001. Identification of Muscle Specific Ring Finger Proteins as Potential Regulators of the Titin Kinase Domain. *J Mol Biol* 306:717-726.

Chakraborty I, Das SK, Dey SK. 1995. Differential expression of vascular endothelial growth factor and its receptor mRNAs in the mouse uterus around the time of implantation. *J. Endocrinol* 147:339-352.

Chi R, Olenych S, Kim K, Keller T. 2005. Smooth muscle alpha-actinin interaction with smitin. *Int J Biochem Cell Biol* 37:1470-1482.

Chi RJ, Simon AR, Bienkiewicz EA, Felix A, Keller TCS. 2008. Smooth muscle titin Zq domain interaction with the smooth muscle alpha-actinin central rod. *J. Biol. Chem* 283:20959-20967.

Cleaver O, Melton DA. 2003. Endothelial signaling during development. *Nat. Med* 9:661-668.

Connolly JM, Rose DP. 1998. Enhanced angiogenesis and growth of 12-lipoxygenase gene-transfected MCF-7 human breast cancer cells in athymic nude mice. *Cancer Lett* 132:107-112.

Crane LH, Martin L. 1991. In vivo myometrial activity during early pregnancy and pseudopregnancy in the rat. *Reprod. Fertil. Dev* 3:233-244.

De M, Sanford TR, Wood GW. 1993. Expression of interleukin 1, interleukin 6 and tumour necrosis factor alpha in mouse uterus during the peri-implantation period of pregnancy. *J. Reprod. Fertil* 97:83-89.

Deng C, Capecchi M. 1992. Reexamination of gene targeting frequency as a function of the extent of homology between the targeting vector and the target locus. *Mol Cell Biol* 12:3365-3371.

van Deursen J, Wieringa B. 1992. Targeting of the creatine kinase M gene in embryonic stem cells using isogenic and nonisogenic vectors. *Nucleic Acids Res* 20:3815-3820.

Dey SK, Lim H, Das SK, Reese J, Paria BC, Daikoku T, Wang H. 2004. Molecular cues to implantation. *Endocr. Rev* 25:341-373.

Doetschman T, Gregg R, Maeda N, Hooper M, Melton D, Thompson S, Smithies O. 1987. Targetted correction of a mutant HPRT gene in mouse embryonic stem cells. *Nature* 330:576-578.

- Draeger A, Amos WB, Ikebe M, Small JV. 1990. The cytoskeletal and contractile apparatus of smooth muscle: contraction bands and segmentation of the contractile elements. *J. Cell Biol* 111:2463-2473.
- Du M, Zhou W, Yan F, Zhu X, He Y, Yang J, Li D. 2007. Cyclosporine A induces titin expression via MAPK/ERK signalling and improves proliferative and invasive potential of human trophoblast cells. *Hum. Reprod* 22:2528-2537.
- Evans MJ, Kaufman MH. 1981. Establishment in culture of pluripotential cells from mouse embryos. *Nature* 292:154-6.
- Farina A, Morano D, Arcelli D, De Sanctis P, Sekizawa A, Purwosunu Y, Zucchini C, Simonazzi G, Okai T, Rizzo N. 2009. Gene expression in chorionic villous samples at 11 weeks of gestation in women who develop preeclampsia later in pregnancy: implications for screening. *Prenat. Diagn* 29:1038-1044.
- Fong GH, Rossant J, Gertsenstein M, Breitman ML. 1995. Role of the Flt-1 receptor tyrosine kinase in regulating the assembly of vascular endothelium. *Nature* 376:66-70.
- Fouladi-Nashta AA, Jones CJP, Nijjar N, Mohamet L, Smith A, Chambers I, Kimber SJ. 2005. Characterization of the uterine phenotype during the peri-implantation period for LIF-null, MF1 strain mice. *Dev. Biol* 281:1-21.
- Freiburg A, Gautel M. 1996. A molecular map of the interactions between titin and myosin-binding protein C. Implications for sarcomeric assembly in familial hypertrophic cardiomyopathy. *Eur J Biochem* 235:317-323.
- Freiburg A, Trombitas K, Hell W, Cazorla O, Fougerousse F, Centner T, Kolmerer B, Witt C, Beckmann J, Gregorio C, et al. 2000. Series of exon-skipping events in the elastic spring region of titin as the structural basis for myofibrillar elastic diversity. *Circ Res* 86:1114-1121.
- Frick KM, Berger-Sweeney J. 2001. Spatial reference memory and neocortical neurochemistry vary with the estrous cycle in C57BL/6 mice. *Behav. Neurosci* 115:229-237.
- Gale NW, Yancopoulos GD. 1999. Growth factors acting via endothelial cell-specific receptor tyrosine kinases: VEGFs, angiopoietins, and ephrins in vascular development. *Genes Dev* 13:1055-1066.
- Gautel M, Goulding D, Bullard B, Weber K, Fürst DO. 1996. The central Z-disk region of titin is assembled from a novel repeat in variable copy numbers. *J. Cell. Sci* 109 ( Pt 11):2747-2754.
- Gautel M, Castiglione M, Pfuhl M, Motta A, Pastore A. 1995. A calmodulin-binding sequence in the C-terminus of human cardiac titin kinase. *Eur J Biochem* 230:752-759.

- Gautel M, Leonard K, Labeit S. 1993. Phosphorylation of KSP motifs in the C-terminal region of titin in differentiating myoblasts. *EMBO J* 12:3827-3834.
- Geiger B, Dutton A, Tokuyasu K, Singer S. 1981. Immunoelectron microscope studies of membrane-microfilament interactions: distributions of alpha-actinin, tropomyosin, and vinculin in intestinal epithelial brush border and chicken gizzard smooth muscle cells. *J Cell Biol* 91:614-628.
- Gerhardt H, Golding M, Fruttiger M, Ruhrberg C, Lundkvist A, Abramsson A, Jeltsch M, Mitchell C, Alitalo K, Shima D, et al. 2003. VEGF guides angiogenic sprouting utilizing endothelial tip cell filopodia. *J. Cell Biol* 161:1163-1177.
- Gordon JD, Shifren JL, Foulk RA, Taylor RN, Jaffe RB. 1995. Angiogenesis in the human female reproductive tract. *Obstet Gynecol Surv* 50:688-697.
- Gotthardt M, Hammer R, Hubner N, Monti J, Witt C, McNabb M, Richardson J, Granzier H, Labeit S, Herz J. 2003. Conditional expression of mutant M-line titins results in cardiomyopathy with altered sarcomere structure. *J Biol Chem* 278:6059-6065.
- Granzier H, Kellermayer M, Helmes M, Trombitas K. 1997. Titin elasticity and mechanism of passive force development in rat cardiac myocytes probed by thin-filament extraction. *Biophys J* 73:2043-2053.
- Granzier H, Labeit S. 2004. The giant protein titin: a major player in myocardial mechanics, signaling, and disease. *Circ Res* 94:284-295.
- Granzier HL, Radke MH, Peng J, Westermann D, Nelson OL, Rost K, King NMP, Yu Q, Tschöpe C, McNabb M, et al. 2009. Truncation of titin's elastic PEVK region leads to cardiomyopathy with diastolic dysfunction. *Circ. Res* 105:557-564.
- Gräter F, Shen J, Jiang H, Gautel M, Grubmüller H. 2005. Mechanically induced titin kinase activation studied by force-probe molecular dynamics simulations. *Biophys J* 88:790-804.
- Gregorio CC, Granzier H, Sorimachi H, Labeit S. 1999. Muscle assembly: a titanic achievement? *Curr Opin Cell Biol* 11:18-25.
- Gregorio CC, Trombitás K, Centner T, Kolmerer B, Stier G, Kunke K, Suzuki K, Obermayr F, Herrmann B, Granzier H, et al. 1998. The NH2 terminus of titin spans the Z-disc: its interaction with a novel 19-kD ligand (T-cap) is required for sarcomeric integrity. *J Cell Biol* 143:1013-27.
- Gregorio C, Perry C, McElhinny A. 2006. Functional properties of the titin/connectin-associated proteins, the muscle-specific RING finger proteins (MURFs), in striated muscle. *J Muscle Res Cell Motil*:1-12.
- Gu JL, Pei H, Thomas L, Nadler JL, Rossi JJ, Lanting L, Natarajan R. 2001. Ribozyme-mediated inhibition of rat leukocyte-type 12-lipoxygenase prevents intimal hyperplasia in balloon-injured rat carotid arteries. *Circulation* 103:1446-1452.

- Guilford WH, Warshaw DM. 1998. The molecular mechanics of smooth muscle myosin. *Comp. Biochem. Physiol. B, Biochem. Mol. Biol* 119:451-458.
- Halbert SA, Becker DR, Szal SE. 1989. Ovum transport in the rat oviductal ampulla in the absence of muscle contractility. *Biol. Reprod* 40:1131-1136.
- Halbert SA, Tam PY, Blandau RJ. 1976. Egg transport in the rabbit oviduct: the roles of cilia and muscle. *Science* 191:1052-1053.
- Halder JB, Zhao X, Soker S, Paria BC, Klagsbrun M, Das SK, Dey SK. 2000. Differential expression of VEGF isoforms and VEGF(164)-specific receptor neuropilin-1 in the mouse uterus suggests a role for VEGF(164) in vascular permeability and angiogenesis during implantation. *Genesis* 26:213-224.
- Hama K, Aoki J, Inoue A, Endo T, Amano T, Motoki R, Kanai M, Ye X, Chun J, Matsuki N, et al. 2007. Embryo spacing and implantation timing are differentially regulated by LPA3-mediated lysophosphatidic acid signaling in mice. *Biol. Reprod* 77:954-959.
- Hanahan D, Jessee J, Bloom FR. 1991. Plasmid transformation of *Escherichia coli* and other bacteria. *Meth. Enzymol* 204:63-113.
- Hanson J, Huxley HE. 1953. Structural basis of the cross-striations in muscle. *Nature* 172:530-2.
- Hasselgren PO, Fischer JE. 2001. Muscle cachexia: current concepts of intracellular mechanisms and molecular regulation. *Ann. Surg* 233:9-17.
- Hasty P, Rivera-Pérez J, Bradley A. 1991. The length of homology required for gene targeting in embryonic stem cells. *Mol. Cell. Biol* 11:5586-5591.
- Heierhorst J, Probst WC, Vilim FS, Buku A, Weiss KR. 1994. Autophosphorylation of molluscan twitchin and interaction of its kinase domain with calcium/calmodulin. *J. Biol. Chem* 269:21086-21093.
- Hellström M, Kalén M, Lindahl P, Abramsson A, Betsholtz C. 1999. Role of PDGF-B and PDGFR-beta in recruitment of vascular smooth muscle cells and pericytes during embryonic blood vessel formation in the mouse. *Development* 126:3047-3055.
- Hellström M, Phng L, Hofmann JJ, Wallgard E, Coultas L, Lindblom P, Alva J, Nilsson A, Karlsson L, Gaiano N, et al. 2007. Dll4 signalling through Notch1 regulates formation of tip cells during angiogenesis. *Nature* 445:776-780.
- Helmes M, Trombitas K, Centner T, Kellermayer M, Labeit S, Linke W, Granzier H. 1999. Mechanically driven contour-length adjustment in rat cardiac titin's unique N2B sequence: titin is an adjustable spring. *Circ Res* 84:1339-1352.

Herrera AM, Martinez EC, Seow CY. 2004. Electron microscopic study of actin polymerization in airway smooth muscle. *Am. J. Physiol. Lung Cell Mol. Physiol* 286:L1161-1168.

Hodgkinson JL, Newman TM, Marston SB, Severs NJ. 1995. The structure of the contractile apparatus in ultrarapidly frozen smooth muscle: freeze-fracture, deep-etch, and freeze-substitution studies. *J. Struct. Biol* 114:93-104.

Hoffmeister H, Schulz H. 1961. Light optical and electronoptical findings in the endometrium of the sexually mature woman during the proliferation and secretion phase with special reference to fiber structures. *Beitr Pathol Anat* 124:415-446.

Houmeida A, Holt J, Tskhovrebova L, Trinick J. 1995. Studies of the interaction between titin and myosin. *J Cell Biol* 131:1471-1481.

Hu MC, Wang YP, Mikhail A, Qiu WR, Tan TH. 1999. Murine p38-delta mitogen-activated protein kinase, a developmentally regulated protein kinase that is activated by stress and proinflammatory cytokines. *J. Biol. Chem* 274:7095-7102.

Huang S, Tsai M, Chen G, Wu C, Chen S. 2007. A systematic MS-based approach for identifying in vitro substrates of PKA and PKG in rat uteri. *J Proteome Res* 6:2674-84.

Huxley AF. 1957. Muscle structure and theories of contraction. *Prog Biophys Biophys Chem* 7:255-318.

Huxley AF, Niedergerke R. 1954. Structural changes in muscle during contraction; interference microscopy of living muscle fibres. *Nature* 173:971-973.

Hyder SM, Nawaz Z, Chiappetta C, Stancel GM. 2000. Identification of functional estrogen response elements in the gene coding for the potent angiogenic factor vascular endothelial growth factor. *Cancer Res* 60:3183-3190.

Hyder SM, Stancel GM. 1999. Regulation of angiogenic growth factors in the female reproductive tract by estrogens and progestins. *Mol. Endocrinol* 13:806-811.

Isaacs W, Kim I, Struve A, Fulton A. 1989. Biosynthesis of titin in cultured skeletal muscle cells. *J Cell Biol* 109:2189-2195.

Isaji M, Miyata H, Ajisawa Y, Takehana Y, Yoshimura N. 1997. Tranilast inhibits the proliferation, chemotaxis and tube formation of human microvascular endothelial cells in vitro and angiogenesis in vivo. *Br. J. Pharmacol* 122:1061-1066.

Itoh-Satoh M, Hayashi T, Nishi H, Koga Y, Arimura T, Koyanagi T, Takahashi M, Hohda S, Ueda K, Nouchi T, et al. 2002. Titin Mutations as the Molecular Basis for Dilated Cardiomyopathy. *Biochem Biophys Res Commun* 291:385-393.

- Iwaki T, Sandoval-Cooper MJ, Paiva M, Kobayashi T, Ploplis VA, Castellino FJ. 2002. Fibrinogen stabilizes placental-maternal attachment during embryonic development in the mouse. *Am. J. Pathol* 160:1021-1034.
- Jain RK. 2003. Molecular regulation of vessel maturation. *Nat. Med* 9:685-693.
- Jasper MJ, Tremellen KP, Robertson SA. 2007. Reduced expression of IL-6 and IL-1alpha mRNAs in secretory phase endometrium of women with recurrent miscarriage. *J. Reprod. Immunol* 73:74-84.
- Jeyaseelan R, Poizat C, Baker RK, Abdishoo S, Isterabadi LB, Lyons GE, Kedes L. 1997. A novel cardiac-restricted target for doxorubicin. CARP, a nuclear modulator of gene expression in cardiac progenitor cells and cardiomyocytes. *J. Biol. Chem* 272:22800-22808.
- Kaul A, Koster M, Neuhaus H, Braun T. 2000. Myf-5 revisited: loss of early myotome formation does not lead to a rib phenotype in homozygous Myf-5 mutant mice. *Cell* 102:17-19.
- Keller TC, Eilertsen K, Higginbotham M, Kazmierski S, Kim KT, Velichkova M. 2000. Role of titin in nonmuscle and smooth muscle cells. *Adv. Exp. Med. Biol* 481:265-277; discussion 278-281.
- Kellermayer M, Smith S, Granzier H, Bustamante C. 1997. Folding-unfolding transitions in single titin molecules characterized with laser tweezers. *Science* 276:1112-1116.
- Kennedy TG. 1977. Evidence for a role for prosaglandins in the initiation of blastocyst implantation in the rat. *Biol. Reprod* 16:286-291.
- Kim K, Keller T. 2002. Smitin, a novel smooth muscle titin-like protein, interacts with myosin filaments in vivo and in vitro. *J Cell Biol* 156:101-112.
- Kinbara K, Sorimachi H, Ishiura S, Suzuki K. 1997. Muscle-specific calpain, p94, interacts with the extreme C-terminal region of connectin, a unique region flanked by two immunoglobulin C2 motifs. *Arch Biochem Biophys* 342:99-107.
- Kinoshita K, Satoh K, Ishihara O, Tsutsumi O, Nakayama M, Kashimura F, Mizuno M. 1985. Involvement of prostaglandins in implantation in the pregnant mouse. *Adv. Prostaglandin Thromboxane Leukot. Res* 15:605-607.
- Kirfel J, Pantelis D, Kabba M, Kahl P, Röper A, Kalff JC, Buettner R. 2008. Impaired intestinal wound healing in Fhl2-deficient mice is due to disturbed collagen metabolism. *Exp. Cell Res* 314:3684-3691.
- Klauber N, Rohan RM, Flynn E, D'Amato RJ. 1997. Critical components of the female reproductive pathway are suppressed by the angiogenesis inhibitor AGM-1470. *Nat. Med* 3:443-446.

- Knoll R, Hoshijima M, Hoffman H, Person V, Lorenzen-Schmidt I, Bang M, Hayashi T, Shiga N, Yasukawa H, Schaper W, et al. 2002. The Cardiac Mechanical Stretch Sensor Machinery Involves a Z Disc Complex that Is Defective in a Subset of Human Dilated Cardiomyopathy. *Cell* 111:943-955.
- Knupp C, Luther P, Squire J. 2002. Titin organisation and the 3D architecture of the vertebrate-striated muscle I-band. *J Mol Biol* 322:731-739.
- Kolmerer B, Olivieri N, Witt C, Herrmann B, Labeit S. 1996. Genomic organization of M line titin and its tissue-specific expression in two distinct isoforms. *J Mol Biol* 256:556-563.
- Kong Y, Flick MJ, Kudla AJ, Konieczny SF. 1997. Muscle LIM protein promotes myogenesis by enhancing the activity of MyoD. *Mol. Cell. Biol* 17:4750-4760.
- Kontogianni-Konstantopoulos A, Bloch RJ. 2003. The hydrophilic domain of small ankyrin-1 interacts with the two N-terminal immunoglobulin domains of titin. *J. Biol. Chem* 278:3985-3991.
- Kramerova I, Kudryashova E, Tidball J, Spencer M. 2004. Null mutation of calpain 3 (p94) in mice causes abnormal sarcomere formation in vivo and in vitro. *Hum Mol Genet* 13:1373-1388.
- Labeit S, Barlow D, Gautel M, Gibson T, Holt J, Hsieh C, Francke U, Leonard K, Wardale J, Whiting A, et al. 1990. A regular pattern of two types of 100-residue motif in the sequence of titin. *Nature* 345:273-276.
- Labeit S, Gautel M, Lakey A, Trinick J. 1992. Towards a molecular understanding of titin. *EMBO J* 11:1711-1716.
- Labeit S, Kolmerer B. 1995. Titins: giant proteins in charge of muscle ultrastructure and elasticity. *Science* 270:293-296.
- Labeit S, Lahmers S, Burkart C, Fong C, McNabb M, Witt S, Witt C, Labeit D, Granzier H. 2006. Expression of distinct classes of titin isoforms in striated and smooth muscles by alternative splicing, and their conserved interaction with filamins. *J Mol Biol* 362:664-681.
- Lange S, Auerbach D, McLoughlin P, Perriard E, Schafer B, Perriard J, Ehler E. 2002. Subcellular targeting of metabolic enzymes to titin in heart muscle may be mediated by DRAL/FHL-2. *J Cell Sci* 115:4925-4936.
- Lange S, Xiang F, Yakovenko A, Vihola A, Hackman P, Rostkova E, Kristensen J, Brandmeier B, Franzen G, Hedberg B, et al. 2005. The Kinase Domain of Titin Controls Muscle Gene Expression and Protein Turnover. *Science* 308:1599-1603.
- de Lange WJ, Halabi CM, Beyer AM, Sigmund CD. 2008. Germ line activation of the Tie2 and SMMHC promoters causes noncell-specific deletion of floxed alleles. *Physiol. Genomics* 35:1-4.



- Li Q, Cheon Y, Kannan A, Shanker S, Bagchi IC, Bagchi MK. 2004. A novel pathway involving progesterone receptor, 12/15-lipoxygenase-derived eicosanoids, and peroxisome proliferator-activated receptor gamma regulates implantation in mice. *J. Biol. Chem* 279:11570-11581.
- Lim H, Gupta RA, Ma WG, Paria BC, Moller DE, Morrow JD, DuBois RN, Trzaskos JM, Dey SK. 1999. Cyclo-oxygenase-2-derived prostacyclin mediates embryo implantation in the mouse via PPARdelta. *Genes Dev* 13:1561-1574.
- Lim H, Paria BC, Das SK, Dinchuk JE, Langenbach R, Trzaskos JM, Dey SK. 1997. Multiple female reproductive failures in cyclooxygenase 2-deficient mice. *Cell* 91:197-208.
- Lindahl P, Johansson BR, Levéen P, Betsholtz C. 1997. Pericyte loss and microaneurysm formation in PDGF-B-deficient mice. *Science* 277:242-245.
- Linke W, Ivemeyer M, Olivieri N, Kolmerer B, Ruegg J, Labeit S. 1996. Towards a molecular understanding of the elasticity of titin. *J Mol Biol* 261:62-71.
- Linke W, Rudy D, Centner T, Gautel M, Witt C, Labeit S, Gregorio C. 1999. I-band titin in cardiac muscle is a three-element molecular spring and is critical for maintaining thin filament structure. *J Cell Biol* 146:631-644.
- Liu Y, Wada R, Yamashita T, Mi Y, Deng CX, Hobson JP, Rosenfeldt HM, Nava VE, Chae SS, Lee MJ, et al. 2000. Edg-1, the G protein-coupled receptor for sphingosine-1-phosphate, is essential for vascular maturation. *J. Clin. Invest* 106:951-961.
- Lobov IB, Renard RA, Papadopoulos N, Gale NW, Thurston G, Yancopoulos GD, Wiegand SJ. 2007. Delta-like ligand 4 (Dll4) is induced by VEGF as a negative regulator of angiogenic sprouting. *Proc. Natl. Acad. Sci. U.S.A* 104:3219-3224.
- Loonstra A, Vooijs M, Beverloo HB, Allak BA, van Drunen E, Kanaar R, Berns A, Jonkers J. 2001. Growth inhibition and DNA damage induced by Cre recombinase in mammalian cells. *Proc Natl Acad Sci U S A* 98:9209-9214.
- Ma W, Tan J, Matsumoto H, Robert B, Abrahamson DR, Das SK, Dey SK. 2001. Adult tissue angiogenesis: evidence for negative regulation by estrogen in the uterus. *Mol. Endocrinol* 15:1983-1992.
- Maher PA, Cox GF, Singer SJ. 1985. Zeugmatin: a new high molecular weight protein associated with Z lines in adult and early embryonic striated muscle. *J. Cell Biol* 101:1871-1883.
- Maisonpierre PC, Suri C, Jones PF, Bartunkova S, Wiegand SJ, Radziejewski C, Compton D, McClain J, Aldrich TH, Papadopoulos N, et al. 1997. Angiopoietin-2, a natural antagonist for Tie2 that disrupts in vivo angiogenesis. *Science* 277:55-60.
- Maruyama K, Kimura S, Ohashi K, Kuwano Y. 1981. Connectin, an elastic protein of muscle. Identification of "titin" with connectin. *J. Biochem* 89:701-709.

Maruyama K, Murakami F, Ohashi K. 1977. Connectin, an elastic protein of muscle. *Comparative Biochemistry. J Biochem (Tokyo)* 82:339-345.

Matsumoto H, Ma W, Daikoku T, Zhao X, Paria BC, Das SK, Trzaskos JM, Dey SK. 2002. Cyclooxygenase-2 differentially directs uterine angiogenesis during implantation in mice. *J Biol Chem* 277:29260-7.

Matsuura T, Kimura S, Ohtsuka S, Maruyama K. 1991. Isolation and characterization of 1,200 kDa peptide of alpha-connectin. *J. Biochem* 110:474-478.

Mayans O, van der Ven PF, Wilm M, Mues A, Young P, Fürst DO, Wilmanns M, Gautel M. 1998. Structural basis for activation of the titin kinase domain during myofibrillogenesis. *Nature* 395:863-9.

McElhinny A, Kakinuma K, Sorimachi H, Labeit S, Gregorio C. 2002. Muscle-specific RING finger-1 interacts with titin to regulate sarcomeric M-line and thick filament structure and may have nuclear functions via its interaction with glucocorticoid modulatory element binding protein-1. *J Cell Biol* 157:125-136.

Meegdes BH, Ingenhoes R, Peeters LL, Exalto N. 1988. Early pregnancy wastage: relationship between chorionic vascularization and embryonic development. *Fertil. Steril* 49:216-220.

Mizugishi K, Li C, Olivera A, Bielawski J, Bielawska A, Deng C, Proia RL. 2007. Maternal disturbance in activated sphingolipid metabolism causes pregnancy loss in mice. *J. Clin. Invest* 117:2993-3006.

Mudgett JS, Ding J, Guh-Siesel L, Chartrain NA, Yang L, Gopal S, Shen MM. 2000. Essential role for p38alpha mitogen-activated protein kinase in placental angiogenesis. *Proc. Natl. Acad. Sci. U.S.A* 97:10454-10459.

Mues A, van der Ven PF, Young P, Fürst DO, Gautel M. 1998. Two immunoglobulin-like domains of the Z-disc portion of titin interact in a conformation-dependent way with telethonin. *FEBS Lett* 428:111-114.

Mulholland J, Aplin JD, Ayad S, Hong L, Glasser SR. 1992. Loss of collagen type VI from rat endometrial stroma during decidualization. *Biol. Reprod* 46:1136-1143.

Müller JM, Metzger E, Greschik H, Bosserhoff A, Mercep L, Buettner R, Schüle R. 2002. The transcriptional coactivator FHL2 transmits Rho signals from the cell membrane into the nucleus. *EMBO J* 21:736-748.

Muller-Seitz M, Kaupmann K, Labeit S, Jockusch H. 1993. Chromosomal localization of the mouse titin gene and its relation to "muscular dystrophy with myositis" and nebulin genes on chromosome 2. *Genomics* 18:559-561.

- Nagy A, Gertsenstein M, Vintersten K. 2003a. Introduction of Foreign DNA into Embryonic Stem Cells (Chapter 10). In: *Manipulating the Mouse Embryo*. 3rd ed. Cold Spring Harbor Laboratory.
- Nagy A, Gertsenstein M, Vintersten K. 2003b. Techniques for Visualizing Gene Products, Cells, Tissues, and Organ Systems (Chapter 16). In: *Manipulating the Mouse Embryo*. 3rd ed. Cold Spring Harbor Laboratory.
- Nakao J, Ooyama T, Ito H, Chang WC, Murota S. 1982. Comparative effect of lipoxygenase products of arachidonic acid on rat aortic smooth muscle cell migration. *Atherosclerosis* 44:339-342.
- Natarajan R, Bai W, Rangarajan V, Gonzales N, Gu JL, Lanting L, Nadler JL. 1996. Platelet-derived growth factor BB mediated regulation of 12-lipoxygenase in porcine aortic smooth muscle cells. *J. Cell. Physiol* 169:391-400.
- Natarajan R, Gonzales N, Lanting L, Nadler J. 1994. Role of the lipoxygenase pathway in angiotensin II-induced vascular smooth muscle cell hypertrophy. *Hypertension* 23:142-147.
- Natarajan R, Gu JL, Rossi J, Gonzales N, Lanting L, Xu L, Nadler J. 1993. Elevated glucose and angiotensin II increase 12-lipoxygenase activity and expression in porcine aortic smooth muscle cells. *Proc. Natl. Acad. Sci. U.S.A* 90:4947-4951.
- Nave R, Furst D, Weber K. 1989. Visualization of the polarity of isolated titin molecules: a single globular head on a long thin rod as the M band anchoring domain? *J Cell Biol* 109:2177-2187.
- Neagoe C, Kulke M, del Monte F, Gwathmey J, de Tombe P, Hajjar R, Linke W. 2002. Titin isoform switch in ischemic human heart disease. *Circulation* 106:1333-1341.
- Neuhoff V, Arold N, Taube D, Ehrhardt W. 1988. Improved staining of proteins in polyacrylamide gels including isoelectric focusing gels with clear background at nanogram sensitivity using Coomassie Brilliant Blue G-250 and R-250. *Electrophoresis* 9:255-262.
- Nicholas G, Thomas M, Langley B, Somers W, Patel K, Kemp C, Sharma M, Kambadur R. 2002. Titin-cap associates with, and regulates secretion of, Myostatin. *J Cell Physiol* 193:120-131.
- Nie D, Krishnamoorthy S, Jin R, Tang K, Chen Y, Qiao Y, Zacharek A, Guo Y, Milanini J, Pages G, et al. 2006. Mechanisms regulating tumor angiogenesis by 12-lipoxygenase in prostate cancer cells. *J. Biol. Chem* 281:18601-18609.
- NSFG. 2002. Listing I - Key Statistics from the National Survey of Family Growth. Available from: [http://www.cdc.gov/nchs/nsfg/abc\\_list\\_i.htm#infertility](http://www.cdc.gov/nchs/nsfg/abc_list_i.htm#infertility)

Obermann W, Gautel M, Steiner F, van der Ven P, Weber K, Furst D. 1996. The structure of the sarcomeric M band: localization of defined domains of myomesin, M-protein, and the 250-kDa carboxy-terminal region of titin by immunoelectron microscopy. *J Cell Biol* 134:1441-1453.

Obermann W, Gautel M, Weber K, Furst D. 1997. Molecular structure of the sarcomeric M band: mapping of titin and myosin binding domains in myomesin and the identification of a potential regulatory phosphorylation site in myomesin. *EMBO J* 16:211-220.

Ohtsuka H, Yajima H, Maruyama K, Kimura S. 1997a. Binding of the N-terminal 63 kDa portion of connectin/titin to alpha-actinin as revealed by the yeast two-hybrid system. *FEBS Lett* 401:65-67.

Ohtsuka H, Yajima H, Maruyama K, Kimura S. 1997b. The N-terminal Z repeat 5 of connectin/titin binds to the C-terminal region of alpha-actinin. *Biochem Biophys Res Commun* 235:1-3.

Ohtsuka S, Kimura S, Kawamura Y, Hirono Y, Maruyama K. 1992. Chicken leg muscle alpha-connectin as studied by a monoclonal antibody to the 1200 kDa fragment. *Comp. Biochem. Physiol., B* 103:543-546.

Okagaki T, Weber FE, Fischman DA, Vaughan KT, Mikawa T, Reinach FC. 1993. The major myosin-binding domain of skeletal muscle MyBP-C (C protein) resides in the COOH-terminal, immunoglobulin C2 motif. *J. Cell Biol* 123:619-626.

Ottenheijm CAC, Hidalgo C, Rost K, Gotthardt M, Granzier H. 2009a. Altered contractility of skeletal muscle in mice deficient in titin's M-band region. *J. Mol. Biol* 393:10-26.

Ottenheijm CAC, Kottner AM, Buck D, Luo X, Greer K, Hoying A, Labeit S, Granzier H. 2009b. Tuning Passive Mechanics through Differential Splicing of Titin during Skeletal Muscle Development. *Biophys. J* 97:2277-2286.

Paria BC, Das SK, Andrews GK, Dey SK. 1993. Expression of the epidermal growth factor receptor gene is regulated in mouse blastocysts during delayed implantation. *Proc. Natl. Acad. Sci. U.S.A* 90:55-59.

Parr MB, Parr EL. 1989. The implantation reaction. In: Wynn RM, Jollie WP (eds.), *Biology of The Uterus*. New York: Plenum Press. . p 233-277.

Patricia MK, Natarajan R, Dooley AN, Hernandez F, Gu JL, Berliner JA, Rossi JJ, Nadler JL, Meidell RS, Hedrick CC. 2001. Adenoviral delivery of a leukocyte-type 12 lipoxygenase ribozyme inhibits effects of glucose and platelet-derived growth factor in vascular endothelial and smooth muscle cells. *Circ. Res* 88:659-665.

Peckham M, Young P, Gautel M. 1997. Constitutive and variable regions of Z-disk titin/connectin in myofibril formation: a dominant-negative screen. *Cell Struct Funct* 22:95-101.

- Pelin K, Ridanpää M, Donner K, Wilton S, Krishnarajah J, Laing N, Kolmerer B, Millevoi S, Labeit S, de la Chapelle A, et al. 1997. Refined localisation of the genes for nebulin and titin on chromosome 2q allows the assignment of nebulin as a candidate gene for autosomal recessive nemaline myopathy. *Eur. J. Hum. Genet* 5:229-234.
- Peng J, Raddatz K, Labeit S, Granzier H, Gotthardt M. 2006. Muscle atrophy in Titin M-line deficient mice. *J Muscle Res Cell Motil*:1-8.
- Peng J, Raddatz K, Molkentin J, Wu Y, Labeit S, Granzier H, Gotthardt M. 2007. Cardiac hypertrophy and reduced contractility in hearts deficient in the titin kinase region. *Circulation* 115:743-751.
- Perez Martinez S, Viggiano M, Franchi AM, Herrero MB, Ortiz ME, Gimeno MF, Villalón M. 2000. Effect of nitric oxide synthase inhibitors on ovum transport and oviductal smooth muscle activity in the rat oviduct. *J. Reprod. Fertil* 118:111-117.
- Persechini A, Stull JT. 1984. Phosphorylation kinetics of skeletal muscle myosin and the effect of phosphorylation on actomyosin adenosinetriphosphatase activity. *Biochemistry* 23:4144-4150.
- Piedrahita J, Zhang S, Hagaman J, Oliver P, Maeda N. 1992. Generation of mice carrying a mutant apolipoprotein E gene inactivated by gene targeting in embryonic stem cells. *Proc Natl Acad Sci U S A* 89:4471-4475.
- Pietras K, Ostman A, Sjöquist M, Buchdunger E, Reed RK, Heldin CH, Rubin K. 2001. Inhibition of platelet-derived growth factor receptors reduces interstitial hypertension and increases transcapillary transport in tumors. *Cancer Res* 61:2929-2934.
- Pietras K, Rubin K, Sjöblom T, Buchdunger E, Sjöquist M, Heldin C, Ostman A. 2002. Inhibition of PDGF receptor signaling in tumor stroma enhances antitumor effect of chemotherapy. *Cancer Res* 62:5476-5484.
- Pizon V, Iakovenko A, van der Ven P, Kelly R, Fatu C, Furst D, Karsenti E, Gautel M. 2002. Transient association of titin and myosin with microtubules in nascent myofibrils directed by the MURF2 RING-finger protein. *J Cell Sci* 115:4469-4482.
- Plaks V, Kalchenko V, Dekel N, Neeman M. 2006. MRI analysis of angiogenesis during mouse embryo implantation. *Magn Reson Med* 55:1013-1022.
- Psychoyos A. 1986. Uterine receptivity for implantation. *Ann. N. Y. Acad. Sci* 476:36-42.
- Pusey J, Kelly WA, Bradshaw JM, Porter DG. 1980. Myometrial activity and the distribution of blastocysts in the uterus of the rat: interference by relaxin. *Biol. Reprod* 23:394-397.

- Raab G, Kover K, Paria BC, Dey SK, Ezzell RM, Klagsbrun M. 1996. Mouse preimplantation blastocysts adhere to cells expressing the transmembrane form of heparin-binding EGF-like growth factor. *Development* 122:637-645.
- Raddatz K, Albrecht D, Hochgrafe F, Hecker M, Gotthardt M. 2008. A proteome map of murine heart and skeletal muscle. *Proteomics* 8:1885-1897.
- Radke M, Peng J, Wu Y, McNabb M, Nelson O, Granzier H, Gotthardt M. 2007. Targeted deletion of titin N2B region leads to diastolic dysfunction and cardiac atrophy. *Proc Natl Acad Sci U S A* 104:3444-3449.
- Ray J, Leach R, Herbert J, Benson M. 2001. Isolation of vascular smooth muscle cells from a single murine aorta. *Methods Cell Sci* 23:185-188.
- Reddy MA, Kim Y, Lanting L, Natarajan R. 2003. Reduced growth factor responses in vascular smooth muscle cells derived from 12/15-lipoxygenase-deficient mice. *Hypertension* 41:1294-1300.
- Reddy MA, Thimmalapura P, Lanting L, Nadler JL, Fatima S, Natarajan R. 2002. The oxidized lipid and lipoxygenase product 12(S)-hydroxyeicosatetraenoic acid induces hypertrophy and fibronectin transcription in vascular smooth muscle cells via p38 MAPK and cAMP response element-binding protein activation. Mediation of angiotensin II effects. *J. Biol. Chem* 277:9920-9928.
- Reese J, Das SK, Paria BC, Lim H, Song H, Matsumoto H, Knudtson KL, DuBois RN, Dey SK. 2001. Global gene expression analysis to identify molecular markers of uterine receptivity and embryo implantation. *J. Biol. Chem* 276:44137-44145.
- Reynolds LP, Caton JS, Redmer DA, Grazul-Bilska AT, Vonnahme KA, Borowicz PP, Luther JS, Wallace JM, Wu G, Spencer TE. 2006. Evidence for altered placental blood flow and vascularity in compromised pregnancies. *J. Physiol. (Lond.)* 572:51-58.
- Rockwell LC, Pillai S, Olson CE, Koos RD. 2002. Inhibition of vascular endothelial growth factor/vascular permeability factor action blocks estrogen-induced uterine edema and implantation in rodents. *Biol. Reprod* 67:1804-1810.
- Rodriguez C, Buchholz F, Galloway J, Sequerra R, Kasper J, Ayala R, Stewart A, Dymecki S. 2000. High-efficiency deleter mice show that FLPe is an alternative to Cre-loxP. *Nat Genet* 25:139-140.
- Rogers PA, Murphy CR, Squires KR, MacLennan AH. 1983. Effects of relaxin on the intrauterine distribution and antimesometrial positioning and orientation of rat blastocysts before implantation. *J. Reprod. Fertil* 68:431-435.
- Rowe RW. 1973. The ultrastructure of Z disks from white, intermediate, and red fibers of mammalian striated muscles. *J. Cell Biol* 57:261-277.

Ruhrberg C, Gerhardt H, Golding M, Watson R, Ioannidou S, Fujisawa H, Betsholtz C, Shima DT. 2002. Spatially restricted patterning cues provided by heparin-binding VEGF-A control blood vessel branching morphogenesis. *Genes Dev* 16:2684-2698.

Sainson RCA, Aoto J, Nakatsu MN, Holderfield M, Conn E, Koller E, Hughes CCW. 2005. Cell-autonomous notch signaling regulates endothelial cell branching and proliferation during vascular tubulogenesis. *FASEB J* 19:1027-1029.

Sanger JW, Sanger JM. 2001. Fishing out proteins that bind to titin. *J Cell Biol* 154:21-24.

Sato TN, Tozawa Y, Deutsch U, Wolburg-Buchholz K, Fujiwara Y, Gendron-Maguire M, Gridley T, Wolburg H, Risau W, Qin Y. 1995. Distinct roles of the receptor tyrosine kinases Tie-1 and Tie-2 in blood vessel formation. *Nature* 376:70-74.

Schaffner W, Weissmann C. 1973. A rapid, sensitive, and specific method for the determination of protein in dilute solution. *Anal Biochem* 56:502-514.

Schlafke S, Enders AC. 1975. Cellular basis of interaction between trophoblast and uterus at implantation. *Biol. Reprod* 12:41-65.

Small JV, Gimona M. 1998. The cytoskeleton of the vertebrate smooth muscle cell. *Acta Physiol. Scand* 164:341-348.

Smith A, Heath J, Donaldson D, Wong G, Moreau J, Stahl M, Rogers D. 1988. Inhibition of pluripotential embryonic stem cell differentiation by purified polypeptides. *Nature* 336:688-690.

Smith WL. 1989. The eicosanoids and their biochemical mechanisms of action. *Biochem. J* 259:315-324.

Snell G. 1941. *Biology of the laboratory mouse*. Philadelphia: The Blakiston Co.

Song H, Lim H, Paria BC, Matsumoto H, Swift LL, Morrow J, Bonventre JV, Dey SK. 2002. Cytosolic phospholipase A2alpha is crucial for 'on-time' embryo implantation that directs subsequent development. *Development* 129:2879-2889.

Sorimachi H, Kinbara K, Kimura S, Takahashi M, Ishiura S, Sasagawa N, Sorimachi N, Shimada H, Tagawa K, Maruyama K. 1995. Muscle-specific calpain, p94, responsible for limb girdle muscular dystrophy type 2A, associates with connectin through IS2, a p94-specific sequence. *J Biol Chem* 270:31158-62.

Sorimachi H, Freiburg A, Kolmerer B, Ishiura S, Stier G, Gregorio C, Labeit D, Linke W, Suzuki K, Labeit S. 1997. Tissue-specific expression and alpha-actinin binding properties of the Z-disc titin: implications for the nature of vertebrate Z- discs. *J Mol Biol* 270:688-695.

- Spencer JA, Eliazar S, Ilaria RL, Richardson JA, Olson EN. 2000. Regulation of microtubule dynamics and myogenic differentiation by MURF, a striated muscle RING-finger protein. *J Cell Biol* 150:771-84.
- Spiegel S, Milstien S. 2003. Sphingosine-1-phosphate: an enigmatic signalling lipid. *Nat. Rev. Mol. Cell Biol* 4:397-407.
- Stewart CL, Kaspar P, Brunet LJ, Bhatt H, Gadi I, Köntgen F, Abbondanzo SJ. 1992. Blastocyst implantation depends on maternal expression of leukaemia inhibitory factor. *Nature* 359:76-79.
- Suchting S, Freitas C, le Noble F, Benedito R, Bréant C, Duarte A, Eichmann A. 2007. The Notch ligand Delta-like 4 negatively regulates endothelial tip cell formation and vessel branching. *Proc Natl Acad Sci U S A* 104:3225-30.
- Suri C, Jones PF, Patan S, Bartunkova S, Maisonpierre PC, Davis S, Sato TN, Yancopoulos GD. 1996. Requisite role of angiopoietin-1, a ligand for the TIE2 receptor, during embryonic angiogenesis. *Cell* 87:1171-1180.
- Taveau M, Bourg N, Sillon G, Roudaut C, Bartoli M, Richard I. 2003. Calpain 3 is activated through autolysis within the active site and lyses sarcomeric and sarcolemmal components. *Mol Cell Biol* 23:9127-9135.
- Thomas K, Capecchi M. 1987. Site-directed mutagenesis by gene targeting in mouse embryo-derived stem cells. *Cell* 51:503-512.
- Thurston G, Suri C, Smith K, McClain J, Sato TN, Yancopoulos GD, McDonald DM. 1999. Leakage-resistant blood vessels in mice transgenically overexpressing angiopoietin-1. *Science* 286:2511-2514.
- Torry DS, Torry RJ. 1997. Angiogenesis and the expression of vascular endothelial growth factor in endometrium and placenta. *Am. J. Reprod. Immunol* 37:21-29.
- Trombitas K, Freiburg A, Centner T, Labeit S, Granzier H. 1999. Molecular dissection of N2B cardiac titin's extensibility. *Biophys J* 77:3189-3196.
- Trombitas K, Greaser M, Labeit S, Jin J, Kellermayer M, Helmes M, Granzier H. 1998. Titin extensibility in situ: entropic elasticity of permanently folded and permanently unfolded molecular segments. *J Cell Biol* 140:853-859.
- Truett GE, Heeger P, Mynatt RL, Truett AA, Walker JA, Warman ML. 2000. Preparation of PCR-quality mouse genomic DNA with hot sodium hydroxide and tris (HotSHOT). *BioTechniques* 29:52, 54.
- Tskhovrebova L, Trinick J. 2003. Titin: properties and family relationships. *Nat Rev Mol Cell Biol* 4:679-689.



Turnacioglu KK, Mittal B, Dabiri GA, Sanger JM, Sanger JW. 1997. Zeugmatin is part of the Z-band targeting region of titin. *Cell Struct. Funct* 22:73-82.

Turnacioglu KK, Mittal B, Sanger JM, Sanger JW. 1996. Partial characterization of zeugmatin indicates that it is part of the Z-band region of titin. *Cell Motil. Cytoskeleton* 34:108-121.

Udy G, Parkes B, Wells D. 1997. ES cell cycle rates affect gene targeting frequencies. *Exp Cell Res* 231:296-301.

Vizza E, Correr S, Muglia U, Marchioli F, Motta PM. 1995. The three-dimensional organization of the smooth musculature in the ampulla of the human fallopian tube: a new morpho-functional model. *Hum. Reprod* 10:2400-2405.

Vuorela P, Carpén O, Tulppala M, Halmesmäki E. 2000. VEGF, its receptors and the tie receptors in recurrent miscarriage. *Mol. Hum. Reprod* 6:276-282.

Vuorela P, Halmesmäki E. 2006. Vascular endothelial growth factor, its receptors, and the tie receptors in the placental bed of women with preeclampsia, diabetes, and intrauterine growth retardation. *Am J Perinatol* 23:255-263.

Wakui S, Yokoo K, Muto T, Suzuki Y, Takahashi H, Furusato M, Hano H, Endou H, Kanai Y. 2006. Localization of Ang-1, -2, Tie-2, and VEGF expression at endothelial-pericyte interdigitation in rat angiogenesis. *Lab. Invest* 86:1172-1184.

Wang HM, Zhang X, Qian D, Lin HY, Li QL, Liu DL, Liu GY, Yu XD, Zhu C. 2004. Effect of ubiquitin-proteasome pathway on mouse blastocyst implantation and expression of matrix metalloproteinases-2 and -9. *Biol. Reprod* 70:481-487.

Wang J, Shaner N, Mittal B, Zhou Q, Chen J, Sanger J, Sanger J. 2005. Dynamics of Z-band based proteins in developing skeletal muscle cells. *Cell Motil Cytoskeleton* 61:34-48.

Wang K, McClure J, Tu A. 1979. Titin: major myofibrillar components of striated muscle. *Proc Natl Acad Sci U S A* 76:3698-3702.

Wang SM, Jeng CJ, Sun MC. 1992. Studies on the interaction between titin and myosin. *Histol. Histopathol* 7:333-337.

Warren C, Krzesinski P, Campbell K, Moss R, Greaser M. 2004. Titin isoform changes in rat myocardium during development. *Mech Dev* 121:1301-1312.

Warren C, Krzesinski P, Greaser M. 2003. Vertical agarose gel electrophoresis and electroblotting of high-molecular-weight proteins. *Electrophoresis* 24:1695-1702.

Watanabe K, Nair P, Labeit D, Kellermayer M, Greaser M, Labeit S, Granzier H. 2002. Molecular mechanics of cardiac titin's PEVK and N2B spring elements. *J Biol Chem*.

- Weinert S, Bergmann N, Luo X, Erdmann B, Gotthardt M. 2006. M line-deficient titin causes cardiac lethality through impaired maturation of the sarcomere. *J Cell Biol* 173:559-570.
- Willis MS, Ike C, Li L, Wang D, Glass DJ, Patterson C. 2007. Muscle ring finger 1, but not muscle ring finger 2, regulates cardiac hypertrophy in vivo. *Circ. Res* 100:456-459.
- Witt CC, Witt SH, Lerche S, Labeit D, Back W, Labeit S. 2008. Cooperative control of striated muscle mass and metabolism by MuRF1 and MuRF2. *EMBO J* 27:350-360.
- Witt S, Granzier H, Witt C, Labeit S. 2005. MURF-1 and MURF-2 target a specific subset of myofibrillar proteins redundantly: towards understanding MURF-dependent muscle ubiquitination. *J Mol Biol* 350:713-722.
- Wobus A, Wallukat G, Hescheler J. 1991. Pluripotent mouse embryonic stem cells are able to differentiate into cardiomyocytes expressing chronotropic responses to adrenergic and cholinergic agents and Ca<sup>2+</sup> channel blockers. *Differentiation* 48:173-182.
- Wong EA, Capecchi MR. 1987. Homologous recombination between coinjected DNA sequences peaks in early to mid-S phase. *Mol. Cell. Biol* 7:2294-2295.
- Xie K, Hou X, Li M, Li D. 2010. nm23-H1 at human maternal-fetal interface down-regulates titin expression and invasiveness of trophoblast cells via mitogen-activated protein kinase pathway in early pregnancy. *Reproduction* [Internet]. Available from: <http://www.ncbi.nlm.nih.gov/pubmed/20145075>
- Xin H, Deng K, Rishniw M, Ji G, Kotlikoff M. 2002. Smooth muscle expression of Cre recombinase and eGFP in transgenic mice. *Physiol Genomics* 10:211-215.
- Yamaguchi M, Izumimoto M, Robson RM, Stromer MH. 1985. Fine structure of wide and narrow vertebrate muscle Z-lines. A proposed model and computer simulation of Z-line architecture. *J. Mol. Biol* 184:621-643.
- Yamasaki R, Berri M, Wu Y, Trombitas K, McNabb M, Kellermayer M, Witt C, Labeit D, Labeit S, Greaser M, et al. 2001. Titin-actin interaction in mouse myocardium: passive tension modulation and its regulation by calcium/S100A1. *Biophys J* 81:2297-2313.
- Yamasaki R, Wu Y, McNabb M, Greaser M, Labeit S, Granzier H. 2002. Protein kinase A phosphorylates titin's cardiac-specific N2B domain and reduces passive tension in rat cardiac myocytes. *Circ Res* 90:1181-1188.
- Ye X, Hama K, Contos JJA, Anliker B, Inoue A, Skinner MK, Suzuki H, Amano T, Kennedy G, Arai H, et al. 2005. LPA3-mediated lysophosphatidic acid signalling in embryo implantation and spacing. *Nature* 435:104-8.
- Young P, Ehler E, Gautel M. 2001. Obscurin, a giant sarcomeric Rho guanine nucleotide exchange factor protein involved in sarcomere assembly. *J Cell Biol* 154:123-136.

## 9 Supplement

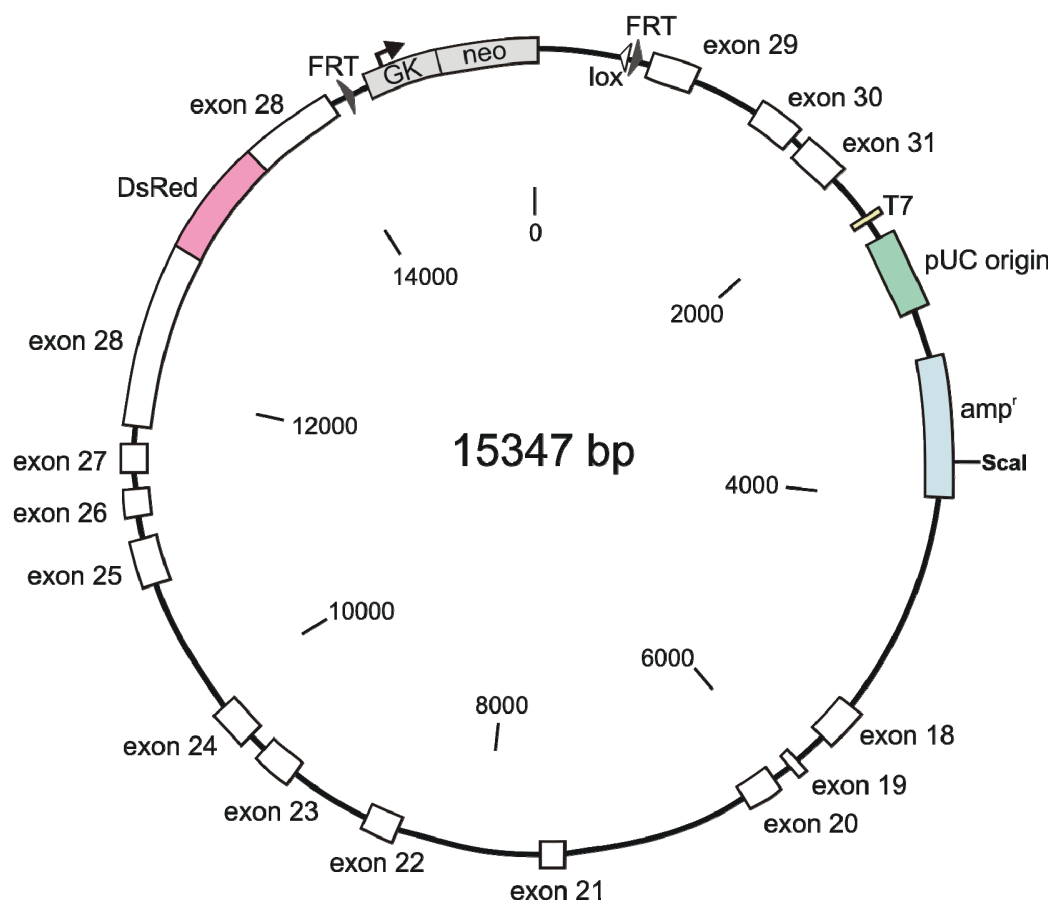


**Figure 30: Map of the targeting vector DsRedKI.** The targeting vector had a size of 15347 bp spanning the genomic region from titin's exon 18 to exon 31 with the DsRed incorporated in exon 28 and the neomycin resistance cassette with the glucokinase promoter (GK) flanked by 2 FRT-sites between exon 28 and exon 29. The plasmid also includes the pUC origin for propagation in *E. coli*, the T7 promoter, and the ampicillin resistance gene (*amp<sup>r</sup>*) for antibiotic selection in *E. coli*. The restriction site of *ScaI* that linearizes the targeting vector is indicated.

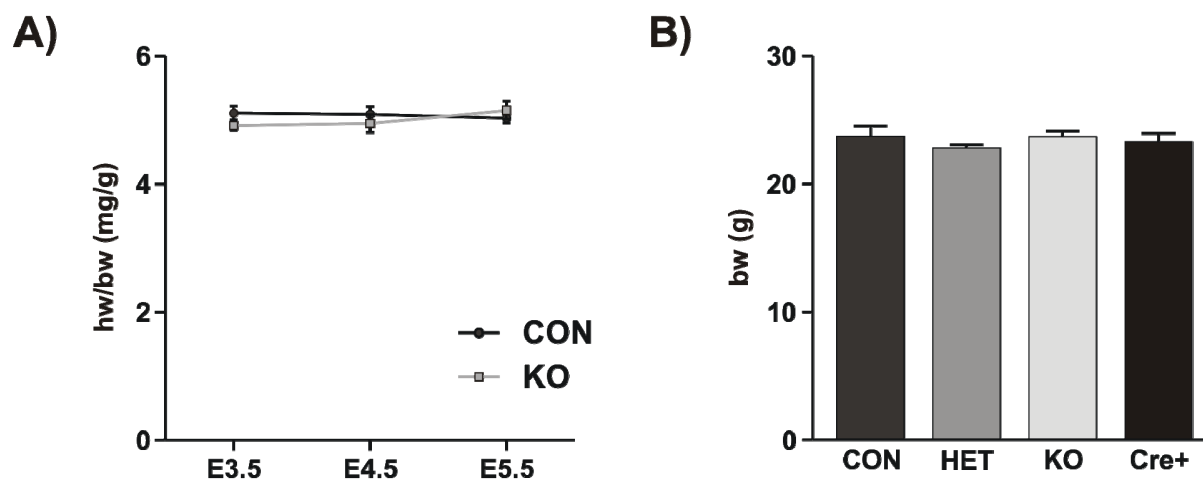


**Figure 31: Adult smooth muscle knockout animals did not have an obvious phenotype.** A) Deletion of titin's kinase region in knockout (KO) animals did not change the heart weight to body weight ratio in comparison to control (CON) animals, which was shown for E3.5 (KO n=10; CON n=11), E4.5 (KO n=5; CON n=7), and E5.5 (KO n=7; CON n=6; mean with SEM; Two-way ANOVA  $P>0.05$ ). E3.5 was confirmed by the presence of blastocysts. B) Control, heterozygous (HET), knockout, and Cre+ control mice (Cre+) had the same body weight so that the reduced uterine weight to body weight ratio in knockout animals was due the loss of titin's kinase region (CON n=6; HET n=5; KO n=7; Cre+ n=3; mean with SEM; one-way ANOVA  $P>0.05$ ).

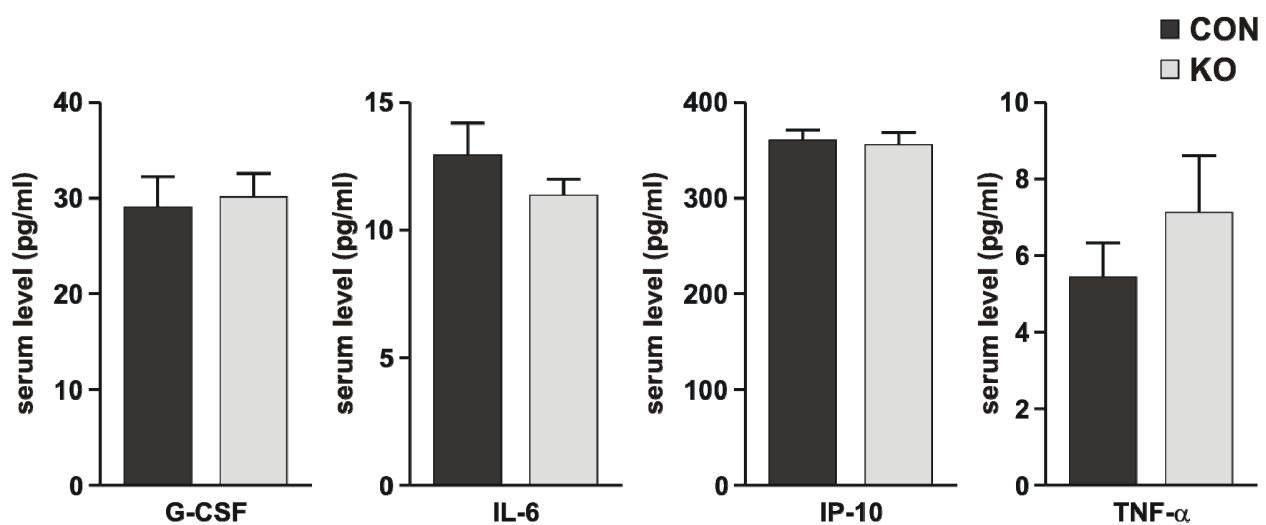


**Figure 32: Increase in the PDGF-B serum levels was not accompanied by changes in selected cytokines.** Multiplex bead immunoassay to measure cytokines in pregnant E3.5 mice revealed no difference in the serum levels of G-CSF, IL-6, IP-10, and TNF- $\alpha$  between knockout animals (KO; n= 13) and control animals (CON; n=14; mean with SEM; T-test  $P>0.05$ ). The metabolite concentration is illustrated per serum volume.

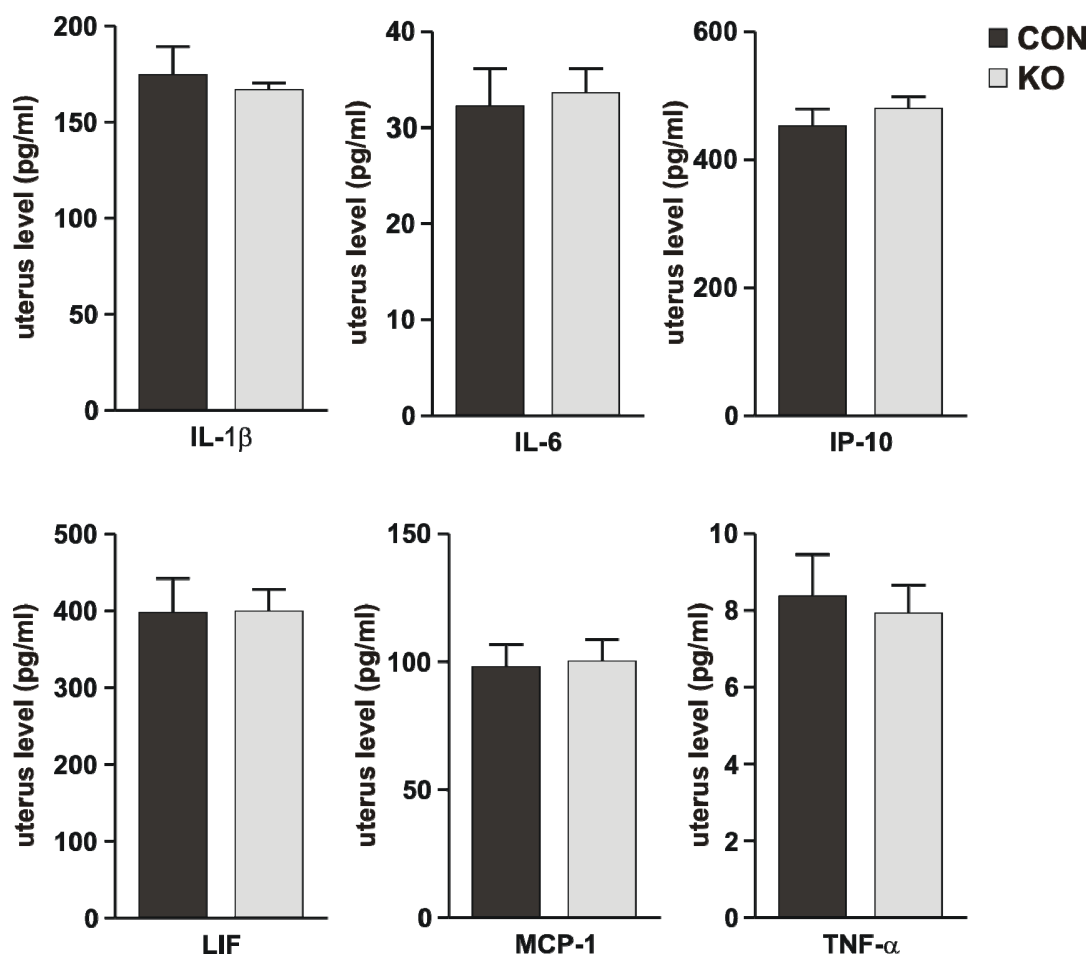


**Figure 33: LIF, an important factor of embryo implantation, was unchanged in pregnant E3.5 knockout uteri.** The cytokines IL-1 $\beta$ , IL-6, IP-10, LIF, MCP-1, and TNF- $\alpha$  were unchanged in pregnant E3.5 uteri comparing knockout (KO; n=13) and control animals (CON; n=14; mean with SEM; T-test  $P>0.05$ ). Values were determined using the multiplex bead immunoassay. The metabolite concentration is illustrated per lysate volume that was normalized against its total protein concentration.

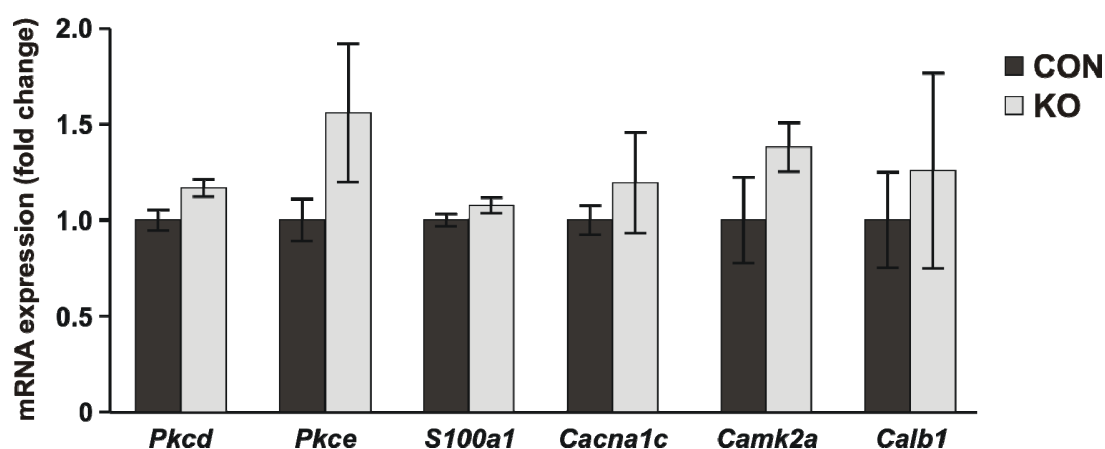


**Figure 34: The transcript level of genes encoding selected calcium-related proteins was unchanged.** Real-Time PCR analysis revealed that the expression of the genes *Prkcd*, *Prkce*, *S100a1*, *Cacna1c*, *Camk2a*, and *Calb1* encoding selected calcium-related proteins did not differ between knockout (KO; n=3) and control (CON; n=3) uteri pregnant at E3.5. The mRNA levels were normalized to 18S RNA and expression is displayed as fold change relative to the control (mean with SEM; T-test comparing CON and KO of one primer/probe set  $P>0.05$ ).

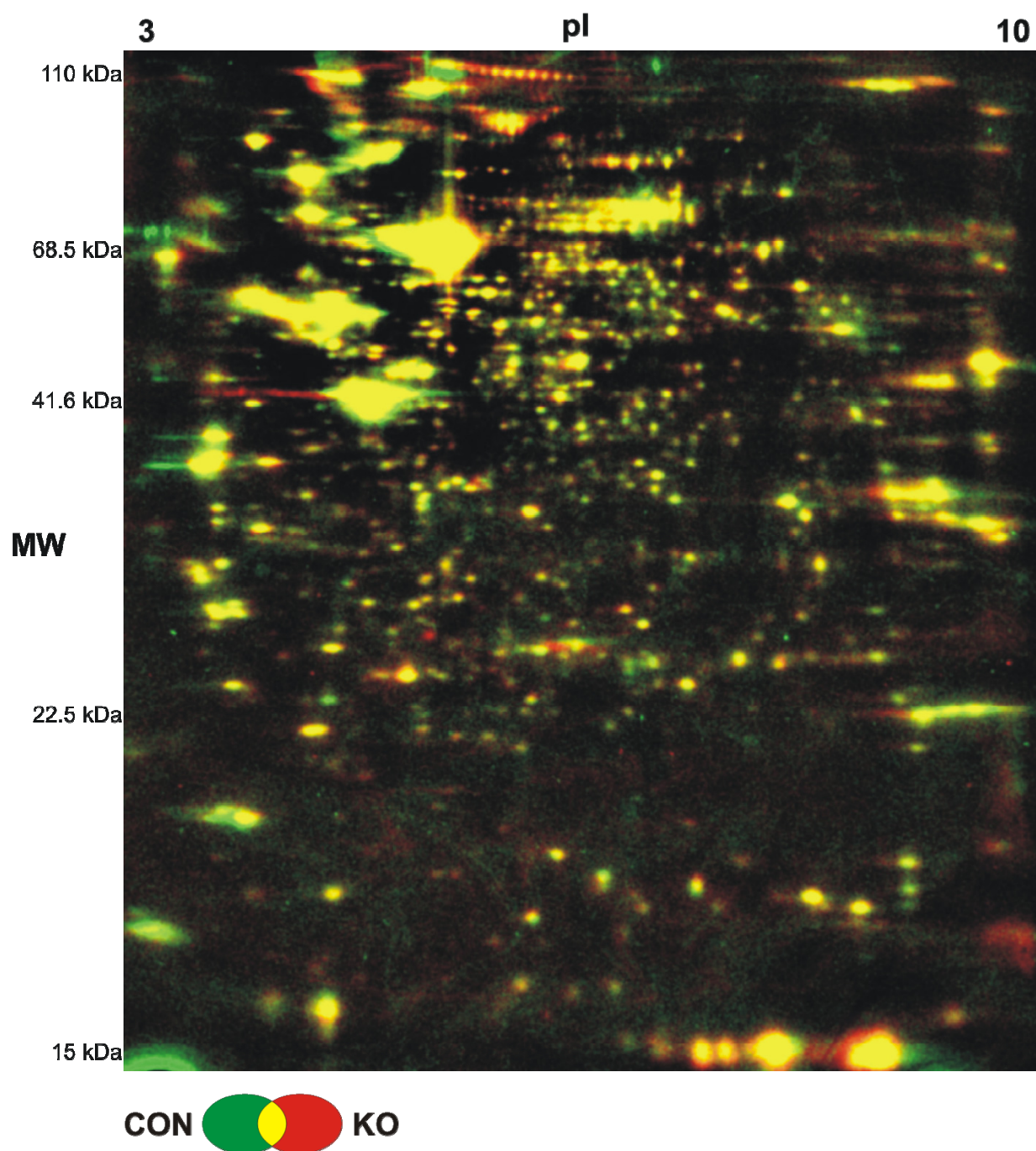


**Figure 35: Dual view of knockout and control 2D-gel.** 2D-gel electrophoresis was performed for proteome analysis of pregnant E3.5 knockout (KO; n=6) in comparison to control (CON; n=6) uteri. A dual view of a representative control and knockout gel is shown, which was generated using the Delta2D software. Thereby, the software colorized the control protein spots green and the knockout protein spots red leading by overlay in the dual view to yellow spots, if the same amount of protein is present in both groups. Proteins in knockout samples that are downregulated are indicated by green spots (32 proteins) and that are accumulated (74 proteins) are indicated by red spots in the dual view (T-test  $P < 0.1$  \*).

**Table 11: Differentially regulated proteins in E3.5 pregnant knockout uteri.** The table shows the mean of control (CON n=6) and knockout (KO n=6) percent volume value (% V) of protein spots obtained by evaluation of 2D-gels comparing pregnant E3.5 knockout and control uteri. Furthermore, the %V ratios between knockout and control mean as well as the results of the T-test are listed. Thereby, proteins with a ratio value of < 0.8 and > 1.3 were considered to be less or more synthesized, respectively (T-test  $P < 0.1$  \*).

Protein	Protein name	Mean % V CON	Mean % V KO	Ratio % V KO/ CON	T-test
ANXA2	annexin A2	0.108	0.084	0.78	0.006
ARPC2	actin related protein 2/3 complex	0.081	0.11	1.36	0.037
CAPG	capping protein	0.029	0.042	1.43	0.064
CAR2	carbonic anhydrase 2	0.068	0.091	1.34	0.011
CKB	brain creatine kinase	0.233	0.18	0.77	0.01
COL6A2	collagen type VI alpha 2	0.069	0.101	1.46	0.074
COL6A2	collagen type VI alpha 2	0.042	0.076	1.79	0.009
DNAJA1	DnaJ (Hsp40) homolog	0.03	0.045	1.49	0.038
ETFDH	electron transferring flavoprotein dehydrogenase	0.031	0.043	1.37	0.024
FGA	fibrinogen	0.032	0.05	1.57	0.014
HNRNPAB	heterogeneous nuclear ribonucleoprotein A/B	0.034	0.05	1.48	0.036
HSPB1	heat shock protein 1	0.191	0.141	0.74	0.024
NDUFS3	NADH dehydrogenase (ubiquinone) Fe-S protein 3	0.03	0.068	2.24	0.003
PCX	pyruvate carboxylase	0.029	0.044	1.57	0.026
PDIA4	protein disulfide-isomerase A4	0.253	0.205	0.79	0.015
PSMC2	proteasome 26S subunit ATPase 2	0.039	0.026	0.68	0.019
SFRS3	splicing factor arginine/serine-rich 3	0.05	0.068	1.35	0.029
TAGLN	transgelin	0.498	0.4	0.79	0.016
TPI1	triosephosphate isomerase 1	0.167	0.217	1.3	0.021
VIM	vimentin	0.018	0.027	1.48	0.05

